5-2019

Enhancing the Macroscopic Properties of Parts Printed via Fused Filament Fabrication by Incorporating Nanoscopic Additives

Dayton Phillip Street
University of Tennessee, dstreet4@vols.utk.edu

Enhancing the Macroscopic Properties of Parts Printed via Fused Filament Fabrication by Incorporating Nanoscopic Additives

A Dissertation Presented for the
Doctor of Philosophy
Degree
The University of Tennessee, Knoxville

Dayton Phillip Street
May 2019

Dedication

This dissertation is dedicated to my parents, David and Jan Street, and to my wife, Mary Beth Street. Their endless encouragement and support have allowed me to develop as an individual and as a scientist.

"It is good to have an end to journey toward, but it is the journey that matters in the end."
-Ernest Hemmingway

ACKNOWLEDGEMENTS

First, I would like to thank my advisor, Prof. S. Michael Kilbey II, for his unwavering support and guidance during my graduate studies. His dedication to teaching and developing students as professional research scientists is unrivaled. I know that selecting Dr. Kilbey as an advisor was the correct choice: Dr. Kilbey has taught me how to succeed as an independent scientist, work collaboratively, and more importantly, he has demonstrated how to be a leader and above all else, a professional. I would also like to thank Dr. Kilbey for teaching me to convey scientific results in a clear and concise method. Scientific writing is something I struggled with prior to and during graduate school. However, through his constant support and efforts have helped me grow and improve, and I now have a sense of pride and confidence regarding my writing abilities. In addition to being my adviser, Dr. Kilbey has become a great friend whom I trust and I know I can rely on as my career begins. And for that, I am truly thankful.

I want to express my deep gratitude to my wife, Mary Beth Street. Your steadfast love and support throughout my graduate studies were essential to my success and they are cherished more than you'll ever know. Thank you for always standing beside me through my trials and successes. Although my graduate studies took time away from our weekends and weeknights, you never complained – instead, you have been a constant source of encouragement. Your reassurance has helped me through the tribulations associated with graduate school and has allowed me to pursue my educational goals and develop as a professional and a research scientist.

I also would like to thank my parents, David and Jan Street, for their continual love and support throughout my life. My mother is the strongest person I know. She has never let any obstacle stand in the way of her aspirations. She is an inspiration to me daily and is a constant source of encouragement and support. My father has been a role model and best friend throughout my graduate studies and my life. In all aspects of life, during failures or victories, I know that I will always be able to confide in them and that I will never walk alone. I would not be the person I am today without my parents' guidance and encouragement. I will carry the values they have instilled in me everywhere I go and apply them daily. I will always be grateful for both of them.

I thank all of the Kilbey group members, both past and present, that have provided support, laughs, and most of all, friendship over the years. I especially thank Jesse Davis, Bethany Aden, and Graham Collier, who are extraordinary colleagues and mentors. Additionally, I am thankful for friendships with other group members, including Kamlesh Bornani, Zach Seibers, Rachel Ramirez, Sina Sabury, Will Ledford, Elizabeth O'Connell, Nia Parker, Dani Chun, Evan Boone, Ben Hopkins, Natalie Czarnecki, Samantha Cahill, and Abigail Allison.

Finally, I would like to thank my collaborators. I sincerely thank Deanna L. Pickel for her advice and help with filament fabrication. I thank Adeline H. Mah and Dr. Gila E. Stein for their insight, advice, and help with X-ray measurements and data fitting. I thank Max Heres, Emmanuel Mapesa, and Dr. Joshua Sangoro, who introduced me to broadband dielectric spectroscopy, which motivated our collaborative studies of the relaxation dynamics of polymer nanocomposites. I am grateful to Jamie M. Messman of the Kansas City National Security Center, who brought me on-site multiple times for training and

assistance with tensile testing and other mechanical measurements. Additionally, I would like to acknowledge the assistance and contributions of collaborators from Oak Ridge National Laboratory. Specifically, I thank John Ankner, who helped me with neutron reflectivity data collection and analysis, and Brad Loktiz, who provided guidance and assistance with instrument training. Lastly, I acknowledge my graduate committee members, Dr. Chris Baker, Dr. Bin Zhao, and Dr. Joshua Sangoro: whether it was during candidacy or proposal defenses, in classes, or serving on committees together, each of you have helped to mold me into the research scientist that I am today, and for that, I thank you.

ABSTRACT

Additive Manufacturing (AM), or 3D printing, provides an alternative route to generate end-stage products by coupling advanced manufacturing techniques with computer modeling. However, parts fabricated by AM are known to have inferior mechanical properties compared to parts prepared by traditional methods, such as injection molding. This principal drawback is attributed to the presence of voids and inefficient adhesion between adjacent filaments, or beads, due to limited diffusion of polymer chains across interbead interfaces. Together these shortcomings also lead to anisotropic mechanical properties in printed parts. While optimizing print conditions or applying post-printing procedures decreases the anisotropy, these methods are incapable of obtaining significant enhancements in material properties. To address this, my dissertation work examines how incorporating nanoscopic additives, including bare (unfunctionalized) nanoparticles, poly(methyl methacrylate)-grafted-nanoparticles (PMMA-g-NPs), and macromolecules containing self-complementary, multiple hydrogen bonding motifs that trigger supramolecular assembly, into PMMA filaments affects structure formation at the nanoscale and impacts the resultant macroscopic properties of PMMA parts manufactured by Fused Filament Fabrication (FFF). Results indicate that incorporating bare nanoparticles, which arrange as well-dispersed mass fractals throughout the matrix, into PMMA filaments leads to a slight increase the thermomechanical properties. Adding PMMA-g-NPs significantly improves material properties relative to samples printed with bare nanoparticles. These enhancements are attributed to increased interactions across grafted nanoparticle/matrix interfaces because there is a direct correlation between loading

level and changes in thermomechanical properties. In addition to using inorganic additives, my research efforts demonstrate that copolymeric additives capable of forming thermoreversible physical crosslinks are advantageous. They increase part performance at use temperatures, but the dissociation of physical crosslinks at high temperatures (used for polymer melt processing) alleviates any deleterious effect on the viscosity, rendering them highly processable. These results demonstrate that molecular engineering can be used to effectively manage interactions on the nanoscale, leading to substantial increases in the performance of FFF-printed parts. These studies, which highlight the importance and potential of non-bonded interactions, provide a compelling and useful pathway for addressing challenges associated with the inferior performance of 3D printed polymeric materials.

TABLE OF CONTENTS

Chapter 1: Introduction 1

1.1 Interfaces in Polymeric Materials 2

1.2 Motivation 5

1.2.1 Polymer Nanocomposites 7

1.2.2 Polymer Grafted Nanocomposites 9

1.2.3 Supramolecular Blends 12

1.3 Synthesis and Characterization of Nanoscopic Additives 16

1.4 Characterization and Thermomechanical Properties 21

1.5 Research Objectives 24

Chapter 2: Interfacial Interactions in PMMA/Silica Nanocomposites Enhance the Performance of Parts Created by Fused Filament Fabrication 28

2.1 Abstract 29

2.2 Introduction 30

2.3 Experimental Methods 34

2.4 Results and Discussion 38

2.5 Conclusions 52

Chapter 3: Tailoring Interfacial Interactions Using Polymer Grafted Nanoparticles Improves Performance of Parts Manufactured by 3D Printing 53

3.1 Abstract 54

3.2 Introduction 54

3.3 Experimental Methods 58

3.3.1 Synthesis of Materials 58
3.3.2 Extrusion of Filament and FFF 61
3.3.3 Instrumentation and Characterization 62
3.4 Results and Discussion 66
3.5 Conclusions 82
Chapter 4: Self-Complementary Multiple Hydrogen Bonding Additives Enhance Thermomechanical Properties of PMMA Structures Created by Fused Filament Fabrication 84
4.1 Abstract 85
4.2 Introduction 86
4.3 Experimental Methods 90
4.3.1 Materials and Copolymer Synthesis 90
4.3.2 Extrusion of Filament and FFF 91
4.3.3 Instrumentation and Characterization 92
4.4 Results and Discussion 94
4.5 Conclusions 108
Chapter 5: Summary, Conclusions, and Future Works 110
5.1 Summary 111
5.2 Future Work 114
5.2.1 Random Copolymer Grafted Nanocomposites 115
5.2.2 Surface-Active Additives Promote Diffusion Across Bead-Bead Interfaces 118
5.3 Conclusions 120
List of References 122

Appendices 144

Appendix A – Supporting Information for Chapter 2: Interfacial Interactions in PMMA/Silica Nanocomposites Enhance the Performance of Parts Created by Fused Filament Fabrication 145

Appendix B – Supporting Information for Chapter 3: Tailoring Interfacial Interactions Using Polymer Grafted Nanoparticles Improves Performance of Parts Manufactured by 3D Printing 149

Appendix C – Supporting Information for Chapter 4: Self-Complementary Multiple Hydrogen Bonding Additives Enhance Thermomechanical Properties of PMMA Structures Created by Fused Filament Fabrication 158

Vita 164

LIST OF TABLES

Table 2.1. Mechanical properties of PMMA nanocomposite samples manufactured by FFF.[a] 41

Table 2.2. Unified fit parameters obtained from SAXS measurements on PMMA nanocomposite specimens. 50

Table 3.1. Optimized model parameters based on fits of at least 12 independent measurements at each particle loading level. P_1 is the Porod exponent for the low-q region, R is the particle radius, R_{HS} is the hard sphere interaction radius, and φ is the volume fraction of particles in a cluster. independent measurements, and the uncertainty is reported as ± 1 standard deviation. 68

Table 3.2. Mechanical properties of PMMA nanocomposite samples containing PMMA-g-NPs manufactured by FFF.[a] 80

Table 4.1. Molecular characteristics of p(MMA-r-UPyMA) additives synthesized via free radical polymerization. 95

Table 4.2. Mechanical properties of FFF-printed parts containing p(MMA-r-UPyMA) copolymer additives. 100

LIST OF FIGURES

Figure 1.1. The surface properties of polymeric materials can be altered using myriad methods such as (A) energetic treatments, (B) chemical modification, and (C) surface active additives..... 3

Figure 1.2. Illustration of how FFF can be used to generate polymeric scaffolds from polymer feedstock. FFF operates by heating a thermoplastic filament to a semi-molten state and extruding it in a layer-by-layer, or “bottom-up”, build process..... 6

Figure 1.3. The nanoscale organization of densely-grafted nanoparticles in a symmetric, athermal, system is controlled by entropic interactions. Specifically, when the matrix chain molecular weight is larger than the graft chain molecular weight particle clusters are observed, while dispersed particles are observed when the matrix chain molecular weight is smaller than the graft chain molecular weight. 11

Figure 1.4. Functionalizing telechelic chain ends of poly(propylene-block-ethylene oxide) oligomers with UPy groups that participate in thermoresponsive, physical crosslinks is demonstrated to result in a denser, thermodynamically stable network compared to oligomers covalently crosslinked through hydroxyl groups. 14

Figure 1.5. Incorporating UPyMA comonomers into the backbone of poly(butyl acrylate-co-UPyMA) random copolymers is demonstrated to increase the melt flow characteristics at temperatures below the dissociation temperature of UPy groups, while no deleterious impact is observed at temperatures above the dissociation temperature. 15

Figure 1.6. Uncontrolled free radical polymerizations, which are used to create self-complementary, multiple hydrogen bonding additives in Chapter 4, have three main mechanistic steps including: Initiation, Propagation, and Termination. 17

Figure 1.7. RAFT polymerization exhibits a fast, dynamic equilibrium due to degenerative fragmentation-chain transfer that allows control over the polymerization, resulting in narrow dispersity control over molecular weight of polymer chains. 19

Figure 1.8. Amino-silane functionalized nanoparticles are reacted with a dithioester CTA to generate CTA-functionalized nanoparticles that are then used to grow polymer chains from the surface of Si NPs. 20

Figure 1.9. DMA works by applying an oscillating force to a sample and measuring the sinusoidal response. By observing differences in the phase shift and/or amplitude one can investigate the thermomechanical properties of polymeric materials. 22

Figure 1.10. DMA strain-sweep (amplitude-sweep) measurements are used to determine both the linear viscoelastic region and the Young's Modulus of printed parts. 22

Figure 2.1. DMA results show an increase in the Young's modulus with increasing amount of Si NP incorporated into the filament. Values of the Young's modulus given in the legend are based on measurements of five replicate samples. 39

Figure 2.2. Tensile testing of nanocomposite samples shows an increase in Young's modulus, ultimate tensile strength, and elongation-at-break as the Si NP loading increases. A representative trace from a series of replicate tests is shown for each loading level and the values of tensile modulus provided in the legend are based on measurements of five replicate samples. 40

Figure 2.3. Constant-strain temperature ramp measurements completed on PMMA nanocomposite samples produced by FFF as a function of Si NP loading show that the glass transition temperature (A) and storage (B) and loss moduli (C) increase with increasing filler content..... 43

Figure 2.4. Rheological measurements show that the storage modulus (A) and complex viscosity (B) of FFF-printed PMMA nanocomposite specimens increase as the loading level of Si NPs increases. A reference temperature of 170 °C was used for time-temperature superposition. The y-axis scale used to create the plot inset in (A) is intended to accentuate the increase in storage modulus with loading level. 46

Figure 2.5. Scanning Electron Microscopy shows that Si NPs, present here at a 1 wt% loading level, are well-dispersed throughout the FFF-printed PMMA nanocomposite specimen. This image is a top-down view of a DMA sample printed by FFF. 49

Figure 2.6. Corrected scattered intensity curves from SAXS measurements of FFF-printed PMMA nanocomposite specimens containing Si NPs at various loading levels..... 50

Figure 3.1. Average of all SAXS profiles for each PMMA-g-NP loading level (open symbols) and best-fit to the model described by Equations 3.1 and 3.2..... 68

Figure 3.2. Rheological measurements show that increasing the loading level of PMMA-g-NPs in FFF-printed PMMA parts increases both the storage modulus (A) and complex viscosity (B). A reference temperature of 170 °C was used to create time-temperature superposition master curves displayed here..... 71

Figure 3.3. Constant-strain temperature ramp measurements show that the glass transition temperature (A), storage modulus (B), and loss modulus (C) of nanocomposite PMMA parts containing PMMA-g-NPs increase with increasing filler content..... 74

Figure 3.4. DMA results show that all samples display a significant increase in the Young's modulus even at low loading levels (≤ 1.0 wt% based on Si), with the largest increase (61%) observed at 0.3 wt%. Values of the Young's modulus given in the legend are based on measurements of five replicate samples and the corresponding standard deviation. 77

Figure 3.5. Representative tensile tests show an increase in the tensile modulus and UTS as the loading level of PMMA-g-NPs increases. While the sets of data shown are from single measurements, values of the tensile modulus given in the legend are based on measurements of five replicate samples. 78

Figure 4.1. DMA results show an increase in the Young's modulus of all FFF-printed parts containing copolymer additives compared to the unmodified PMMA. Moreover, the Young's modulus increases as the UPyMA composition increase from 1 mol% to 5 mol%. Values of the Young's modulus given in the legend are averages based on measurements of five replicate samples. 97

Figure 4.2. Multicomponent blends containing random copolymer additives having SCMHB UPy groups show increases in tensile modulus and ultimate tensile strength as the UPyMA content present in the copolymer additive increases up to 5 mol%. A representative trace from a series of replicate tests is shown for each copolymer additive, and the values of tensile modulus provided in the legend are based on measurements of five replicate samples. 98

Figure 4.3. Constant-strain temperature ramp measurements of PMMA-based samples containing SCMHB random copolymer additives produced by FFF as a function of the UPyMA content show that the (A) glass transition temperature, (B) storage

modulus, and (C) loss modulus increase with increasing UPyMA content. These enhancements are attributed to hydrogen bonding interactions between UPy groups, which serve as physical crosslinks. 103

Figure 4.4. Melt rheology measurements show that the storage modulus (A) and complex viscosity (B) of FFF-printed PMMA multicomponent blends are unaffected by the presence of p(MMA-r-UPyMA) additives. A reference temperature of 180 °C was used for time-temperature superposition. 107

Figure 5.1. A series of methacrylate-based monomers that provide access to various copolymer Tg values. Using random copolymer-grafts based on various methacrylate comonomers offers an innovative way to change the nature of the interfacial layer and potentially control interactions across the grafted-nanoparticle/PMMA matrix interface..... 117

Figure 5.2. Surface active polymer bottlebrushes can promote diffusion across interbead interfaces and increase the mechanical properties of FFF-printed parts..... 119

Figure A.1. Frequency shift factors (a_T) for FFF-printed PMMA nanocomposites. 146

Figure A.2. Small amplitude oscillatory shear measurements completed at 170 °C display a monotonic increase in the storage (A) and complex viscosity (B) as the loading level of Si NPs increases..... 147

Figure A.3. Uncorrected SAXS and WAXS results of FFF-printed PMMA nanocomposites with increasing loading levels of Si NPs. As noted in the *Article*, the WAXS signal ($0.85 < q$ ($Å^{-1}$) < 2.69) is the same for all samples..... 148

Figure B.1. ^1H NMR spectrum (500 MHz, 25 °C, $CDCl_3$) of the modified CTA; δ (ppm): 7.90 (d,2H,CH), 7.56 (t, 1H, CH), 4.59(t, 2H, CH_2), 3.62 (m, 2H, CH_2), 3.30 (t, 2H,

CH_2), 2.50-2.70 (m, 2H, CH_2), 1.95 (s, 3H, CH_3). Solvent residual peaks for chloroform and ethyl acetate (EA) are identified. 150

Figure B.2. GPC trace of PMMA graft chains cleaved (using HF) from 14 nm Si NPs measured using dRI detection. 151

Figure B.3. TGA traces reflect an increase in mass loss after bare Si NPs (black trace) are functionalized with the aminosilane (red trace) and after PMMA chains are grown from the NP surface (blue trace). 152

Figure B.4. WLF-type frequency shift factors, $a_{T,}$ generated using time-temperature superposition for PMMA nanocomposites containing PMMA-g-NPs. 153

Figure B.5. Uncorrected SAXS and WAXS data for FFF-printed PMMA nanocomposites containing PMMA-g-NPs at various loading levels. The red line represents the average trace. 154

Figure B.6. SAXS parameter plots for the (A) Porod Exponent, (B) Radius, (C) Hard Sphere Radius, and (D) volume fraction. 155

Figure B.7. Angular frequency-dependent storage modulus master curves show how the melt flow characteristics of FFF-printed PMMA parts are significantly affected by the addition of PMMA-g-NPs compared to bare (unfunctionalized) Si NPs at (A) 0.1 wt% and (B) 1.0 wt%. 156

Figure B.8. Angular frequency-dependent complex viscosity master curves reflect an increase in the melt flow properties of PMMA parts containing PMMA-g-NPs compared to bare Si NPs at equivalent loading levels, such as (A) 0.1 wt% and (B) 1.0 wt%. 157

Figure C.1. ^{1}H NMR spectrum (500 MHz, 25 °C, $CDCl_3$) of UPyMA monomer; δ (ppm): 12.97 (s,1H,NH), 11.95 (s, 1H, NH), 10.50 (s, 1H, NH), 6.18 (s, 1H, CH), 5.78 (s, 1H, CH), 5.54 (s, 1H, CH), 4.27 (s, 2H, CH_2), 3.58 (s, 2H, CH_2), 2.23 (s, 3H, CH_3), 1.93 (s, 3H, CH_3)..... 159

Figure C.2. Representative ^{1}H NMR spectrum (500 MHz, 25 °C, $CDCl_3$) of MMA-r-UPyMA copolymer (3 mol% UPyMA); δ (ppm): 12.96 (s, 1H, NH in UPyMA units), 11.94 (s, 1H, NH in UPyMA units), 10.49 (s, 1H, NH in UPyMA units), 5.78 (s, 1H, CH in UPyMA units), 3.59 (s, 3H, CH_3 in MMA units), 3.48 (s, 2H, CH_2 in UPyMA units), 0.8-2.3 (b, CH_2, CH_3 in MMA and UPyMA units). 160

Figure C.3. GPC traces of p(MMA-r-UPyMA) copolymer additives synthesized via free radical polymerization measured using dRI detection.. 161

Figure C.4. Frequency shift factors (a_t) generated by time-temperature superposition for PMMA multicomponent blends printed via FFF.. 162

Figure C.5. Storage and loss moduli master curves measured for the PMMA matrix polymer (A) and multicomponent blends with 1 wt.% random copolymer additive of different composition (B-E) display liquid-like behavior in the terminal regime, G”(ω) > G’(ω), regardless of the UPyMA content. This suggest that at temperatures exceeding the dissociation temperature (taken to be T = 80 °C) the physical crosslinks are, in essence, broken. 163

CHAPTER 1: INTRODUCTION

1.1 Interfaces in Polymeric Materials

As described in Jones and Richards' book, *Polymers at Surfaces and Interfaces*, the examination of any material generally starts with a thorough investigation of the material's bulk properties.[1] However, the stark reality is that all materials, even bulk phases, consist of myriad constituents that interact and assemble on a variety of length scales.[1] Therefore, being able to design and control the properties of interfaces is essential for expanding the known boundaries of material-property space. Polymer interfaces are found abundantly in nature and are utilized in various technologies such as paints, coatings, lubricants, and adhesives.[2,3] The versatility of polymeric materials, which originates in the diversity of monomer types, has significant impact on their surface properties. For instance, by changing the chemical and physical composition of polymers, surface properties such as wettability, friction, chemical resistivity, and lubricity can be effectively managed.[4] In addition to using synthetic polymer chemistry to tune or manipulate surface or interfacial properties, it is essential to assess physical properties and chemical functionality properties of polymer interfaces with advanced characterization techniques.[2] Structure-property relationships established from these types of research efforts allow one to understand and alter interfacial interactions, so that products with tailored functionalities and performance can be produced.[2]

Various methods can be used to modify the interface of polymeric materials including energetic treatments, chemical functionalization and additive migration, as seen in Figure 1.1. Energetic treatments, such as corona or plasma treatments, are demonstrated to enhance the wetting and adhesion of polymer surfaces. For example, corona treatments accelerate electrons into a polymer surface to fracture macromolecules at the surface.[5]

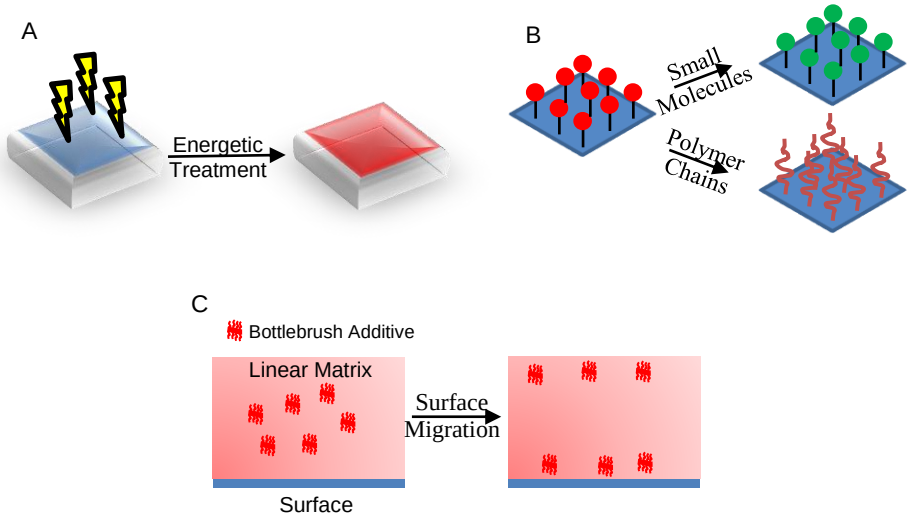

Figure 1.1. The surface properties of polymeric materials can be altered using myriad methods such as (A) energetic treatments, (B) chemical modification, and (C) surface active additives.

Next, the surface is subjected to ozone treatment which functionalizes the surface with carbonyl groups. The presence of carbonyl groups on the surface increases the hydrophilicity thus increasing both the wettability and adhesion compared to untreated polymer surfaces.[5]

In addition to using energetic treatments, recently researchers have demonstrated that the wettability and adhesion of surfaces can be modified by varying the chemical and physical composition of substrates functionalized with either small molecules or polymer chains. For instance and as demonstrated by Lokitz *et al.*, the wettability of poly(2-vinyl-4,4-dimethyl azlactone) (PVDMA) brushes attached to silicon substrates can be effectively managed by gradually immersing the polymer-modified substrate in a chloroform solution containing an alkyl-amine, 1-tetradecylamine (TDA), at 0.25 wt%.[6] Specifically, they

demonstrate that increasing the amount of TDA integrated in the brush layer of PVDMA-modified substrates increases the hydrophobicity of the polymer-decorated surface. For example, PVDMA-modified surfaces displayed a contact angle of 68°, while PVDMA surfaces allowed to react with TDA for 2 and 5 hours displayed a contact angle of 81° and 94°, respectively. Increases in the hydrophobicity of TDA modified PVDMA surfaces were attributed to presence of hydrophobic alkyl chains.

Lastly, research efforts have shown that surface-active additives can be used to tailor the interfacial properties of polymeric materials. As reported by Stein *et al.*, incorporating polymer bottlebrush (BB) additives, which are driven to interfaces via entropy, in a linear polymer matrix provides an alternative route to tune the wettability of polymer thin films.[7] Specifically, copolymer BBs containing poly(dimethylsiloxane) (PDMS) and poly(lactic acid) (PLA) side chains were incorporated in a linear PLA matrix. As compared to pure PLA thin films, which had a contact angle of 66°, increasing the mol% of PDMS in PDMS-co-PLA BBs increased the hydrophobicity of PLA films. For instance, increasing the mol% of PDMS in PDMS-co-PLA BBs from 26 mol% to 74 mol% is demonstrated to increase the contact angle from 95° to 107°, respectively. These results were attributed to the fact that copolymer BBs accumulate at the surface. Therefore, increasing the PDMS mol % increases the hydrophobic content present at the surface which manifest as an increase in the hydrophobicity of PLA thin films containing copolymer BBs.

While these reports highlight how modifications to polymer surfaces impact wetting and adhesion, they stress how altering surface, or interfacial, properties provides a novel route to control the performance of polymer materials. For instance and as demonstrated in Chapter 2, utilizing favorable, physical interactions across the

matrix/additive interface is demonstrated to enhance the properties of printed materials printed with polymer nanocomposite filament. As exhibited in Chapter 3, the number density and strength of interfacial interactions across the matrix/additive interface can be effectively managed by decorating nanoparticle surfaces with polymer chains which results in a significant increase in the mechanical properties as compared to parts containing bare (unfunctionalized) additives. Additionally, Chapter 4 investigates how non-bonding thermoresponsive interactions impact performance and processability of printed materials. In total, the scope of my dissertation work examines how manipulating interfacial interactions present in either polymer nanocomposites, or polymer blends, can be used to control assembly on the nanoscale and increase the properties of parts manufactured by 3D printing.

1.2 Motivation

Polymers are suitable for myriad applications due to their ease of processing and wide range of functionality and properties that can be conveyed by different types of monomers. Inspired by their thermoplastic behavior and processability, polymer-based Additive Manufacturing (AM) methods have generated interest as a viable way to rapidly and efficiently produce 3D-printed structures. AM works by coupling computer-aided modeling with various material processing techniques to manufacture end-stage parts of complex design in a layer-by-layer process. As compared to traditional manufacturing techniques that require the use of pre-designed molds, AM provides a novel route to fabricate prototype parts that can be assessed for performance prior to production. Fused Filament Fabrication (FFF), a subcategory of AM, creates polymer scaffolds by heating a

thermoplastic polymer filament to a semi-molten state and extruding it onto a position-controlled build platform to create a structure in a in layer-by-layer procedure, as displayed in Figure 1.2.

As compared to specimens fabricated by injection molding, parts created by FFF have inferior mechanical properties due to the presence of cavities between adjacent filaments, or beads, and poor interfacial adhesion between beads due to limited diffusion of polymer chains across interbead interfaces during the build process. These shortcomings are inherent to the FFF printing process, and they also lead to anisotropic properties. While researchers have demonstrated that the build direction and printing conditions can be optimized to lessen the anisotropy or maximize mechanical properties in a particular direction, these efforts do not address the fundamental issue: weak interbead interfaces are responsible for the poor performance of parts generated by FFF. To address this principal

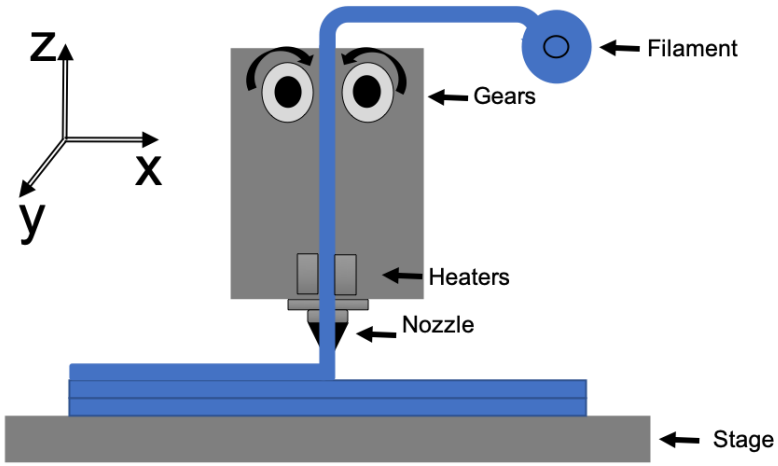

Figure 1.2. Illustration of how FFF can be used to generate polymeric scaffolds from polymer feedstock. FFF operates by heating a thermoplastic filament to a semi-molten state and extruding it in a layer-by-layer, or “bottom-up”, build process.

drawback, my research takes a fundamentally different approach. My dissertation research focuses on how polymer nanocomposites and "active", functional additives can be utilized to increase the mechanical properties of parts manufactured by FFF. Specifically, I examine how tailoring interfacial interactions in polymer nanocomposites and polymer blends can be used to direct the structure at the nanoscale and promote interdiffusion across printed layers. These are expected to increase the mechanical properties of parts made by the non-isothermal, nonequilibrium (vide infra) FFF process.

1.2.1 Polymer Nanocomposites

Compared to ceramics and metals, polymers have low mechanical properties, such as strength and strain, which limit their use as structural materials. To improve the performance of polymeric materials, research efforts have focused on utilizing polymer nanocomposites, which consist of a polymer matrix imbedded with inorganic additives having at least one dimension on the nanoscale. Polymer nanocomposites are known to exhibit superior mechanical properties compared to the native polymer matrix containing no additives. By blending the properties of hard and soft matter, polymer nanocomposites allow one to retain the processability associated with polymers while improving the material performance. However, it is well-known that the material properties of polymer nanocomposites depend significantly on interfacial interactions between the inorganic additive and polymer matrix. Favorable interactions generally lead to improvements in the material properties, but repulsive interactions typically lead to a decrease in the performance compared to that of the pure (unfilled) polymer. For instance, Brinson *et al.* reported significant increases in the mechanical properties of poly(methyl methacrylate)

when single-wall nanotubes (SWNTs) were incorporated. Specifically, they observed a 48% increase in the storage modulus when SWNTs were incorporated in a PMMA matrix at a 1 wt% loading. This increase was attributed to favorable interactions between the SWNTs and the PMMA matrix, which reduced the mobility of polymer chains in contact with the surface of the nanotubes and increased the stress-transmission from the matrix to the particle.[8] On the other hand, Schadler *et al.* reported a decrease in the glass transition temperature, T_g, Young's modulus and ultimate tensile strength for PMMA nanocomposites containing alumina nanoparticles.[9] They proposed that decreases in the thermomechanical properties were due to repulsive interactions between matrix chains and nanoparticle surfaces. Images acquired by transmission electron microscopy supported this claim, as they displayed voids around nanoparticles where polymer chains were expected to be present.

Although these reports provide insight into how the properties of polymer nanocomposites at equilibrium are governed by the interfacial interactions that occur on the nanoscale, only a few research efforts have been devoted to the use of polymer nanocomposites in the context of additive manufacturing, which is inherently a nonequilibrium situation. For instance Chen *et al.* investigated how the mechanical properties of ABS parts created via FFF were impacted by the incorporation of various inorganic additives, including silica, calcium carbonate, montomorillonite, and others, which were added at a 1 wt% loading level.[10] They observed that in all cases, regardless of the type of nanofiller, the tensile strength and flexural strength were increased as compared to virgin (unfilled) ABS parts. They suggested that the increase in performance was due either to the orientation and dispersity of the additives or to polymer-particle interactions.

On the other hand, a study by Roberson *et al.* determined that mechanical properties of ABS parts generated by FFF decreased significantly when nanofillers such as titanium oxide, strontium titanate, and alumina oxide were added at a 5 wt% loading level (relative to parts created with pure ABS).[11] Decreases in the material properties with all additives were attributed to the presence of voids within the structure and agglomeration of nanoparticles.

In total, these reports clearly demonstrate that the mechanical properties of polymeric materials modified with nanofillers depend on the interfacial interactions at the nanofiller/ matrix interface. These studies proved that interfacial interactions affect not only the spatial distribution of the nanoparticles within the matrix, but also control the efficiency of stress-transfer from the polymer matrix to the nanoparticle. Therefore, the ability to control or manipulate interactions across internal interfaces may provide a useful route to improve the macroscopic properties of parts created by AM methods such as FFF. In particular, designs and methods that promote particle/matrix interactions and enhance diffusion across interbead interfaces may be especially effective.

1.2.2 Polymer Grafted Nanocomposites

While it is well-known that the material properties of polymer nanocomposites depend on the nanoscale organization of nanoparticles within the polymer matrix, controlling the spatial distribution of bare (unfunctionalized) nanoparticles is exceedingly difficult due to strong van der Waals interactions between particles.[12–14] As a result, various strategies have been used to control the nanoscale organization of nanoparticles over multiple length scales. For instance, recent research efforts have examined how varying

the shape of the nanofiller, applying magnetic fields, or utilizing electrostatic repulsion can be used to alter the organization of nanoparticles.[15] In addition to these methods, modifying the nanoparticle surface with ligands or polymer grafts has proven to be an effective way to control the interfacial interactions between nanoparticles, allowing hierarchal structures to be generated in the nanocomposite.[12,16–18]

Advances in polymer synthesis have allowed researchers to systematically investigate how varying the chemical composition, molecular weight, dispersity, and grafting density of tethered chains that create polymer grafted nanoparticles impacts the resultant nanostructure.[12] While all of these molecular parameters affect the spatial distribution of polymer grafted nanoparticles in a symmetric system – a system in which homopolymer chains grafted to the nanoparticle surface are chemically identical to matrix chains – recent efforts suggest that the grafting density and ratio of the graft to matrix molecular weight are the most important parameters for controlling the state of nanoparticles.[12] For instance and as described by Jayaraman, at high grafting densities the graft chains extend due to crowding and adopt a brush conformation. When these polymer-grafted particles are placed in a chemically similar matrix (athermal system) they aggregate if the matrix chain molecular weight is higher than that of the graft, but disperse if the matrix chain molecular weight is lower than that of the grafted chains, as seen in Figure 1.3.[12,17] This is because when the molecular weight of the matrix chains are smaller than the grafted chains, the conformational entropy penalty is smaller than the gain in the entropy of mixing.[12,17] Therefore, entropic mixing favors a dispersed state of polymer grafted nanoparticles. However, in the opposite case when the matrix MW > graft MW, the conformational entropic penalty for rearrangement of the grafted chains is higher than

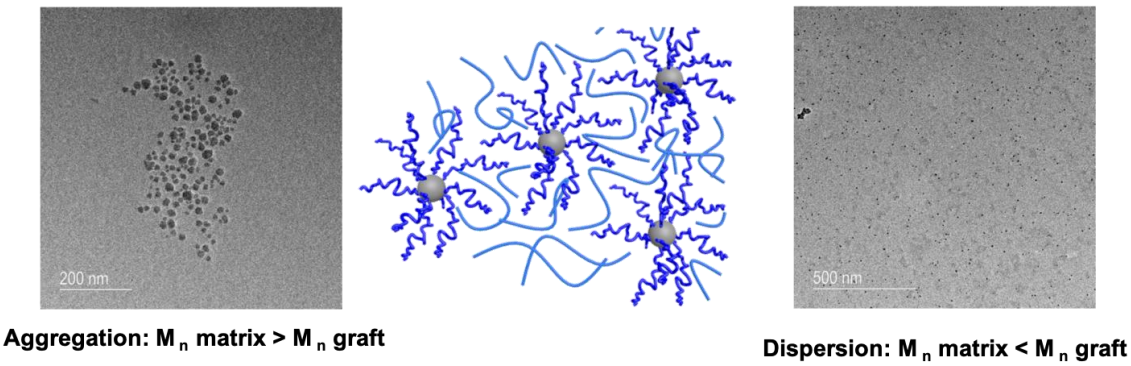

Figure 1.3. The nanoscale organization of densely-grafted nanoparticles in a symmetric, athermal, system is controlled by entropic interactions. Specifically, when the matrix chain molecular weight is larger than the graft chain molecular weight particle clusters are observed, while dispersed particles are observed when the matrix chain molecular weight is smaller than the graft chain molecular weight.

the entropy gained by mixing. At low grafting densities, the grafted polymers do not completely cover the NP surface. In this case, the polymer-grafted NP has character like an amphiphile, and the organization of nanoparticles is controlled by interactions between the exposed surface of nanoparticles and the matrix and grafted chains.[12] Recent research by Kumar *et al.* have shown that polymer grafted nanoparticles having various grafting densities can arrange in a variety of nanostructures that include connected sheets, strings, aggregates and well dispersed.[19,20] These reports suggest that the spatial distribution of the grafted particles relies heavily on the molecular weight of the graft and matrix polymers and also the grafting density.

In addition to altering interfacial interactions to control the spatial distribution of polymer grafted nanoparticles, recent efforts have demonstrated that polymer-grafted

nanomaterials provide an alternative way to increase the performance of the resulting nanocomposites. For example Friedrich *et al.* determined that as compared to polypropylene nanocomposites containing unfunctionalized silica nanoparticles, polypropylene nanocomposites having polystyrene grafted nanoparticles displayed a 17 % increase in the tensile strength at a 5 wt% loading level. This increase was attributed to an increase in the number density of interactions between the polymer matrix and polymer graft. Specifically, they suggested that the increase in the number density of polymer/particle interactions were conveyed through interdiffusion and entanglements between the graft and matrix chains.

These works are highlighted because they demonstrate that both the spatial distribution and nanocomposite properties can be manipulated by polymer grafted nanoparticles. More importantly, these examples stress the importance of interfacial interactions. Thus, strategies that tune the interfacial interactions can be used to manipulate both the nanoscale structure and macroscopic material properties.

1.2.3 Supramolecular Blends

Advances in the field of supramolecular chemistry have resulted in the development of novel classes of macromolecules that utilize non-bonded interactions to direct molecular assembly. As described by Meijer *et al.*, supramolecular assembly of polymers can be classified by the physical nature of the interaction used to dictate formation of the resultant supramolecular network.[21] With this classification scheme, supramolecular assembly of polymers are categorized according to the major types of interactions: π-π interactions, hydrophobic interactions, metal-ligand binding, and hydrogen bonding interactions.[21]

Among these, strategies to generate responsive polymeric materials utilizing complementary hydrogen bonding interactions have received interest due to their thermosensitive nature.[22] Specifically, incorporating groups that direct assembly via complementary hydrogen bonding interactions in macromolecules has resulted in the development of novel thermoresponsive polymers that adopt and retain their supramolecular structure at use temperatures, but display low viscosities during processing due to the thermoreversible dissociation of hydrogen bonding interactions that occur at high (melt processing) temperatures.[23–27]

For instance and as reported by Meijer *et al.*, functionalizing the hydroxyl groups of telechelic poly(propylene-block-ethylene oxide) oligomers with a self-complementary multiple hydrogen bonding group, 2-ureido-4[1*H*]-pyrimidone (UPy), leads to self-assembly that significantly impacts the melt flow characteristics. Specifically, Meijer *et al.* compared the melt flow properties of poly(propylene-block-ethylene oxide) oligomers covalently crosslinked through their hydroxyl end groups to the melt flow characteristics of poly(propylene-block-ethylene oxide) oligomers modified with UPy groups, which participate in physical crosslinks, as seen in Figure 1.4.[28] They determined that copolymers modified with UPy end groups displayed a substantially higher plateau modulus and exhibited a rubbery plateau in the storage modulus compared to covalently crosslinked analogues. Both of these results, an increase in the plateau modulus and the formation of a rubbery plateau in the storage modulus for UPy-modified oligomers, were attributed to the self-dimerization of UPy end groups that form an interconnected and thermodynamically stable network at use temperatures. Whereas poly(propylene-block-ethylene oxide) oligomers covalently crosslinked through hydroxyl groups represent a kinetically

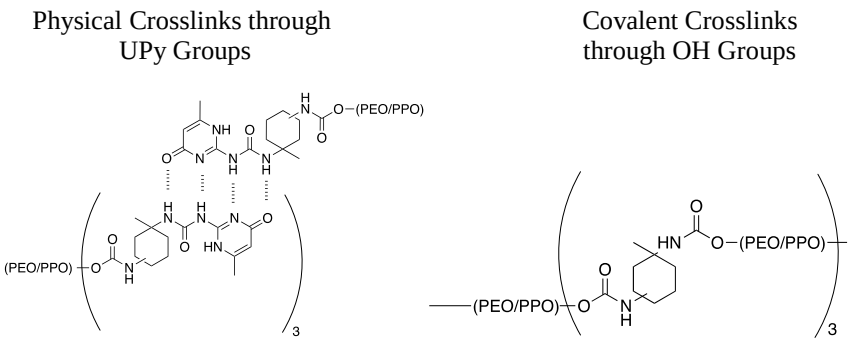

Figure 1.4. Functionalizing telechelic chain ends of poly(propylene-block-ethylene oxide) oligomers with UPy groups that participate in thermoresponsive, physical crosslinks is demonstrated to result in a denser, thermodynamically stable network compared to oligomers covalently crosslinked through hydroxyl groups.

controlled system.[21,28] In addition to investigating how self-complementary hydrogen bonding interactions installed at chain ends impact the properties of oligomers, others have investigated how hydrogen bonding groups present as pendent groups on the repeating units affect the resultant thermal and mechanical properties of macromolecules. For example, Long *et al.* examined how the thermal properties of poly(butyl acrylate) polymers were impacted as the content of a hydrogen bonding comonomer increased from 0 to 10 mol%. To accomplish this, they synthesized four random butyl acrylate copolymers made from butyl acrylate and a hydrogen bonding comonomer, 2-ureido-4[1*H*]-pyrimidone methacrylate (UPyMA) having different molar compositions with respect to the UPyMA comonomer (1 mol%, 3 mol%, 5 mol%, and 10 mol%), as seen in Figure 1.5. They determined that increasing the UPyMA comonomer content resulted in a linear increase the T_g. Increases in the glass transition temperature were attributed to the self-dimerization of UPy groups, which decreases free volume and manifest as an increase in T_g.

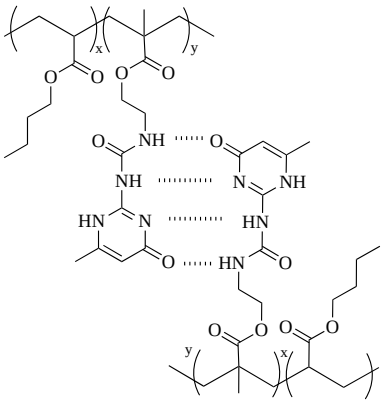

Figure 1.5. Incorporating UPyMA comonomers into the backbone of poly(butyl acrylate-co-UPyMA) random copolymers is demonstrated to increase the melt flow characteristics at temperatures below the dissociation temperature of UPy groups, while no deleterious impact is observed at temperatures above the dissociation temperature.

Additionally, rheometric studies were completed to investigate how increasing the UPyMA comonomer content affected the melt flow characteristics. They determined that poly(butyl acrylate-co-UPyMA) random copolymers containing UPyMA at 3 mol% increased the melt viscosity by an order of a magnitude compared to homopolymers of poly(butyl acrylate) having analogous molecular weight. Further increases in UPyMA comonomer content resulted in higher melt viscosities. These results, increases in the melt viscosity as the UPyMA comonomer content increases, were attributed to physical crosslinks between UPy groups that create an interconnected, physically crosslinked network. However, at temperatures above the dissociation temperature (80 °C) the melt viscosities for all poly(butyl acrylate-co-UPyMA) copolymers were nearly identical to that of the poly(butyl acrylate) homopolymer, thus highlighting the thermoreversible nature of the hydrogen bonding groups.

Moreover, Long *et al.* investigated how the mechanical properties of poly(2-ethylhexyl methacrylate-co-UPyMA) random copolymers were affected as the UPyMA comonomer content was increased.[23] Results from tensile testing indicated that increasing the UPyMA commoner content from 0 mol% to 3 mol% changed the deformation pattern from a viscoelastic solid (observed for homopolymers) to a brittle glass. Additionally, increasing the UPyMA content up to 7 mol% resulted in a ten-fold increase in the modulus of these copolymers. They attributed both the increase in the modulus and the change in the deformation pattern to physical crosslinks that formed between the self-complementary hydrogen bonding groups.[23]

These reports highlight how non-bonded interactions can be used to change the thermal and mechanical properties of polymeric materials. Specifically, these research efforts highlight how self-complementary hydrogen bonding groups can be used to create an interconnected, physically crosslinked network that enhances the thermal and mechanical properties at use temperatures but dissociates at elevated temperatures used for melt processing. These studies exemplify how the thermomechanical properties of polymers can be effectively managed by tailoring the number density of hydrogen bonding interactions.

1.3 Synthesis and Characterization of Nanoscopic Additives

In my dissertation research, two different free radical polymerization strategies were used to generate hydrogen bonding copolymers and polymer-decorated silica nanoparticles. Specifically, uncontrolled free radical polymerization and controlled free radical polymerization techniques were used. As stated by Matyjaszewski *et al.*, one of the

main advantages of free radical polymerization is facile statistical copolymerization, especially when monomers having equivalent polarities and similar structures are copolymerized.[29] As described in Chapter 4, uncontrolled free radical polymerizations were used to synthesize random copolymer additives comprised of methyl methacrylate and UPyMA. Uncontrolled free radical polymerizations have three distinct mechanistic steps: initiation, propagation and termination, as seen in Figure 1.6.

In the initiation step, radical species are generated, often by thermal decomposition, or by electrochemical or photochemical reactions. In the propagation step, monomer adds to the radical species in a chain growth process. This propagating radical may continue to add monomeric repeat units, or it may participate in reactions that terminate the kinetic chain. These terminating side reactions may include chain transfer reactions with either solvent molecules, monomer units, or polymer chains. Another termination mechanism that kills the propagating chain is biomolecular termination, which may proceed by either a disproportion or combination mechanism. Long *et al.* successfully used uncontrolled free

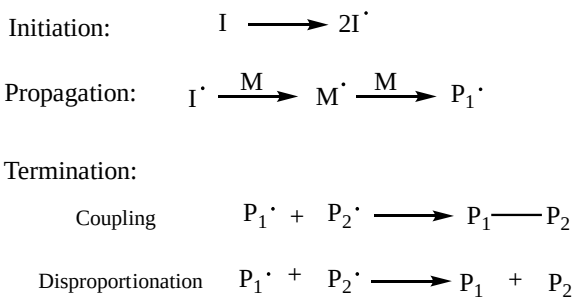

Figure 1.6. Uncontrolled free radical polymerizations, which are used to create self-complementary, multiple hydrogen bonding additives in Chapter 4, have three main mechanistic steps including: Initiation, Propagation, and Termination.

radical polymerizations to randomly incorporate UPyMA comonomers in the backbone of methacrylate based copolymers.[23,24,27] Therefore, self-complementary hydrogen bonding random copolymers described in Chapter 4 were synthesized using this method.

Polymer-grafted nanoparticles, which were studied and are described in Chapter 3, can be synthesized by two main synthetic strategies that are frequently known as "grafting to" and "grafting from". In grafting to, pre-made polymer chains functionalized with a reactive end-group are attached through complementary groups on the surface. Generally, grafting to is used when one desires to purify and characterize polymer chains prior to attachment to the (nanoparticle) surface. In grafting from, polymer chains are grown from initiation sites that are either attached or adsorbed to the particle surface. As compared to grafting to, grafting from achieves higher grafting densities because steric crowding inherent to attaching polymer chains to the nanoparticle surface are avoided. In either method, living (controlled) free-radical polymerizations are often used to make the polymers. Specific variants include atom transfer radical polymerization (ATRP), nitroxide-mediated polymerization (NMP) or Reversible Addition Fragmentation Chain Transfer (RAFT) polymerization.

Among these, RAFT polymerization distinguishes itself due to its ability to control the molecular weight of polymer chains and its ability to produce polymers having a narrow dispersity (Đ <1.2). Furthermore, RAFT polymerization is tolerant of oxygen and water, and avoids contamination from a metal catalyst. As compared to ATRP, which uses a metal-ligand complex to establish an equilibrium between growing "active" chains and dormant "inactive" chains, RAFT utilizes a chain transfer agent (CTA) that forms a fast, dynamic equilibrium between the propagating species and the dormant (stabilized radical)

CTA. This fast, dynamic equilibrium allows for propagating chains to grow at the same rate, which results in a narrow molecular weight distribution, and provides control over the molecular weight of the polymer chains, as seen in Figure 1.7.

While most CTAs are comprised of either a trithiocarbonate or dithioester group, CTAs also contain two functionalities, "R" and "Z", that are essential for preserving the living character. Specifically and as seen in Figure 1.7, the R group must be able to homolytic cleave and reinitiate the polymerization, while the Z group controls the fragmentation and addition rate and stabilizes the intermediate radical. Myriad CTAs have been synthesized with diverse "R" and "Z" group functionalizes which allows RAFT polymerizations to be used with a wide range of monomers. Furthermore, the number-average molecular weight (M_n) of chains polymerized via RAFT can be controlled by tailoring the ratio of monomer concentration ([M]) to RAFT CTA concentration ([CTA]) as seen in Equation 1.1:

$$M_n\ (theo) = \frac{[M]}{[RAFT]} * M_o \qquad (1.1)$$

As denoted by Odian *et al.*, this equation is based on the assumption that both the CTA and monomer are fully consumed during the reaction and that the number of initiator-derived

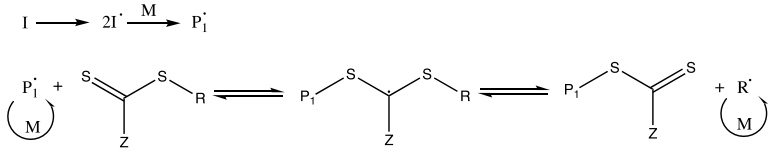

Figure 1.7. RAFT polymerization exhibits a fast, dynamic equilibrium due to degenerative fragmentation-chain transfer that allows control over the polymerization, resulting in narrow dispersity control over molecular weight of polymer chains.

chains is negligible. (M_o denotes the molecular weight of the monomeric repeat unit.) As demonstrated in Chapter 3 of my dissertation, RAFT polymerization is used to grow polymer chains that have a narrow dispersity and controlled molecular weights from the surface of silica nanoparticles (Si NPs). Specifically, this was accomplished by functionalizing the surface of Si NPs with an amino-silane that was subsequently reacted with a CTA, as seen in Figure 1.8. Those CTA-modified nanoparticles were used to synthesize poly(methyl methacrylate)-grafted Si NPs (PMMA-g-NPs).

The physical properties of polymer-grafted nanoparticles and random copolymer additives are characterized using standard techniques. Specifically, ^{1}H nuclear magnetic resonance (NMR) spectroscopy is used to determine the relative comonomer content in random copolymer additives. Additionally, the molecular weight and dispersity of polymer grafts and random copolymers are determined using gel-permeation chromatography (GPC). Thermal gravimetric analysis (TGA) is used to determine the grafting density (chains/area) of chains attached to Si NPs. Furthermore, thermal transitions, specifically

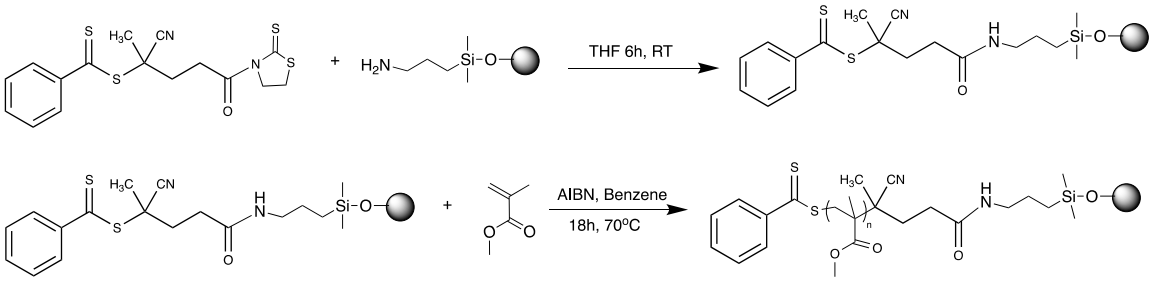

Figure 1.8. Amino-silane functionalized nanoparticles are reacted with a dithioester CTA to generate CTA-functionalized nanoparticles that are then used to grow polymer chains from the surface of Si NPs.

the glass transition temperature, T_g, of random copolymers are determined via dynamic scanning calorimetry (DSC).

1.4 Characterization and Thermomechanical Properties

As mentioned throughout Section 1.2, tailoring the polymer design and nature of interactions that operate at the nanoscale to enhance the macroscopic properties of polymeric materials is the principal objective of my dissertation work. Therefore, it is imperative to assess how nanoscopic additives impact the macroscopic properties of FFF-printed parts. To accomplish this, numerous techniques were utilized including tensile tests, dynamic mechanical analysis (DMA), and rheology. Of these, DMA and rheology will be discussed; however, because these measurement techniques are extensive, the purpose of this section is to provide context regarding the type of measurements completed and what material properties are examined.

DMA is used to examine thermal transitions and the thermomechanical properties of polymeric materials. In general, DMA applies a force in an oscillatory fashion and measures the material's response, as depicted in Figure 1.9. By measuring the response and expressing it in terms of a change in amplitude or phase shift, myriad thermomechanical properties are determined. In my dissertation work, two types of DMA measurements were used. First, dynamic strain sweeps were completed to identify the linear viscoelastic region (LVR) and to measure the Young's modulus of FFF-printed polymer structures. This testing method examines a materials response to increasing deformation. Specifically, DMA strain-sweeps increase the amplitude, or strain, while keeping the frequency and temperature constant as seen in Figure 1.10. From this measurement one can determine

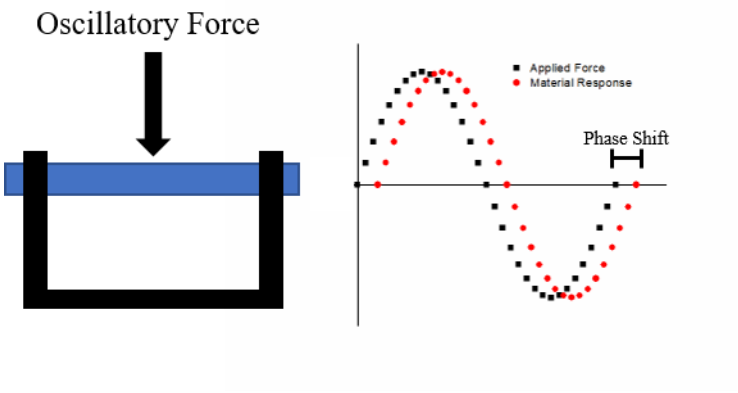

Figure 1.9. DMA works by applying an oscillating force to a sample and measuring the sinusoidal response. By observing differences in the phase shift and/or amplitude one can investigate the thermomechanical properties of polymeric materials.

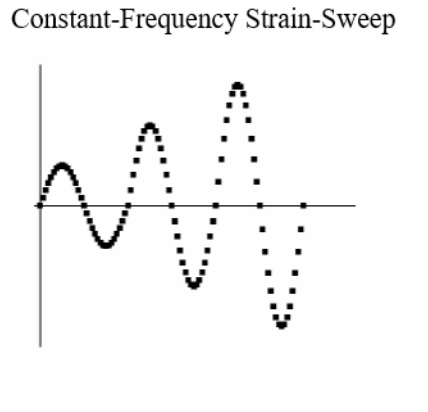

Figure 1.10. DMA strain-sweep (amplitude-sweep) measurements are used to determine both the linear viscoelastic region and the Young's Modulus of printed parts.

both the LVR and the Young's modulus of the polymer sample by plotting either the storage modulus versus strain or stress versus strain. Identifying the LVR is imperative for further DMA experiments. For example, measurements that alter frequency or temperature must be completed in the LVR so that the applied sinusoidal force results in a sinusoidal response (i.e. modulus is independent of strain). This allows one to investigate changes in the phase shift. Specifically and as exhibited in my dissertation work, DMA constant-strain temperature ramp measurements are completed in the LVR. During this testing method, both the frequency and amplitude (strain) of the sinusoidal force are held constant while the temperature is ramped. By examining how the phase shift between the applied force and material's response is impacted during a temperature ramp, one can discern the glass transition temperature and examine how the storage and loss moduli of FFF-printed parts are affected by temperature.

Rheology, or the study of deformation and flow of matter, is primarily used to investigate the behavior of complex fluids, or materials that do not follow Newton's law of viscosity or Hooke's law of elasticity.[30–32] Because the melt characteristics of polymers influence the fluid and heat transfer properties during processing, and dictate the performance of the polymer at use temperatures,[33] it is imperative to investigate the rheological response of FFF-printed materials containing additives. Therefore, I have used small-amplitude oscillatory shear (SAOS) measurements as part of my studies of polymer nanocomposites and multicomponent polymer blends, which provide perspective as to how nanoscopic additives impact the relaxation behavior of the matrix chains. In a similar fashion to DMA and as seen in Figure 1.9, SAOS measurements work by perturbing a material with an oscillating shear force and measuring the material's response. In my

dissertation work, SAOS frequency sweeps were completed at a variety of temperatures using a fixed strain. By measuring the phase shift between the applied force and material response, the storage and loss moduli (G', G") and complex viscosity (|η*|) of FFF-printed parts could be determined. Additionally, by using time-temperature superposition master curves were constructed, which allow one to examine the relaxation behavior of matrix chains over a broad range of frequencies. By comparing master curves of unfilled (pure) FFF-printed parts to those containing nanoscopic additives, I investigate how the addition of nanoscopic additives affect the relaxation processes of matrix chains.

In my dissertation research, I couple melt rheology measurements, which describe the flow characteristics and deformation behavior of polymers, with assessments obtained from DMA and tensile testing. By combining these results, I examine how altering interactions across the polymer/additive interfaces controls organization on the nanoscale and affects the performance of FFF-printed materials.

1.5 Research Objectives

The main focus of my dissertation work is to examine how interfacial interactions that function at the nanoscale can be effectively used to augment the macroscopic properties of polymer nanocomposites and multicomponent blends. The structure-property relationships I develop in my work provide proof-of-concept that the thermomechanical properties of polymeric structures created by FFF can be manipulated through those interactions, which provides a novel route to address key limitations of polymeric parts created via additive manufacturing. Specifically, the goals of my research are to:

1. Investigate how increasing the number density of interfacial interactions between bare (unfunctionalized) silica nanoparticles and PMMA matrix chains impacts the thermomechanical properties of PMMA nanocomposites;
2. Examine how tailoring interactions across the polymer matrix/particle interface, accomplished by decorating nanoparticle surfaces with polymer chains, impacts both the organization on the nanoscale and the thermomechanical properties of FFF-printed nanocomposites; and
3. Develop design-structure-property relationships that describe how self-complementary, multiple hydrogen bonding interactions, conveyed through pendant groups present along the backbone of random copolymer additives affect the melt flow characteristics of the multicomponent blends and mechanical properties of FFF-printed parts.

Chapter 2 presents a fundamental study describing how the incorporation of bare Si NPs into PMMA nanocomposites affects properties and performance of parts fabricated by FFF. In this effort, Si NPs were mechanically mixed with PMMA beads and extruded to generate nanocomposite filaments that were used to create PMMA nanocomposites by FFF. By keeping the processing conditions, type of inorganic additive, and polymer matrix constant, I systematically examined how increasing the number density of interactions between the Si NP surface and the PMMA matrix chains, which increase as the loading level of Si NPs increases, affects the performance of FFF-printed nanocomposites. Improvements in mechanical properties appear to be due to attractive hydrogen bonding interactions between hydroxyl groups on the Si NP surface and carbonyl groups present in the PMMA backbone.

Motivated by this work, the studies presented in Chapter 3 describe how grafting chains onto Si NPs to create polymer-grafted nanocomposites affects properties and performance of FFF-printed samples. For this, PMMA chains were end-anchored to the surface of Si NPs, incorporated in PMMA to make filaments (at comparable loading levels to the system described in Chapter 2), and printed. Macroscopic assessments indicate the performance of parts containing PMMA-g-NPs markedly surpass those containing similar loadings levels of bare Si NPs, with the average Young's modulus of parts containing the lowest loading level of PMMA-g-NPs exceeding the value obtained at the highest loading level with bare Si NPs. Rheology measurements suggest that grafting polymer chains to Si NP surfaces having the same chemical identity as the polymer matrix promotes interdiffusion and entanglements across the graft/matrix interface. Analogous to patterns of behavior observed in "bare" systems, increasing the number of interactions between the matrix and PMMA-g-NP effectively improves stress-transfer in the nanocomposite. This work provides proof-of-concept that tailoring interactions at interfaces through graft copolymer design can be exploited to control the properties of polymer nanocomposites printed via FFF.

In addition to using polymer nanocomposites, Chapter 4 describes how increasing the content of a self-complementary multiple hydrogen bonding commoner present in random copolymer additives impacts thermomechanical properties of FFF-printed parts. Specifically, random copolymers additives comprised of methyl methacrylate and 2-ureido-4-pyrimidone methacrylate (UPyMA) were incorporated into printed parts at a 1 wt% loading level. The UPyMA comonomer was chosen due to its thermoreversible, self-complementary quadruple hydrogen bonding interactions offered through UPy groups. The

results of DMA and tensile testing show remarkable improvements in mechanical properties: For example, more than a 50% increase was observed in the Young's modulus, while the tensile modulus increased by ~100% as the UPyMA comonomer content increases up to 5 mol%. The thermoreversible nature of UPy hydrogen bonding interactions allows facile processing, but strong dimerization strengthens printed parts at use temperatures.

Finally, Chapter 5 provides a brief summary of the main findings of my dissertation research and also highlights the importance with regard to the fields of polymer science and additive manufacturing. This chapter concludes with an outlook on how fundamental research efforts expounded upon here provide a starting point for future investigations.

CHAPTER 2: INTERFACIAL INTERACTIONS IN PMMA/SILICA NANOCOMPOSITES ENHANCE THE PERFORMANCE OF PARTS CREATED BY FUSED FILAMENT FABRICATION

This chapter describes the work published in Polymer, 157, (2018), 87-94. I manufactured all of the printed parts in this work and completed all of the thermomechanical characterizations. Coauthors include Adeline H. Mah and Prof. Gila E. Stein, who performed and fit SAXS and WAXS measurements, and Steven Patterson, James A Bergman, and Jamie M. Messman, who provided initial insight and training for rheology and tensile measurements. Additional coauthors include Deanna L. Pickel, who provided helpful suggestions regarding filament and specimen fabrication, and Prof. S. Michael Kilbey II, who advised this work.

2.1 Abstract

As an additive manufacturing method, Fused Filament Fabrication (FFF) is conceptually attractive due to its agility and adaptability. However, FFF-printed parts exhibit poor mechanical properties as compared to parts manufactured by traditional methods. Here, the addition of silica nanoparticles (Si NPs) into FFF-printed parts is demonstrated to markedly improve a variety of thermomechanical properties. Specifically, dynamic mechanical analysis (DMA) and tensile tests indicate that the glass transition temperature, Young's modulus, elongation at break, ultimate tensile strength, and storage and loss moduli all increase with the Si NP loading. Small-angle X-ray scattering (SAXS) and scanning electron microscopy (SEM) demonstrate similar hierarchical structures in all FFF-printed nanocomposites, which suggests that improvements in material properties with Si NP loading are likely due to an increasing number of hydrogen bonding interactions between PMMA matrix chains and hydroxyl groups on the Si NP surface. The potential of nanocomposite filaments to increase the thermomechanical properties of FFF-printed

specimens provides a facile route to overcome limitations in FFF-printed part strength by combining the properties of hard and soft matter.

2.2 Introduction

Additive Manufacturing (AM), colloquially referred to as 3D printing, combines computer modeling with manufacturing technologies to produce prototypes and early stage models that facilitate evaluation of design, fit, and performance prior to full-scale manufacturing.[34–37] AM has been used to create and test parts for automobiles, airplanes, and microelectromechanical systems, and to produce anti-biofouling inserts for marine vessels, tissue scaffolds for biomedical engineering, as well as prototypes for defense applications.[38–43] Fused Filament Fabrication (FFF) is one of the most widely used AM techniques, and it is used to produce functional end-stage parts of complex design and shape from polymeric feedstocks without the need for further assembly.[44,45] This is a result of the build process in which a solid polymer filament is heated to a semi-molten state and subsequently extruded and deposited in a layer-by-layer (bottom-up) fashion until the final product is created.[46–48]

Although FFF has considerable potential as a production platform compared to traditional manufacturing techniques, parts created by FFF have significantly lower strength due to the formation of voids and poor adhesion between successive layers and adjacent filaments (or "beads").[45] To address these limitations, many researchers have investigated how printing parameters, build orientation, and post-processing treatments can be manipulated in order to optimize the mechanical properties of printed materials.[42,44,48–51] For example, Bagsik *et al.* examined how changing the build direction affects the

mechanical properties of FFF-printed specimens made of a polyetherimide (Ultem*9085™). They changed directionality of the build, printing tensile samples on their edge, flat against the build plate, or vertically, which they denoted as X, Y, and Z-directions, respectively. They reported that tensile specimens printed in the Y-direction contained voids between raster beads that led to voids within the cross-section, while parts printed in the X- and Z-directions contained voids between the contour and raster beads. The location and directionality of voids between adjacent filaments creates a strong relationship between break patterns and mechanical properties of FFF-printed specimens and the build direction: specimens printed in the X-direction had the highest ultimate tensile strength and elongation at break while specimens printed in the Z-direction had the highest compressive strength.[44]

Although this report by Bagsik *et al*. is one of many highlighting how the build conditions can be effectively managed to improve the macroscopic performance of FFF-printed parts, the mechanical properties of these parts are still inferior to their injection molded counterpart. This is commonly attributed to weak inter-bead adhesion that arises because of limited chain diffusion across bead-bead interfaces.[52,53] The addition of fillers into polymer matrices is generally regarded as a useful way to enhance properties. Initial efforts focused on blending micron-sized additives with polymers to increase thermomechanical properties, such as the T_g and modulus.[54,9] However, with micron-sized fillers, it is generally appreciated that high loadings are required before material properties change.[9] On the other hand, creating a polymer nanocomposite (PNC) by incorporating nanometer sized particles, which have significantly higher surface-to-volume ratios, leads to increases in material properties at lower loading levels. For example, in their studies of

the mechanical properties of polypropylene Sumita *et al.* reported a 1.3-fold increase in the yield stress and a 1.7-fold increase in Young's modulus when nanoparticles were incorporated as compared to microparticles.[55] Similarly, Petrovic and Zhang compared the performance of elastomeric polyurethanes filled with silica nanoparticles and micron-sized silica spheres (12 nm and 1.4 μm, respectively). Relative to unfilled samples, they reported a 6-fold increase in the elongation at break and a 3-fold increase in the tensile strength when silica nanoparticles were used, but only a 2-fold increase in elongation at break and a 1.7-fold increase in the tensile strength when the micron-sized silica particles were used.[56] Due to enhancements in thermomechanical properties and the ability to combine properties of dissimilar materials, PNCs have widespread applicability across several technological applications, including structural materials, gas separation membranes, energy conversion and storage, and microelectronics.[13,15,17,57–60]

While the incorporation of nanoscale inorganic additives into polymeric materials by melt blending or solution-based processing has received considerable attention, only a few studies have focused on incorporating nanoparticles into polymer matrices in the context of additive manufacturing. Wiria *et al*. examined how imbedding hydroxyapatite (HA) sintered powder into poly-ε-caprolactone scaffolds manufactured by selective laser sintering (SLS) impacts the resulting mechanical properties. They showed that as the loading level of HA was increased from 10 wt% to 30 wt%, the Young's modulus and yield stress increase by a factor of 1.5.[61] Similarly, Chung *et al.* investigated how the amount of Si NPs incorporated into Nylon-11 affected the mechanical properties of nanocomposite specimens fabricated by SLS. They determined that the tensile modulus increased from 620 MPa to 720 MPa as the loading level increased from 4 wt% to 10 wt% and showed

that the compressive modulus increased from 1175 MPa to 1425 MPa as the loading level was increased from 2 wt% to 10 wt%.[62] Lastly, Chen *et al.* investigated how the mechanical properties and thermal properties of ABS nanocomposite parts printed by FFF were affected by the presence of different inorganic additives. They incorporated calcium carbonate, montmorillonite clay, multiwalled carbon nanotubes, and silica, each at a 1% loading by mass, and printed test specimens from the corresponding nanocomposite filament. They observed enhancements – more than 10% but less than 30% in all cases – in the mechanical properties of all FFF-printed specimens regardless of the inorganic additive, but none of the FFF-printed nanocomposites exhibited material properties comparable to parts made by injection molding of virgin ABS.[10] It is also worth noting that a recent set of studies by Roberson and Chen suggest that the mechanical properties of FFF-printed nanocomposite parts made with ABS as the matrix may be improved or diminished, depending on the type of inorganic additive incorporated into the printed specimen.[10,11]

Drawing inspiration from these reports, with this work I sought to provide a fundamental understanding describing how the addition of inorganic nanoparticles provides material reinforcement in printed parts made by the non-isothermal, non-equilibrium (*vide infra*) FFF process. To achieve this, I systematically examine how increasing the amount of silica nanoparticles in poly(methyl methacrylate) affects mechanical and thermal properties of polymer nanocomposites specimens created by FFF and assess their dispersion in nanocomposite printed specimens. The combination of assessments of macroscale performance, rheology, and nanoscopic structure points to particle-polymer interactions, which increase as the loading level of the additive increases,

as governing the response to deformation, thereby providing a basis for understanding for the reinforcement effect of FFF-printed nanocomposites.

2.3 Experimental Methods

Filament Preparation. Prior to filament extrusion, atactic poly(methyl methacrylate) beads having a nominal molecular weight, MW = 100,000 g/mol (Polysciences Inc.) were dried by heating at 100 °C under vacuum for 12 hours to remove any residual moisture. Silica nanoparticles (Si NPs) (diameter of 14 ± 4 nm) dispersed in 2-butanone (supplied as a gift from Nissan Chemical) were isolated by precipitation into chilled hexanes followed by centrifugation at 3500 RPM for 15 minutes. The supernatant was decanted, and the nanoparticles were collected and dried overnight at 100 °C under vacuum. A Discovery Series thermogravimetric analyzer coupled with a mass spectrometer (TGA-MS) was used to determine if residual solvent and moisture were removed from Si NPs prior to their incorporation into PMMA filaments. In a typical TGA-MS procedure, vacuum oven-dried Si NPs (0.5-2.0 mg in a 100 μL high temperature platinum pan) were subjected to a temperature ramp from 30 to 800 °C at a rate of 20 °C/min. Si NPs were considered dry and used for filament preparation when the mass loss was ≤ 3.0%. All other materials were used as received unless stated otherwise.

To create nanocomposite filaments, Si NPs were combined with PMMA beads at predetermined loading levels that are based on the mass of silica. After physically mixing with a stirring rod, the mixture was added to a Magic Bullet® 250 W blender and pulsed for five to ten cycles of one to three seconds each until the mixture appeared homogenous. This mixture was then added to the hopper of a Filabot EX2 extruder. The Filabot EX2

consist of a single-screw extruder with one heating zone. The extrusion screw has an L/D ratio of 10:1. For this study, the heating zone was set to 205 °C and the nanocomposite mixture was extruded at 25 RPM through a 2.85 mm circular die. After solidification, the extruded nanocomposite filament was collected and measured with calipers to ensure variation in the filament diameter was < 0.2 mm. Prior to printing by FFF, all filaments were dried overnight in a vacuum oven at 100 °C to remove any residual moisture.

3D printing of test specimens. Specimens for dynamic mechanical analysis (DMA) and tensile testing were drawn in accordance with ASTM D7028 and ASTM D638 (standard V) specifications, respectively, using Autodesk® AutoCad® 2017. Each sample template was saved in STL format, transferred to the computer used to control the Lulzbot Mini 3D printer, and opened using the Lulzbot 3D printing software (Cura). This Lulzbot Mini 3D printer was used to print at least five PMMA test specimens for each measurement type. Each sample was printed in the X-Y plane at 230 °C with a +45/−45 raster angle. The bed temperature was set to 110 °C. In a typical print, the printer settings were as follows: 0.5 mm nozzle size, 0.425 mm initial layer thickness, 0.25 mm layer height with a 100% fill density, and all other settings were left at standard values set by the Cura software for ABS. After each print and in order to minimize sample deformation, the bed was allowed to cool to room temperature prior to removing the sample.

Instrumentation and Characterization. Tensile tests were performed on an MTS Criterion Model 43 system with a 10 kN load cell. “Dog bone” specimens were tested following the ASTM D638 procedure in which the samples were set at a grip separation distance of 25.4 mm and were elongated at 1 mm/s. The Young’s modulus, storage and loss moduli, and the glass transition temperature (T_g) of FFF-printed nanocomposite specimens were

determined using a TA DMA Q800 equipped with a dual cantilever clamp. Samples were first equilibrated at 30 °C. To determine the Young's modulus, an amplitude sweep from 20 to 2000 μm was completed using a constant frequency of 1 Hz at 30 °C. The T_g and storage and loss moduli were determined using a constant-strain temperature ramp protocol in which a strain of 0.1% was applied to the specimen while the temperature was ramped from 30 to 140 °C at a rate of 3 °C/min. From these measurements, T_g was assigned based on the peak of tan δ.[63]

A TA Discovery Hybrid Rheometer-3 was used to determine the complex viscosity and storage and loss moduli of FFF-printed nanocomposite specimens. An experimental protocol consisting of a constant-strain frequency sweep method at various temperatures was used so that a master curve could be constructed by time-temperature-superposition. In a typical procedure, the FFF-printed sample was placed between parallel plates (25 mm diameter) and heated to 210 °C. After that temperature was reached, the molten polymer sample was compressed to set a gap of 1000 μm between the plates. Then, frequency sweeps from 0.1 to 100 Hz at a strain of 0.1% were performed at various temperatures, beginning at 210 °C and decreasing to 130 °C using decrements of 20 °C. The superposed master curves were generated by the TA Discovery software after setting the reference temperature of the frequency sweeps to 170 °C. The temperature-dependent frequency shift factors (a_T, WLF type) used to generate the master curves are presented in Figure A.1. (See Appendix A.)

Small-angle and wide-angle x-ray scattering (SAXS and WAXS, respectively) were used to characterize the nanoscale structure of FFF-printed nanocomposite

specimens. SAXS and WAXS data were acquired at the 12-ID-B beamline at the Advanced Photon Source (APS) at Argonne National Laboratory. Samples were measured at room temperature in air with a 13.3 keV X-ray beam and a sample-to-detector distance of 2.3 meters. The scattered radiation was recorded as a function of scattering angle 2θ using a Pilatus 2M detector for SAXS and a Pilatus 300 detector for WAXS. For each sample, 3 measurements were taken at different positions (1 mm spacing) with a 0.1 second exposure time. The 2-dimensional (2D) scattering images were then reduced to 1-dimensional (1D) scattering curves by an azimuthal integration method using the SAXSLee software developed at the 12-ID-B beamline. All data are reported as scattered intensity I as a function of q, where $q = 4\pi/\lambda \sin(\theta)$. The scattering data for each nanocomposite sample was corrected by subtracting the average intensity of a virgin (unfilled) PMMA FFF-printed specimen. The q-range detected was 0.004 – 0.89 $Å^{-1}$ for SAXS measurements and 0.85 – 2.69 $Å^{-1}$ for WAXS measurements. The WAXS signal disappears after subtracting the signal of the pure PMMA specimen.

SAXS data were analyzed using the Unified Fit model (Equation 2.1) in the Irena software package (Version 2.63) published by APS:[64,65]

$$I(q) = \sum_{i=1}^{2} G_i \exp\left(\frac{-q^2 {R_{gi}}^2}{3}\right) + \; B_i (q^*)^{-P_i} \tag{2.1}$$

where $q^* = q/\left[\text{erf}\left(qR_{gi}/6^{1/2}\right)\right]^3$, i is the population/structural level, G_i is the Guinier prefactor, R_{gi} is the radius of gyration, B_i is the power-law prefactor and P_i is the Porod exponent. This model is used to evaluate the size distribution and dispersion behavior of the nanoparticles in the PMMA matrix. In the present study, two levels of structure were needed to describe the SAXS data: one level captures the larger-scale structure from

collections of nanoparticles (low q), and a second level that captures the sizes, dispersion, and interfacial characteristics of the primary nanoparticles. The parameters extracted from Equation 2.1 are used to characterize the hierarchical structure of the composite: P_i >3 indicates surface fractal scattering, $2 < P_i < 3$ indicates mass fractal scattering, and $P_i > 4$ is consistent with a diffuse interface.[66] For a spherical particle, the radius R_i can be calculated from R_{gi} by Equation 2.2:

$$R_i = \sqrt{5/3}\, R_{gi} \tag{2.2}$$

Scanning electron microscopy (SEM) was used in addition to SAXS and WAXS to provide further insight into the structural formation of Si NPs incorporated into PMMA parts printed by FFF. In a typical procedure, carbon paint was applied to the edge of FFF-printed parts to increase the conductivity and then images were collected using a Zeiss Auriga with a 0.5 keV electron beam.

2.4 Results and Discussion

The reinforcement effect of Si NPs incorporated into FFF-printed PMMA specimens was examined by DMA, tensile tests and rheology. Representative DMA stress-strain curves presented in Figure 2.1 show an increasing slope as the loading level of Si NPs is increased. The Young's modulus (values are reported in the legend as the average ± standard deviation determined from measurements of five replicate samples) consistently increases with nanofiller loading: a 44% increase relative to specimens printed from pure PMMA filaments is observed for samples containing Si NPs at 1.0 wt.% loading.

While DMA measurements were used to probe the linear response regime, tensile test measurements were completed to provide additional insight into the mechanical

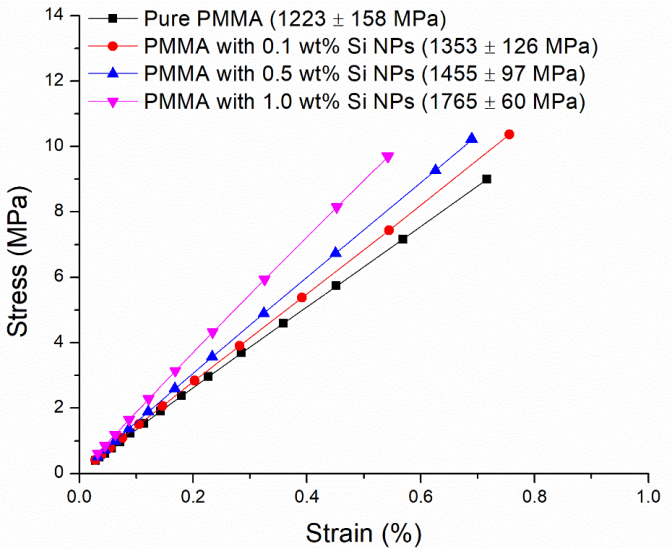

Figure 2.1. DMA results show an increase in the Young's modulus with increasing amount of Si NP incorporated into the filament. Values of the Young's modulus given in the legend are based on measurements of five replicate samples.

properties of FFF-printed nanocomposites through macroscopic failure. Representative stress-strain curves shown in Figure 2.2 also reflect improvements in the mechanical properties as nanofiller is added, which is analogous to behaviors observed from DMA. The results show that all samples exhibit the same pattern of behavior: elastic deformation gives way to yielding of the PMMA matrix (signified by the transition from elastic deformation and the formation of a plateau)[67,68] followed by stain-hardening. However, even though the deformation patterns are similar, the mechanical properties are drastically affected by the incorporation of Si NPs. For instance, the Young's modulus, which is determined from the slope of the stress-strain curve prior to plastic deformation, increases as the loading level of Si NPs increases. More specifically, an 87% increase in tensile modulus is seen for PMMA samples containing Si NPs at a 1.0 wt.% as compared to FFF-

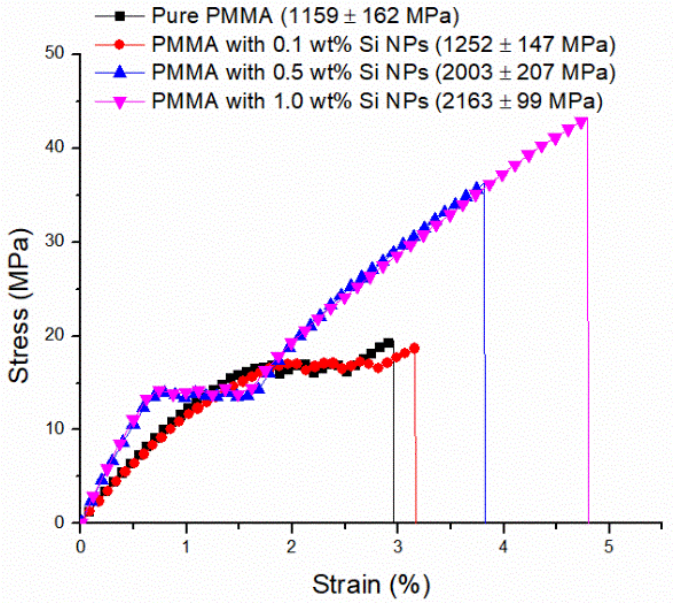

Figure 2.2. Tensile testing of nanocomposite samples shows an increase in Young's modulus, ultimate tensile strength, and elongation-at-break as the Si NP loading increases. A representative trace from a series of replicate tests is shown for each loading level and the values of tensile modulus provided in the legend are based on measurements of five replicate samples.

printed specimens made from virgin PMMA filaments. In addition to increases in modulus, the ultimate tensile strength (UTS), which is the maximum stress a material can withstand prior to fracture, and elongation at break increase as the amount of Si NPs incorporated into PMMA filament increases. Virgin PMMA-printed parts had (on average) an UTS of 17.6 MPa and an elongation-at-break of 2.3% while FFF-printed parts containing Si NPs at a 1 wt.% loading level show a dramatic increase (137%) in the UTS to 41.8 MPa and a substantial improvement (91% increase) in elongation-at-break to 4.4%. It should be noted that the addition of nanoparticle additives generally leads to reductions in the elongation at

break;[69,70] however, some researchers recently have observed increases in the elongation at break with the introduction of nanoparticles.[9,71,72] The reason for this enhancement is still a point of debate. Lastly, as the loading level of Si NPs increases a decrease in the yield stress is observed, as seen in Figure 2.2. This reduction in the yield stress for polymer nanocomposites has been attributed to strong interfacial adhesion between the matrix polymer and nanoparticle additive.[73] The averages for all specimens are reported in Table 2.1, and the results obtained from tensile tests coupled with those obtained from DMA suggest that incorporating Si NPs into PMMA to create nanocomposite filaments increases the mechanical properties of FFF-printed specimens. Furthermore, as seen from the other properties reported in Table 2.1, not only do the mechanical properties increase as the loading level of Si NPs increases, but this trend is preserved across multiple measurement techniques.

Table 2.1. Mechanical properties of PMMA nanocomposite samples manufactured by FFF.[a]

Loading Level	**Ultimate Tensile Strength (MPa)**	**Young's Modulus Tensile Test (MPa)**	**Elongation at break (%)**	**Young's Modulus DMA (MPa)**
Pure PMMA	18 ± 3	1159 ± 162	2.3 ± 0.9	1223 ± 159
0.1 wt% Si NPs	21 ± 3	1252 ± 147	2.8 ± 0.4	1353 ± 126
0.5 wt% Si NPs	37 ± 5	2003 ± 207	4.5 ± 0.8	1455 ± 97
1.0 wt% Si NPs	42 ± 4	2163 ± 99	4.4 ± 0.6	1765± 60

[a]All values (average ± the standard deviation) result from measurement of 5 replicate samples.

Constant-strain temperature ramp experiments were also used to examine how incorporating Si NPs into PMMA filaments impacts the thermomechanical properties, such as T_g, and the storage and loss moduli. Two main observations can be deduced from these results, which are displayed in Figure 2.3. First, as the loading level of Si NPs increases, the T_g of the FFF-printed test specimens increases. (Values are given in the legend and as noted previously, T_g is taken to be the maximum in the dissipation factor, tan δ.[63]).Changes in the T_g of polymer nanocomposites have been attributed to interactions between the matrix polymer and inorganic additives that impact the mobility of polymer chains at or near the internal interface.[9,74] Generally, a depression in T_g from the bulk value is attributed to repulsive interactions between the polymer and filler,[9,74,75] and increases in T_g are indicative of attractive interactions between the nanoparticle and polymer that decrease the mobility of chains near the surface.[74,76–78] As seen from the normalized tan δ curves presented in Figure 2.3A, relative to the T_g extracted for pure FFF-printed PMMA (109 °C), as the loading level of Si NPs increases to 1 wt.%, the T_g of the nanocomposite increases to 114 °C. It is understood that the carbonyl groups of PMMA hydrogen bond with hydroxyl groups on Si NP surfaces, and this non-bonded, attractive interaction reduces the dynamics of chains at nanoparticle/matrix interfaces, which manifests as an increase in T_g.[77,79,80] Moreover, the increase in T_g as the loading level of Si NPs is consistent with an increase in the number of hydrogen bonding interactions within the nanocomposite.

In addition, the pattern of behavior seen in the values of storage modulus, E', and loss modulus, E", (Figures 2.3B and 2.3C, respectively) derived from constant-strain temperature ramp experiments complement those obtained from tensile testing and from the DMA strain-sweep experiments: All show that modulus increases as the loading level

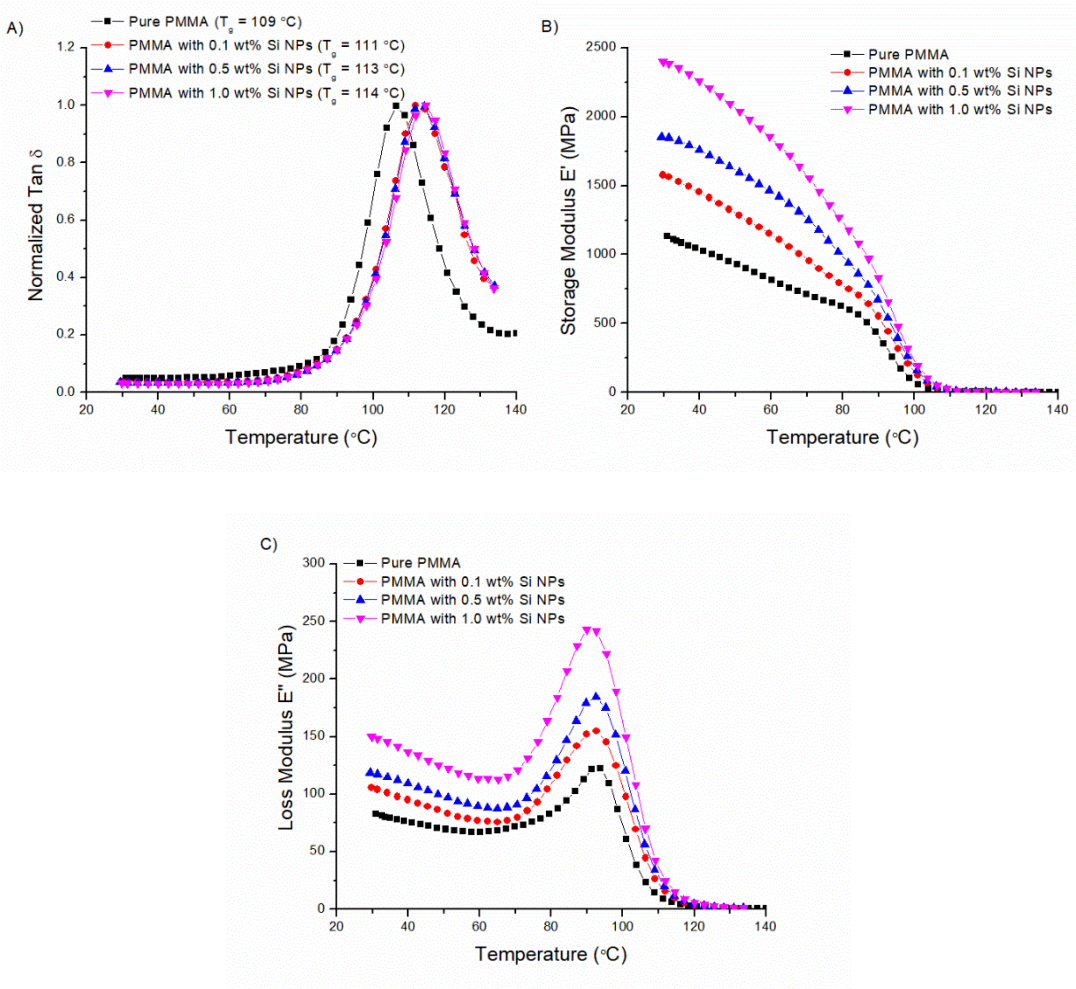

Figure 2.3. Constant-strain temperature ramp measurements completed on PMMA nanocomposite samples produced by FFF as a function of Si NP loading show that the glass transition temperature (A) and storage (B) and loss moduli (C) increase with increasing filler content.

of Si NPs incorporated into FFF-printed PMMA nanocomposites increases. My research shows that both the storage and loss moduli of the nanocomposite specimens in the glassy state increases as the loading level of Si NPs incorporated in the printed PMMA nanocomposites increases. A 72% increase in E' is seen at the highest loading level (1 wt% Si NP) compared to unfilled PMMA samples, and a 55% increase in the loss modulus E", which is indicative of the energy dissipated during deformation, is observed when Si NPs are incorporated at 1 wt.% (relative to virgin PMMA samples). As suggested by Menard,[63] although the storage modulus obtained from DMA only represents the elastic response of a material, it can be considered essentially analogous to the Young's modulus as long as the test is performed at low strain. Here, this analogy between the storage modulus, indicative of elastic recovery, and Young's modulus is preserved because the low strain (0.1%) used in the constant-strain temperature ramp experiments is within the linear response regime (see Figures 2.1 and 2.2) and values of E" are relatively small. Therefore, not only are the moduli determined from three different experiments self-consistent, the pattern of increasing modulus with loading level is also consistently observed. In addition, the constant-strain temperature ramp results displayed herein align with reports by Ramanathan *et al.* and Wong *et al.* who determined that the T_g, E', and E" of PMMA nanocomposites increased as the loading level of graphite nanoplatelets and expanded graphite increased, respectively. Both reports ascribe the improvements to favorable interfacial interactions between the polymer matrix and inorganic additive, which led to reduced polymer chain dynamics at the interface.[78,81] Finally, the increase in the E' and E" as the loading level of Si NPs increases also agrees with previous reports suggesting that

the mechanical property enhancements are due to the material properties of the additive.[8,78,81,82]

While these assessments of macroscopic behavior allow inferences regarding the origin of the nanocomposite reinforcement to be made, it is useful to pair these with perspectives of phenomena that occur on the nanoscale. In order to assess whether increasing the amount of Si NPs imbedded into PMMA FFF-printed specimens increases the number of polymer-surface interactions, rheometric studies using low-amplitude oscillatory-shear measurements were completed. As suggested by Paul and Zheng, the storage modulus ($G'(\omega)$) and complex viscosity ($|\eta^*|$) are more sensitive to subtle changes in the melt behavior of polymer nanocomposites,[83,84] and for that reason, I will focus the discussion to how the patterns of behavior in these properties are impacted as Si NPs are added. Figure 2.4 shows the angular frequency dependence of storage modulus and complex viscosity of FFF-printed PMMA specimens containing no Si NPs (pure PMMA) and nanocomposites containing Si NPs at 0.1 and 1.0 wt.% loading levels. From the behavior of the elastic modulus (Figure 2.4A), it is clear that incorporating Si NPs affects the nanocomposite properties denoted by the increase in $G'(\omega)$ as the loading level of Si NPs increases; however, regardless of the amount of additive incorporated into the nanocomposite, all samples display a liquid-like behavior in the terminal regime. The absence of a solid-like behavior within the terminal regime indicates that a percolated network and the agglomeration of particles was avoided at these loading levels.[84–87] These results align with similar reports that determined that the percolation threshold for ~14 nm silica nanoparticles in polypropylene, polystyrene and poly(butyl acrylate), where solid-like behavior arises, does not develop until the loading level of spherical nanoparticles is

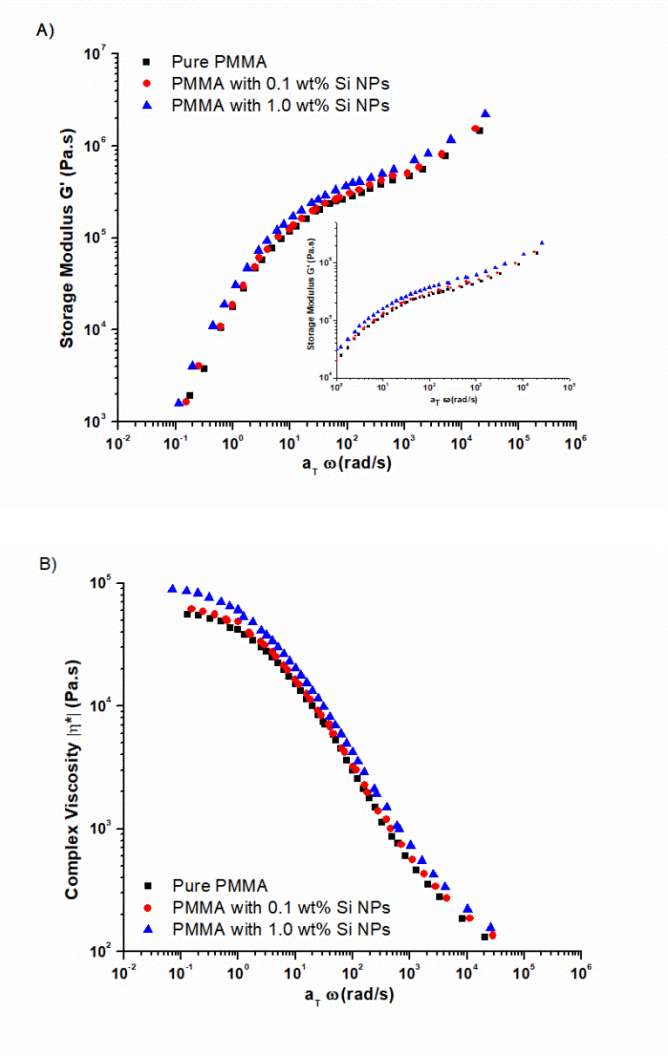

Figure 2.4. Rheological measurements show that the storage modulus (A) and complex viscosity (B) of FFF-printed PMMA nanocomposite specimens increase as the loading level of Si NPs increases. A reference temperature of 170 °C was used for time-temperature superposition. The y-axis scale used to create the plot inset in (A) is intended to accentuate the increase in storage modulus with loading level.

roughly 2.5 vol%.[88–90] Thus, it is not surprising that liquid-like behavior is observed for the FFF-printed nanocomposite systems studied here because loading levels of 0.1 wt% and 1.0 wt% correspond to 0.04 vol% and 0.4 vol%, respectively. The data also show that compared to the behavior of pure PMMA, the enhancements in G'(ω) observed at a 0.1 wt.% Si NP loading level are minimal. These results suggest that the total interaction energy between the PMMA matrix chains and the Si NP surface, which ostensibly is the product of the number of segment-surface contacts and the fundamental interaction energy, is low. However, as the Si NP loading is increased by an order of magnitude (0.1 wt.% to 1.0 wt.%), the number of non-bonded, physical interactions (hydrogen bonding interactions) between the segments of PMMA chains and surface silanol groups increase, leading to a more substantial increase in G'(w), especially at low frequencies. This view of the nanoscale interactions present in the system and pattern of behavior are consistent with the macroscale behaviors seen from the DMA and tensile tests. Furthermore, the frequency-dependent complex viscosity, which is displayed in Figure 2.4B, shows a monotonic increase in the viscosity of the PMMA nanocomposites as the loading level of Si NPs increases. At low frequencies, the formation of a plateau is clear and the increase in |η*| is more distinct. At high frequencies, the pure PMMA and PMMA nanocomposite samples exhibit shear thinning behavior and the viscosities of all the samples become similar. The monotonic increase observed in both the complex viscosity and storage modulus is further highlighted in the results of small amplitude oscillatory shear measurements, which are presented in Figure A.2 in Appendix A. These results align with reports by Ray *et al.* and Giannelis *et al.*, who ascribed the improvements in G'(ω) and |η*|

in polymer-layered silicate nanocomposites to the decreased mobility of polymer chains confined at the surface and enhanced polymer-surface interactions, respectively.[91,92]

In addition, constant-strain temperature-ramp experiments also show that the complex viscosity of the nanocomposite melt is similar to the melt viscosity of pure PMMA at T >200 °C (data not shown) and is not affected by Si NP loading level. In fact, these experiments were conducted first, and the results used to set the extrusion (T_{ext} = 205 °C) and printing (T_{print} = 230 °C) temperatures used for nanocomposite filament preparation and FFF printing. These results are consistent with other reports indicating that the melt viscosity of nanocomposite parts produced by FFF is not impacted when the amount of added nanofiller is low.[93–95]

Finally, it is widely accepted that the spatial distribution of nanoparticles directly impacts nanocomposite properties. For example, agglomeration of nanoparticles can lead to a significant decrease in the mechanical properties and optical clarity of polymer nanocomposites, while dispersion leads to an increase in the thermal resistance, thermomechanical properties and reduces permeability.[12,96–98] Therefore, SEM and SAXS were used to examine how the spatial distribution of Si NPs was affected by the loading level. The SEM micrograph of an FFF-printed PMMA nanocomposite specimen containing Si NPs at a 1 wt.% loading level, shown as Figure 2.5, illustrates that individual particles are well-dispersed throughout the matrix. Even at the highest loading level used, only a few isolated clusters of nanoparticles are observed, and there are no large-scale aggregates. While the SEM image suggests a well-dispersed system and provides insight about the structure formation of Si NPs at the nanoscale, SAXS was used to calculate an average structure size and particle distribution in nanocomposite samples. The corrected

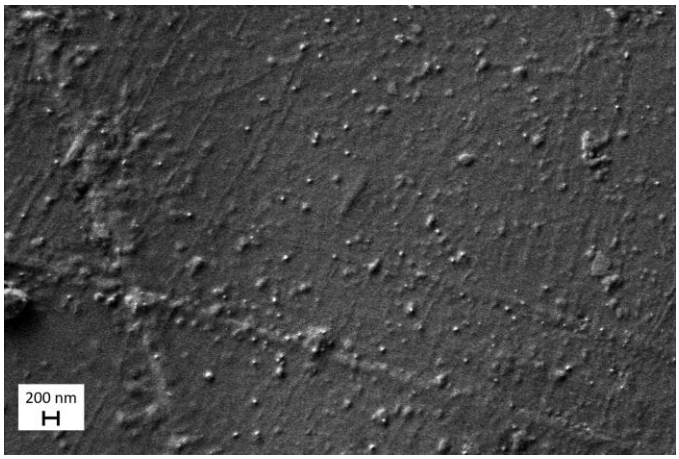

Figure 2.5. Scanning Electron Microscopy shows that Si NPs, present here at a 1 wt% loading level, are well-dispersed throughout the FFF-printed PMMA nanocomposite specimen. This image is a top-down view of a DMA sample printed by FFF.

scattered intensity curves, which are modeled using a Unified Fit, are shown in Figure 2.6. Two samples were measured by SAXS for each particle loading, and data were recorded from three areas on each sample. Each data set was modeled using the Unified Fit, and the average values of the parameters are reported in Table 2.2 with an uncertainty of ±1 standard deviation.

It should be noted that the following discussion focuses solely on the SAXS region (scattering wavevector $q < 0.4$ Å^{-1}) because the WAXS data contain only the scattering contribution from the PMMA matrix as seen in Figure A.3. (See Appendix A.) As expected, the scattered intensity of PMMA nanocomposite specimens increases with increasing Si NP loading levels. Power law exponents, or fractal dimensions, and particle sizes, were determined by using a Unified Fit model (Equation 2.1) to describe the corrected SAXS data, and two levels of structure were needed, as reflected in the results

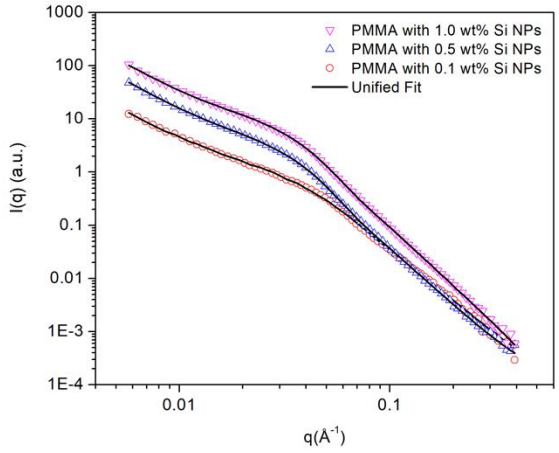

Figure 2.6. Corrected scattered intensity curves from SAXS measurements of FFF-printed PMMA nanocomposite specimens containing Si NPs at various loading levels.

Table 2.2. Unified fit parameters obtained from SAXS measurements on PMMA nanocomposite specimens.

Loading Level	***R* (nm)**	**R_g (nm)**	**Power law exponent (high-q)**	**Power law exponent (low-q)**
0.1 wt% Si NPs	7.49 ± 1.88	5.81 ± 1.46	4.22 ± 0.15	1.78 ± 0.45
0.5 wt% Si NPs	7.36 ± 1.27	5.70 ± 0.98	3.70 ± 0.09	2.30 ± 0.06
1.0 wt% Si NPs	7.44 ± 1.22	5.77 ± 0.94	3.81 ± 0.18	2.31 ± 0.28

presented in Table 2.2. It should be noted that the scattering from the 0.1 wt.% samples was weak and nearly indistinguishable from the PMMA reference, so these data should be interpreted with caution. Each data set was fit without inclusion of a structure factor, which as suggested by Kumar *et al.*, indicates that interparticle interactions are not present within the nanocomposite.[79]

For all of the FFF-printed samples, the primary particle size, reported as the radius of gyration, R_g, was ≈ 6 nm. Not only does this agree with the size of the Si NPs reported by the manufacturer, this calculated particle size does not change as the amount of Si NPs was increased. At low *q*, the Porod exponent for the 1.0 wt.% and 0.5 wt.% FFF-printed nanocomposite samples was determined to be approximately 2, which is indicative of mass-fractal scattering.[9,66,79] The low *q* Porod exponent for the 0.1 wt.% sample is also near 2, but the statistical uncertainty is high, as noted previously. The size of mass fractals could not be determined from these data because resolution is limited to a minimum *q* of approximately 0.005 $Å^{-1}$; however, it is well-established that a Porod exponent of 2 in the low *q* regime is characteristic of a miscible polymer-particle system containing well-dispersed mass fractals[9,79] or soft agglomerates,[99] but values approaching 3 are expected for larger-scale clusters. The high *q* exponent describes the type of surface fractals, or the surface roughness of the polymer-nanoparticle interface. A value of 4 is expected for a smooth surface, while a value of 3 indicates a rough surface. The exponent for all three Si NP loadings is near 4, which is consistent with a smooth PMMA/Si NP interface. Thus, according to results from rheology, which showed no evidence of a secondary plateau in the terminal regime, imaging by SEM, and the calculated R_g values and Porod exponents at low *q* from SAXS, it is inferred that even in the non-equilibrium melt extrusion processes

of FFF, the nanocomposite structure and average structural size are not impacted as the loading level of Si NPs increases. Moreover, at all loading levels the Si NPs appear to be well-dispersed throughout the nanocomposite.

2.5 Conclusions

Coupling assessments of macroscopic thermomechanical performance with insights from SAXS, SEM, and rheometry provide a clear picture of how interfacial interactions and nanoscale structure affect the macroscopic properties of FFF-printed nanocomposite parts. My research shows that the enhancements obtained by the incorporation of inorganic nanoparticles are due to the complex interplay of particle-polymer surface interactions, which I attribute to hydrogen-bonding interactions between the carbonyl groups of PMMA and the hydroxyl groups on the Si NP surface. These interfacial entanglements lead to reduced chain mobility at the surface that enhances stress-transfer from the polymer matrix to the inorganic additive. Moreover, altering the number of interactions by varying loading level of the additive can be used as a way to adjustably improve material properties and performance of FFF-printed parts. While the present study is limited by its focus on a specific homopolymer that exhibits favorable physical interactions with the inorganic additive, additional studies aimed at assessing relations between loading level and polymer-surface interaction strength are discussed in Chapter 3. Overall, the insights established from this work are expected to be generally advance the implementation of additive manufacturing by using nanocomposites to provide a wider range of material properties, thereby providing a way to address challenges associated with inferior performance of FFF-printed parts.

CHAPTER 3: TAILORING INTERFACIAL INTERACTIONS USING POLYMER GRAFTED NANOPARTICLES IMPROVES PERFORMANCE OF PARTS MANUFACTURED BY 3D PRINTING

3.1 Abstract

Decorating nanoparticle surfaces with end-tethered chains provides a way to mediate interfacial interactions in polymer nanocomposites. Here, polymer grafted nanoparticles are investigated for their impact on the performance of polymer structures created by fused filament fabrication (FFF). The nanoscale organization of poly(methyl methacrylate)-grafted nanoparticles (PMMA-g-NPs) in PMMA matrices are examined via small-angle X-ray scattering (SAXS). SAXS data indicate that all nanocomposites exhibit particle-particle interactions and organize in the polymer matrix as surface fractals, or as "connected sheets". Additionally, increasing the loading level of PMMA-g-NPs produces modest changes in T_g, but significant increases in the complex viscosity and storage modulus, suggesting that the number density of entanglements between graft chains and the matrix polymer increases with increasing PMMA-g-NP content. Increasing the number density of entanglements and the formation of connected sheets manifest at the macroscale: Dynamic mechanical analysis and tensile testing show that FFF-printed PMMA-g-NPs/PMMA nanocomposites display a 65% increase in the Young's modulus, 116% increase in the ultimate tensile strength, and a 120% increase in the storage modulus compared to parts printed with pure (unfilled) PMMA. This research effort highlights how molecular engineering can enhance interactions on the nanoscale and improve the macroscopic properties of parts printed by FFF.

3.2 Introduction

Layers of surface tethered polymers are routinely used to alter interfacial properties. The diversity of monomer types and richness of copolymer design space provides a

tractable way to alter the range, strength, and nature of interfacial interactions and surface properties. Along these lines, decorating the surface of NPs with end-anchored polymer chains to create polymer-grafted nanoparticles (PGNPs) has proven to be a useful way to mediate interparticle and particle-matrix interactions,[15,19,100] thereby affecting the nanocomposite performance and spatial arrangement.[13,20,101,102] For instance, polystyrene (PS) will not wet "bare" (unfunctionalized) silica nanoparticles (Si NPs),[103] and as a result, the addition of Si NPs to PS at modest loading levels (1-10 wt%) decreases the mechanical properties relative to neat (unfilled) PS.[104] However, Douglas *et al.* showed that incorporating PS-grafted nanoparticles at a 5 wt% loading level increased the Young's modulus and facture strain of PS-grafted nanocomposites by 52% and 157% compared to neat PS, respectively.[100] They reasoned that the polymer grafts effectively shield unfavorable polymer-particle interactions and increase the number density of interfacial interactions between the PS-grafted nanoparticles and PS matrix chains. This effectively enhances stress transmission from the polymer matrix to the reinforcing Si NPs. Similarly, Friedrich *et al.* showed that the addition of unmodified Si NPs lowered the tensile strength of polypropylene nanocomposites, but nanocomposites with a 1 wt% loading level of polypropylene-grafted nanoparticles generated a ~22% increase in the tensile strength.[105] The increase in mechanical performance also was attributed interdiffusion and entanglements between the graft and matrix chains.

In addition to enhancing the performance of nanocomposites, Akcora *et al*., demonstrated that the spatial arrangement of PS-grafted nanoparticles in a PS matrix can be altered by varying the ratio of the graft to matrix chain length and the grafting density of chains decorating the nanoparticle surfaces.[19] Specifically, PS-grafted nanoparticles

with high grafting densities equilibrated in a polystyrene matrix were well-dispersed (aggregated) when the graft chain to matrix chain ratio was large (small), which are consistent with well-known behaviors of athermal systems that are dominated by competition between mixing and conformational entropy.[17,106–110] In addition, various anisotropic nanostructures such as strings, fractals, and connected sheets were observed as both the grafting density and graft to matrix chain length ratio were varied. Presumably, these anisotropic nanostructures emerge because incomplete shielding of the nanoparticle surface leads to non-symmetric inter-particle interactions.[19,97] These studies highlight how the performance and spatial arrangement of polymer nanocomposites can be improved by effectively managing interfacial interactions between the polymer matrix and nanoparticle additive.

Inspired by these reports, herein I assess how tailoring interfacial interactions across the matrix-additive interface can be used to improve the performance of 3D printed parts generated by fused filament fabrication (FFF). While FFF provides a novel route to create complex polymeric scaffolds, parts manufactured by FFF exhibit inferior mechanical properties compared to parts created by traditional manufacturing methods. This principal drawback is due to inefficient interfacial adhesion between adjacent filaments, or beads, which is attributed to inability of polymer chains to diffuse and entangle across bead-bead interfaces during processing.[111–117] To address the issue of poor mechanical performance, recent efforts have examined how polymer nanocomposites can be utilized to provide mechanical reinforcement in printed systems.[10,11,95,118–120] For instance, in Chapter 2 I determined that the thermomechanical properties of PMMA specimen fabricated by FFF could be improved by the addition of Si NPs.[121] Specifically,

results from dynamic mechanical analysis and tensile tests show a 44% increase in the Young's modulus and a 87% increase in the tensile modulus at a 1.0 wt% Si NPs loading level compared to unfilled PMMA, respectively. Rheology measurements suggest that these improvements are due to hydrogen bonding interactions between the hydroxyl groups on nanoparticle surfaces and carbonyl groups along the polymeric backbone. The physical non-bonded interaction tends to confine polymer chains at the nanoparticle surface, which enhances stress-transfer from the polymer matrix to the additive, manifesting as an increase in the mechanical properties.

While Chapter 2 demonstrates how the thermomechanical properties of FFF printed scaffolds can be enhanced by the addition of bare nanoparticles, to the best of my knowledge, there have been no reports describing how the incorporation of PGNPs impacts the performance of FFF-printed parts. PGNPs are expected to be an inherently tailorable platform that can be used to improve the mechanical properties of FFF-printed part. For instance and as described earlier, compared to unfunctionalized additives, PGNPs provide a novel route to shield unfavorable particle/polymer interactions and are reported to increase the number density of entanglements between the matrix and nanoparticle, thus enhancing stress-transmission. Herein, I systematically examine how increasing the loading level of poly(methyl methacrylate)-grafted nanoparticles (PMMA-g-NPs) in PMMA parts manufactured by FFF impacts structural organization and properties of the resultant nanocomposites. Assessments of nanoscale structure formation and thermomechanical properties underscore the importance of interfacial interactions and suggest that the mechanical properties improvements of FFF-printed parts containing

PMMA-g-NPs are due to interfacial interactions between graft chains with neighboring polymer-decorated particles and the polymer matrix, which effectively dissipates stress.

3.3 Experimental Methods

3.3.1 Synthesis of Materials

Methyl methacrylate (Aldrich, 99%) was passed through a basic alumina column to remove inhibitor. 2,2'-Azobis(2-methylpropionitrile) (AIBN, Aldrich, 98%) was recrystallized twice from methanol. Atactic poly(methyl methacrylate) [MW = 100,000 g mol^{-1}] beads obtained from Polysciences Inc. were heated *in vacuo* at 100 °C to remove residual moisture before use. All other materials were used as received unless stated otherwise.

Synthesis of CTA-Functionalized Silica Nanoparticles. The chain transfer agent, 4-cyanopentanoic acid dithiobenzoate, was activated by coupling 2-mercaptothiazoline as described by Benicewicz *et al.*[122] In a typical procedure, 1.40 g (5.0 mmol) of 4-cyanopentanoic acid dithiobenzoate, 1.24 g (6.0 mmol) of dicyclohexylcarbodiimide, and 0.596 g (5.0 mmol) of 2-mercaptothiazoline were added to a 50 mL round bottom flask containing 20 mL dichloromethane. Next, 61 mg (0.50 mmol) of 4-(dimethylamino)pyridine was added to the solution dropwise and the reaction was stirred at room temperature for 6 h. At that time, the salt was removed by filtration and the activated 4-cyanopentanoic acid dithiobenzoate (ACPDB) was recovered by column chromatography using a 5:4 mixture of hexane to ethyl acetate as the mobile phase, and characterized via ^{1}H NMR.[122] (See Figure B.1 in Appendix B.) Next, Si NPs (14 ± 4 nm dispersed in methyl ethyl ketone (MEK)) supplied by Nissan Chemical were modified to

present amine groups as reported by Schadler *et al.*[74] To accomplish this, 0.5 mL of 3-aminopropyldimethylethoxysilane was added to a 100 mL flame-dried, round bottom flask containing 16 mL of Si NPs dissolved in MEK and 50 mL of THF. This mixture was refluxed at 75 ºC for 24 h and subsequently quenched by precipitating the reaction mixture in 500 mL of chilled hexanes. The amine-modified nanoparticles were isolated by decanting the supernatant after centrifugation at 4000 rpm for 10 minutes. The modified nanoparticles were then re-dispersed in THF. This sequence of precipitation-centrifugation-redispersion was completed three more times to ensure unreacted silanes were removed. Next, the ACPDB was attached to the amine-decorated Si NPs following protocols described by Benicewicz *et al*.[122] Briefly, 3.6 g of the amine-functionalized Si NPs were dispersed in g 30 mL THF. This solution was added to a 100 mL round-bottom flask containing 0.5 g (1.3 mmol) of ACPDB dissolved in 30 mL of THF. The reaction mixture was stirred at room temperature for 6 h. After that time, the solution was precipitated in a 4:1 (v/v) mixture of cyclohexane and ethyl acetate, and the ACPDB-functionalized NPs were isolated by centrifugation at 4000 rpm for 10 minutes. After the supernatant was decanted, the particles were re-dispersed in THF and then precipitated in a 4:1 mixture of cyclohexane and ethyl acetate. As noted by Benicewicz *et al.*, this precipitation-centrifugation-dispersion procedure was repeated until the supernatant remaining after centrifugation was colorless, which indicates that any residual (unattached) ACPDB has been removed from the ACPDB-modified Si NPs.[122] To determine the mass loss for ACPDB-decorated Si NPs, a TA Instruments Discovery Series thermogravimetric analyzer (TGA) was used. In a typical procedure, 0.5 to 2 mg of dried ACPDB-modified

NPs were placed in a 100 μL platinum pan, which was subjected to a temperature ramp from 30 to 800 °C at a rate of 10 °C/ min.

Synthesis of Polymer-grafted Nanoparticles. In a typical procedure, 6.0 g (59.92 mmol) of MMA and 2.0 mg (0.0129 mmol) of AIBN were added to a 50 mL round bottom flask containing 30 mL of THF. Next, 1.24 g (0.162 mmol) of ACPDB-functionalized Si NPs were added to a round bottom flask, which then was sparged with argon for 15 minutes. Next, the flask was placed in an oil bath that was heated to 70 °C and allowed to stir for 24 h. After that time elapsed, the reaction was quenched using liquid nitrogen and allowed to thaw. Next, free polymer chains, derived from initiation in solution, were separated from PMMA-g-NPs using a mixed solvent precipitation procedure involving THF and hexanes, as described by Akcora *et al*.[13] In brief, the crude reaction mixture (containing both free polymer chains and PMMMA-g-NPs) was placed in centrifuge tubes and then a non-solvent (hexanes) was added dropwise until the homogenous solution first showed evidence of turbidity. At that point, the solution was centrifuged at 4000 rpm for 10 minutes. The clear supernatant layer, which contains the free polymer, was decanted into hexanes. The PMMA-g-NPs were collected and again dissolved in THF. This precipitation-centrifugation-dispersion procedure was completed at least four more times, or until no precipitate (polymer) was observed when the supernatant was decanted into hexanes.

The grafting density of PMMA-g-NPs was determined by coupling assessments of chain size determined by GPC and mass loss analyzed by TGA. To determine the number-average molecular weight, M_n, of the polymer graft, chains were cleaved from the Si NPs, recovered, and characterized as described by Benicewicz *et al*.[122] To accomplish this, 50 mg of PMMA-g-NPs were dissolved in 3 mL of THF. Next, 0.2 ml of aqueous HF (49%)

were added and the solution stirred overnight. After that time elapsed, the solution was poured into a PTFE dish, which was allowed to sit in a fume hood overnight to remove volatiles. The recovered PMMA was then dissolved in THF and characterized via GPC. Additionally, the amount (areal density) of PMMA chains grafted to Si NPs was determined via TGA, as described above. The assessments of molecular weight by GPC and mass loss corresponding to grafted chains by TGA are displayed in Figure B.2 and B.3 of Appendix B, respectively.

3.3.2 Extrusion of Filament and FFF

Filament Preparation. Polymer-grafted nanocomposite filaments comprised of PMMA containing PMMA-g-NPs were fabricated as reported previously.[121] To make comparisons to our previous report involving PMMA filaments blended with bare Si NPs, the loading level (wt %) of PMMA-g-NPs in the extruded filament is based on the mass of silica. To create polymer-grafted nanocomposite filaments, PMMA-g-NPs were blended with PMMA beads using a Magic Bullet® 250 W blender. This mixture was pulsed for ten cycles of one to three seconds each and then added to the hopper of a Filabot EX2 extruder that had been preheated to 205 °C. (The Filabot EX2 is a single-screw extruder with one heating zone and the extrusion screw has an L/D ratio of 10:1.) For this study, the heating zone was set to 205 °C and the nanocomposite filament was extruded at 25 RPM using a 2.85 mm nozzle head. If the filament diameter deviated by more than 0.2 mm it was pelletized and re-extruded. After successful extrusion, the filament was collected and heated overnight *in vacuo* at 100 °C to remove residual moisture.

3D Printing of Test Specimens. As described previously, DMA and tensile specimen templates were drawn in accordance to ASTM D7028 and ASTM D638 (standard V) specifications using Autodesk® AutoCad® 2017, respectively.[121] Once a specimen template was created, it was exported as an STL file. This file was then opened on a Lulzbot Mini 3D printer that was used to print at least five samples for each testing method (DMA and tensile). All specimens were printed in the x-y plane at 245 °C with a bed temperature of 110 °C and a +45° / -45° raster angle. Additional printer settings (layer thickness, nozzle size, etc.) are reported elsewhere.[121] After each print, the build plate was allowed to cool to room temperature before removing the sample to ensure the sample was not deformed prior to testing.

3.3.3 Instrumentation and Characterization

^{1}H NMR spectra were obtained using a Varian VNMRS 500 MHz spectrometer at 25 °C in deuterated chloroform. A TA Instruments Discovery Series TGA was used to determine the mass loss of silane, ACPBD and PMMA decorated Si NPs following each procedure described above. Number-average molecular weight, M_n, and dispersity, Đ, of the PMMA grafts were determined in THF at room temperature with a flow rate of 1 mL/min using an Agilent 1260 Infinity II GPC. The Agilent GPC is equipped with a Wyatt Dawn® Helios® 8 Multi-Angle Light Scattering Detector, ViscoStar® III, and an Optilab® T-rEX™. Molecular weights were determined using conventional calibration against polystyrene standards. Tensile tests were completed using an MTS Criterion Model 43 system containing a 10 kN load cell. Tensile tests were completed according to the ASTM D638 procedure, in which samples were elongated at 1 mm/s at the gauge length is set to

25.4 mm. A TA Instruments Discovery DMA Q800 equipped with a dual cantilever clamp was used to examine how thermomechanical properties PMMA printed parts containing PMMA-g-NPs. Specifically, strain-sweeps using an amplitude from 20 to 2000 μm and a frequency of 1 Hz were used to determine the Young's Modulus. The glass transition temperature, T_g, and the storage and loss moduli of nanocomposite specimens were determined using constant-strain temperature ramp experiments that applied a strain rate of 0.1% while the temperature was ramped from 30 to 140 °C at 10 °C/ min. Values of T_g for PMMA nanocomposite samples containing PMMA-g-NPs are reported as the peak maximum of the normalized tan delta (tan δ).[63] A TA Instruments Discovery Hybrid Rheometer-3 equipped with 25 mm parallel plates was used to determine the complex viscosity and the storage and loss moduli of FFF-printed PMMA parts containing PMMA-g-NPs. To accomplish this, fractured tensile bars were equilibrated at 210 ºC and the molten polymer was compressed to an interplate (gap) distance of 1000 μm. Then, constant-strain frequency sweeps from 0.1 to 100 Hz at a strain of 0.1% were performed at myriad temperatures, starting at 210 °C and decreasing to 130 °C in decrements of 20 °C. Master curves were constructed by time-temperature-superposition using the TRIOS software and a reference temperature of 170 °C. The temperature-dependent frequency shift factors (a_t, WLF type) used to generate the master curves are presented in Figure B.4. (See Appendix B.)

Small-angle and wide-angle x-ray scattering (SAXS and WAXS) data were used to characterize the nanoscale structure of PMMA-g-NPs in FFF-printed parts. Scattering measurements were completed at the Advanced Photon Source (APS) at Argonne National

Laboratory using beamline 12-ID-B. Simultaneous SAXS and WAXS measurements were completed in air at room temperature using a sample-to-detector distance of 2.3 meters and a 13.3 keV X-ray beam ($\lambda = 0.93$ Å). The scattered radiation was collected using a Pilatus 2M detector and a Pilatus 300 detector for SAXS and WAXS measurements, respectively, which record the intensity as a function of scattering angle (2θ). Three independent samples were measured for each particle loading (0 wt%, 0.1 wt%, 0.3 wt% and 1 wt%), and data were acquired from at least four positions on each sample. The exposure time was 0.1 second for each measurement. SAXSLee software, developed at the12-ID-B beamline, was used to reduce 2-dimensional (2D) scattering images to 1-dimensional (1D) scattering curves via azimuthal integration. These 1D curves are scattered intensity I as a function of scattering vector modulus q, where $q = 4\pi/\lambda \sin(\theta)$. The q-range detected was $0.004 \leq q \leq 0.89$ Å^{-1} for SAXS measurements and $0.85 \leq q \leq 2.69$ Å^{-1} for WAXS measurements. Uncorrected SAXS and WAXS measurements and the average scattering trace for PMMA nanocomposites at various PMMA-g-NP loading levels are shown in Figure B.5 in Appendix B.

The scattering data for each nanocomposite sample were corrected by subtracting the average intensity of a virgin (unfilled) PMMA FFF-printed specimen. (The scattering curves for each nanocomposite sample are scaled to the average PMMA curve, which means the WAXS signal disappears after subtracting the PMMA reference.) SAXS data were then modeled using Porod's law, the Unified Fit,[64,99] and a hard-sphere structure factor. Porod's law and the Unified fit are shown in Equation 3.1:

$$P(q) = B_1 q^{-P_1} + B_2 (q^*)^{-4} + G_2 \exp\left(\frac{-q^2 {R_{g2}}^2}{3}\right) \quad (3.1)$$

B_1 and P_1 are the power-law prefactor and Porod exponent for larger-scale structures, such as nanoparticle clusters, which produce scattering at low q. The parameters B_2, G_2 and R_{g2} are the power-law prefactor, Guinier prefactor and radius of gyration of the primary structure (i.e., nanoparticles), where $q^* = q/\left[\mathrm{erf}\left(qR_{gi}/6^{1/2}\right)\right]^3$. As described by Kumar *et al.*, polymer grafted nanoparticles are expected to behave as objects with well-defined interfaces, thus the high-q Porod exponent value for the primary particles was constrained to 4 in all cases.[101] If the nanoparticles are well-dispersed, then the scattering intensity is $I(q) = P(q)$.[79,121] However, while this approach could fit the SAXS data, the optimized value of R_{g2} was nearly double the expected value. Therefore, the model was amended to include a hard-sphere structure factor, as seen in Equation 3.2:

$$I(q) = P(q)S(q) \tag{3.2}$$

The hard-sphere structure factor, $S(q)$, is a function of the hard-sphere radius (R_{hs}) and the nanoparticle volume fraction within a cluster (φ).[66,99,124] Data were analyzed in Matlab using nonlinear regression with a Cauchy weighting function to optimize the 7 unknown parameters. The parameters of most interest from this analysis are P_1, R_{g2}, R_{hs}, and φ, and these characterize the types of interactions among nanoparticles in the composites. First, the power-law exponent P_1 helps to classify the larger-scale structure: $3 < P_1 < 4$ indicates surface fractal scattering, while $P_1 < 3$ indicates mass fractal scattering.[66] Second, for a spherical particle, the radius is calculated from $R = \sqrt{5/3}\,R_{gi}$. Third, the parameter R_{HS} quantifies the distance of closest approach between particles. Finally, the parameter φ is the local volume fraction of particles (in a cluster), which may deviate from the bulk composition.

3.4 Results and Discussion

Poly(methyl methacrylate)-grafted nanoparticles (PMMA-g-NPs) were synthesized and characterized, and then incorporated in PMMA filaments. Specifically, PMMA chains recovered after HF cleaving were found to have an M_n = 31,000 g/mol and Đ = 1.4. (GPC trace displayed in Figure B.2 in Appendix B) With this information, the grafting density of chains, σ, was determined from the mass loss determined by TGA. Figure B.3 in Appendix B presents TGA for "bare" Si NPs, CTA-modified NPs and PMMA-g-NPs. Following protocols by Jayaraman *et al.*, we find σ_{pmma} = 0.07 chains/nm^2.[125]

It is well-established that the spatial distribution of nanoparticles has a significant impact on the performance of polymer nanocomposites.[15,20,101] For instance, well-dispersed nanoparticles and a variety of anisotropic nanostructures, such as strings and sheets, are demonstrated to enhance the mechanical properties of polymer nanocomposites.[20,59,126] On the other hand, the presence of agglomerated structures are observed to degrade the mechanical properties of polymer nanocomposites.[9] Nanoscale organization and the resultant material properties of polymer nanocomposites are attributed to a complex interplay between interfacial interactions between the polymer matrix and nanoparticles.[20] Therefore, to assess how the mechanical properties of FFF-printed PMMA parts are affected by the addition of PMMA-g-NPs, it is imperative to examine how nanoparticles are organized within the polymer matrix and investigate polymer-particle interactions.

The nanoscale organization of PMMA-g-NPs in PMMA parts printed by FFF are examined with SAXS. SAXS is a popular technique for examining the hierarchical

structure in polymer-based nanocomposites. These data cannot be "inverted" to a real-space picture, so analysis relies on building a model to describe the scattering and then optimizing the model parameters to achieve agreement with the experiment. Figure 3.1 displays the average trace of all SAXS measurements at each PGNP loading (open symbols) and the corresponding fit (solid line) to the model described by Equations 3.1 and 3.2. Table 3.1 reports the optimized model parameters based on fits of at least 12 independent measurements at each particle loading, and the distributions for each parameter are shown in Figures B.6 in Appendix B.

In all samples, the average particle radius (R) is approximately 7 nm, which is the expected value based on manufacturer specification and our prior work.[79,101,121] The hard-sphere radius (R_{HS}), which characterizes the distance of closest approach between two particles in a larger fractal structure, is approximately 8.5 nm. The average Porod exponent P_1, corresponding with the power-law behavior at low q, is approximately 3 for all loading levels. This value marks the transition from mass fractal to surface fractal behavior. However, the average value of P_1 is misleading for nanoparticle loadings of 0.1 and 0.3 wt%, as the distributions are trimodal and bimodal, respectively, as seen in Figure S6. This implies that the hierarchical arrangements of nanoparticles at low loadings is somewhat heterogeneous, and some regions are dominated by surface fractals while others are dominated by mass fractals. Such heterogeneities are difficult to examine more quantitatively with SAXS, as they are too large to be directly detected. The average volume fraction of nanoparticles within the fractal structure increases with particle loading, but the distribution is very broad, so this outcome should be interpreted with caution.

In my prior work, I examined the structure of bare silica NPs in PMMA at loading

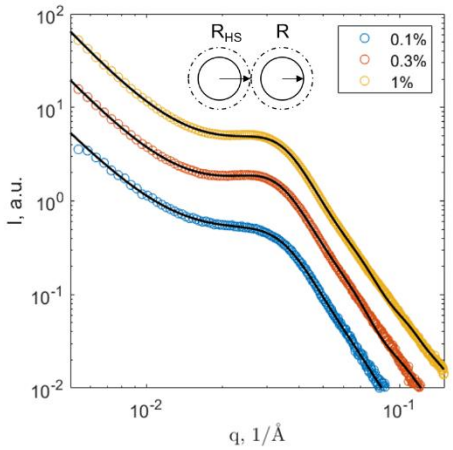

Figure 3.1. Average of all SAXS profiles for each PMMA-g-NP loading level (open symbols) and best-fit to the model described by Equations 3.1 and 3.2.

Table 3.1. Optimized model parameters based on fits of at least 12 independent measurements at each particle loading level. P_1 is the Porod exponent for the low-q region, R is the particle radius, R_{HS} is the hard sphere interaction radius, and φ is the volume fraction of particles in a cluster. independent measurements, and the uncertainty is reported as ± 1 standard deviation.

Loading Level	***R* (nm)**	***R*$_{HS}$ (nm)**	**P$_1$ (low-*q*)**	φ
0.1 wt% PMMA-g-NPs	7.2 ± 0.3	8.4 ± 0.3	3.0 ± 0.4	0.13 ±0.02
0.3 wt% PMMA-g-NPs	7.1 ± 0.3	8.6 ± 0.3	2.8 ± 0.3	0.15 ± 0.03
1.0 wt% PMMA-g-NPs	7.1 ± 0.2	8.6 ± 0.2	3.0 ± 0.1	0.17 ± 0.02

[a] Large uncertainties in low-*q* power law reflect multimodal distributions, as seen in Figure B.6. (See Appendix B.)

levels from 0.1 wt% to 1 wt%, and all SAXS data were consistent with a model for well-dispersed mass fractals.[121] In contrast, incorporating PMMA-g-NPs in FFF-printed PMMA parts at comparable loading levels results in the formation of a larger hierarchical structure, as evident by the increase in the low-*q* exponent from 2 to 3. Although the incorporation of PMMA-g-NPs results in the formation of larger structures, we note that the SAXS results show that both the primary particle size (~7 nm) and low-*q* power law exponent (3) are independent of particle loading, which indicates that the size of the nanostructure is not impacted as the loading level increases.[101] These results – a low-*q* power law exponent of 3 for all loading levels for PMMA-g-NPs – align with previous reports by Kumar *et al*. that focused on the nanoscale organization of polymer-grafted NPs dispersed in a chemically similar polymer matrix.[79,101] Specifically, they observed surface fractals (low-*q* exponents of 3) for nanocomposites (either PMMA or polystyrene) having a low (<1) graft to matrix chain length ratio at numerous grafting densities (0.05 – 0.12 chains/nm^2).[79,101] Furthermore, they determined that these surface fractal nanostructures consist of connected sheets of 3-5 particles each that span up to 1-10 μm. Based on morphology diagrams for polymer-grafted nanocomposites, the grafting density (0.07 chains/nm^2) and graft to matrix chain length ratio (0.3) used here suggests that our PMMA-g-NPs will organize in connected sheets throughout the polymer matrix.[20,79,100,101] Based on this supposition and the results from SAXS, I infer that even after the non-equilibrium, non-isothermal FFF print process used to create these samples, PMMA-g-NPs in FFF-printed PMMA parts are organized as surface fractals, or connected sheets, throughout the PMMA matrix.

Rheometric studies using low-amplitude oscillatory-shear measurements were completed to investigate how increasing the loading level of PMMA-g-NPs affects the

linear viscoelastic properties of FFF-printed nanocomposites. The following discussion will focus on how the storage modulus, G'(ω), and complex viscosity, |η*|, are affected by the addition of PMMA-g-NPs because it is well-known that the these properties are more sentient to changes in the melt flow characteristics of polymer nanocomposites.[83,84,121] The angular frequency dependent storage modulus and complex viscosity master curves, which are generated by time-temperature superposition, are displayed in Figure 3.2A and 3.2B, respectively. Specifically, Figure 3.2A compares the storage modulus of PMMA printed parts containing no filler (pure) and nanocomposite samples containing PMMA-g-NPs at a 0.1 wt% and 1.0 wt%. The G'(ω) curve for pure (unfilled) PMMA exhibits the typical response for an unfilled entangled melt: Specifically, an elastic response is observed at high frequency while a viscous response is displayed at low frequencies.[127] Moreover, the pure PMMA sample exhibits a high-frequency power law exponent of ½, which is expected for an entangled melt, but deviates from the power-law dependency of 2 expected for a monodisperse, entangled melt at low frequencies. This is due to the fact that the PMMA resin utilized here has a large dispersity (Đ = 1.5); thus the characteristic behavior for a monodisperse melt should not be expected.

When PMMA-g-NPs are incorporated in PMMA parts printed by FFF, a noticeable increase in the G'(ω) response is observed across all frequencies. Enhancements in G'(ω) are indicative of interfacial interactions between polymer matrix chains and nanoparticle additives that alter the relaxation dynamics of the matrix polymer.[91,121,127] As expected, increasing the loading level of PMMA-g-NPs by an order of a magnitude (0.1 wt% to 1.0 wt%) increases the number density of interactions, conveyed through either interdiffusion or entanglements between the polymer matrix and polymer graft, which results in an

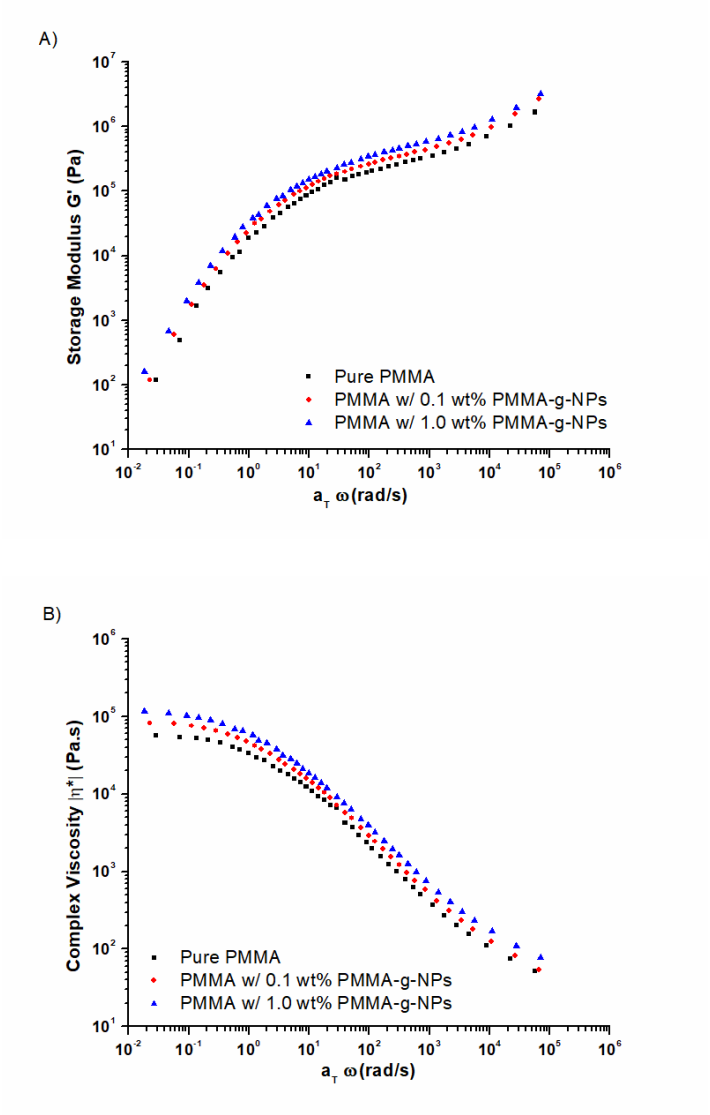

Figure 3.2. Rheological measurements show that increasing the loading level of PMMA-g-NPs in FFF-printed PMMA parts increases both the storage modulus (A) and complex viscosity (B). A reference temperature of 170 °C was used to create time-temperature superposition master curves displayed here.

increase in the melt response. Specifically, at intermediate frequencies (ωa_T > 10 rad/s), G'(ω) increases as the PMMA-g-NP loading level increases. Increases in the storage modulus at intermediate frequencies are attributed to elastic reinforcement provided by the presence of polymer-grafted Si NPs.[127] Moreover, all samples exhibit a liquid-like response in the terminal regime, and samples containing PMMA-g-NPs exhibit the same high-frequency and low-frequency power law exponents as pure PMMA. This type of behavior is expected for polymer nanocomposites containing spherical additives as previous research efforts have determined that a solid-like response does not develop until ~2.5 vol%.[89,90,128] Thus, a liquid-like response is expected since PMMA-g-NP loadings of 0.1 wt% and 1.0 wt% correspond to 0.04 vol% and 0.4 vol%, respectively. However, even though all samples display a liquid-like response in the terminal regime, increasing the loading level of PMMA-g-NPs is demonstrated to increase the G'(ω) response in the terminal region. These results align with previous research efforts investigating the rheological response of polymer-grafted nanoparticles assembled in surface fractal nanostructures.[101,127]

Specifically, Kumar *et al*. observed that the elastic response of polystyrene-grafted nanocomposites having a connected sheet nanostructure increased as the loading level increased from 0.5 to 5.0 wt%.[101] Increases in the G'(ω) response were attributed to interfacial interactions involving graft chains with the graft chains of neighboring polymer-grafted particles and graft chain interactions with polymer matrix chains. Coupling assessments of SAXS and melt rheology, I infer that the PMMA-g-NPs utilized herein organize in connected sheet nanostructures throughout PMMA printed parts. While these nanocomposites do not display a solid-like response, it is apparent that increasing the

loading level of PMMA-g-NPs increases the elastic response. The gradual increase in the G'(ω) response as a function of loading level is attributed to increases in the number density of interfacial interactions between graft chains with graft chains on adjacent particles and with polymer matrix chains.

Furthermore, frequency-dependent complex viscosity curves, which are presented in Figure 3.2B, show a monotonic increase in the complex viscosity of FFF-printed nanocomposites as the loading level of PMMA-g-NPs increases. Increases in |η*| are suggestive of favorable interfacial interactions between the polymer matrix and nanoparticle that alter the relaxation dynamics of the matrix polymer.[91,121] This observation – an increase in the complex viscosity as the loading level of PMMA-g-NPs - is expected because increasing the loading level by an order of magnitude (0.1 wt% to 1.0 wt%) should increase the number of interfacial interactions between the polymer graft and matrix polymer. Although |η*| increases as the nanoparticle content increases, all sample patterns behave similarly. Specifically, at low frequencies the formation of a plateau is present, while at high frequencies all samples exhibit the non-Newtonian behavior of shear thinning.

To assess how the incorporation of PMMA-g-NPs into FFF-printed PMMA parts impacts the thermomechanical properties, such as the glass transition temperature (T_g) and the storage and loss moduli, dynamic mechanical analysis (DMA) using a constant-strain temperature ramp protocol were completed. As seen from the temperature dependence of tan δ, which is presented in Figure 3.3A, the T_g of FFF-printed nanocomposites increases as the loading level of PMMA-g-NPs increases. (As noted previously, the maximum in the normalized dissipation factor tan δ is assigned as the T_g,[63] and values are shown in the

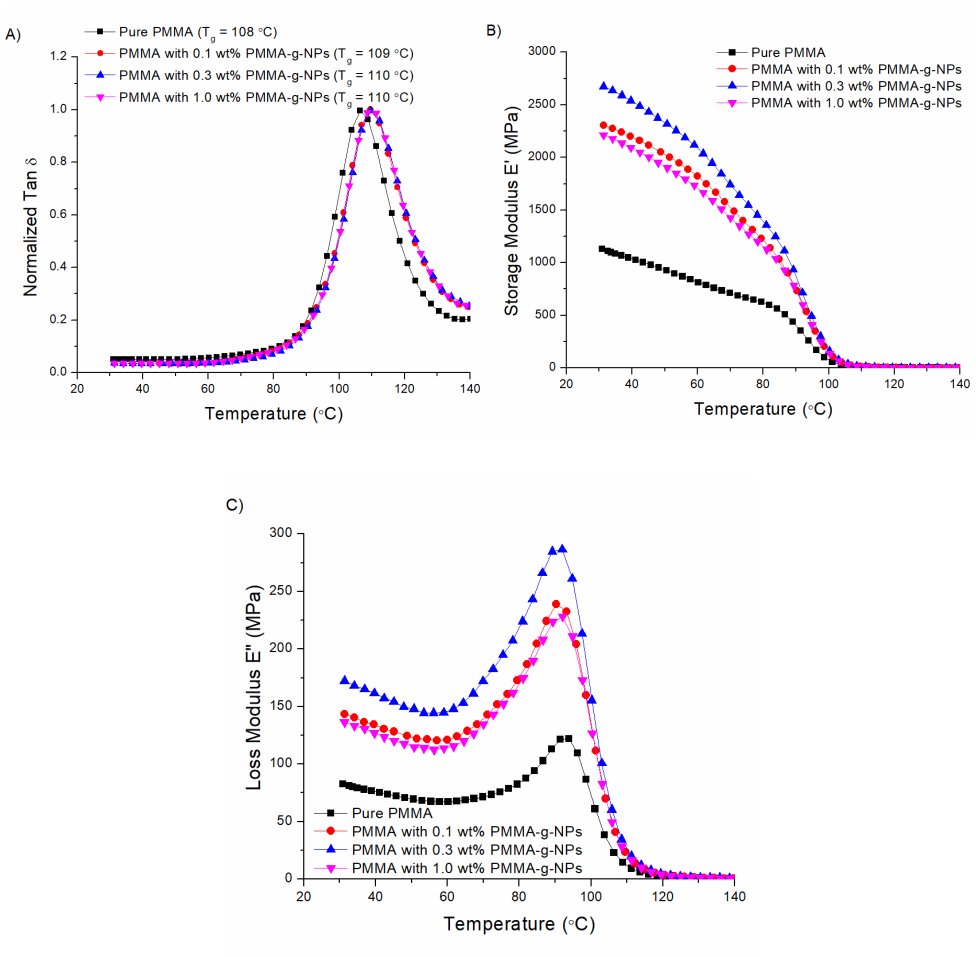

Figure 3.3. Constant-strain temperature ramp measurements show that the glass transition temperature (A), storage modulus (B), and loss modulus (C) of nanocomposite PMMA parts containing PMMA-g-NPs increase with increasing filler content.

legend of Figure 3.3A.) Deviations from bulk T_g values for polymer nanocomposites are attributed to interfacial interactions between the additive and polymer matrix that alter chain dynamics within the interfacial zone, which manifest as a change in the T_g of the nanocomposite.[9,74] More specifically, depressions in bulk T_g values are attributed to repulsive interactions,[9,74,75] while increases from bulk T_g values suggest favorable interactions between the nanoparticle and polymer.[74,76–78] As seen from the normalized tan δ curves displayed in Figure 3.3A, relative to the bulk T_g value for pure (unfilled) FFF-printed PMMA (108 °C), as the loading level of PMMA-g-NPs increases to 1 wt% the T_g of the nanocomposite increases to 110 °C. These results compliment rheology measurements, which suggest that increases in melt rheology were due to interfacial interactions involving graft and matrix chains. Furthermore, these results are consistent with those reported by Dubois *et al.*, who observed increases in the T_g of poly(ε-caprolactone) nanocomposites as the loading level of polymer-grafted cellulose nanocrystals increased. As described by Dubois *et al.*, increases in the T_g of nanocomposites suggests that interfacial interactions, such as interdiffusion and entanglements between the graft and polymer matrix chains, restrict the molecular motions of polymer matrix chains, resulting in an increase in the T_g.[129]

Furthermore and as seen in Figure 3.3B and 3.3C, increasing the loading level of PMMA-g-NPs up to 0.3 wt% increases both the storage, E', and loss, E", moduli of FFF-printed PMMA nanocomposites. Specifically, compared to virgin PMMA samples, a 120% increase in E' and a 118% increase in E" is observed in the glassy regime when PMMA-g-NPs are incorporated at a 0.3 wt% loading level. These results are consistent with previous research efforts that examined how the thermomechanical properties of polymer

nanocomposites are affected by the addition of polymer-grafted nanofillers.[129,130] For example, Shi *et al.*, observed a 14% increase in the storage modulus when PMMA-g-NPs were incorporated in poly(vinyl chloride) at a 2.5 wt% loading level, while Goh *et al.*, observed a 50% increase in the storage modulus of poly(vinylidene fluoride) nanocomposites containing PMMA-g-NPs at a 0.42 wt%.[130,131] As described by Schadler *et al.*, increases in E' for polymer nanocomposites containing surface-modified additives is indicative of favorable particle-polymer interactions that enhance the stress-transition from the polymer matrix to the nanoparticle additive thereby providing material reinforcement.[132] The combination of DMA results and assessments from rheology support this interpretation.

To assess the effect of incorporating PMMA-g-NPs into PMMA filaments on the macroscopic properties of parts printed by FFF, DMA strain-sweeps and tensile tests were completed. Representative DMA stress-strain curves displayed in Figure 3.4 show that compared to parts printed with pure (unfilled) PMMA, the Young's modulus increases when PMMA-g-NPs are incorporated in PMMA printed parts. While Figure 3.4 shows one set of representative samples, average values of Young's modulus are ~50% higher at all loading levels of PMMA-g-NPs, with the greatest increase (61%) in the Young's modulus observed at 0.3 wt%. As suggested by Kumar *et al*., increases in the Young's modulus for nanocomposites containing particulate additives are expected in the linear response regime because the nanocomposite blends the properties of hard and soft matter.[100]

In addition to DMA strain-sweep measurements that examine the linear response regime, tensile tests were used to investigate how the addition of PMMA-g-NPs impacts the extensional properties of FFF-printed PMMA nanocomposites that are strained to

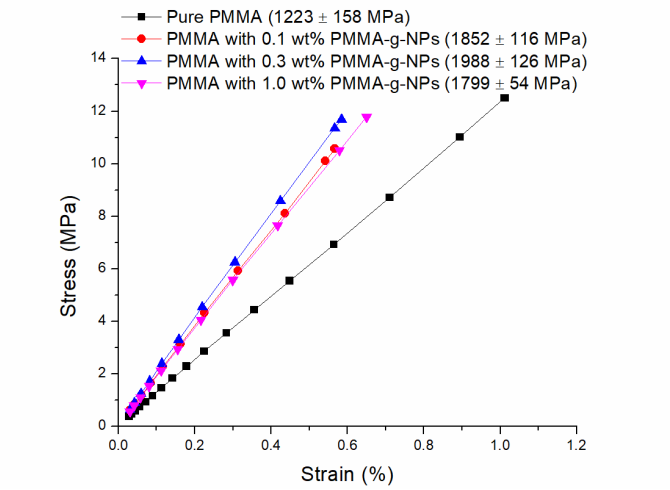

Figure 3.4. DMA results show that all samples display a significant increase in the Young's modulus even at low loading levels (≤ 1.0 wt% based on Si), with the largest increase (61%) observed at 0.3 wt%. Values of the Young's modulus given in the legend are based on measurements of five replicate samples and the corresponding standard deviation.

macroscopic failure. Tensile measurements show an increase in the tensile modulus and ultimate tensile strength (UTS) as the loading level of PMMA-g-NPs increases as displayed in Figure 3.5. These results are similar to the behavior observed from DMA measurements. As seen in Figure 3.5, all samples display analogous deformation patterns regardless of the PMMA-g-NP loading level. The samples exhibit elastic deformation followed by yielding and then stain-hardening. This pattern of behavior has been observed previously for FFF-printed materials containing nanoparticles,[121] and as stated by Vaia *et al.*, when nanocomposite deformation patterns are similar to that of the unfilled polymer, regardless of the additive loading level, it indicates that the macroscopic deformation process is predominantly governed by the matrix polymer.[133] Given the low loading levels used

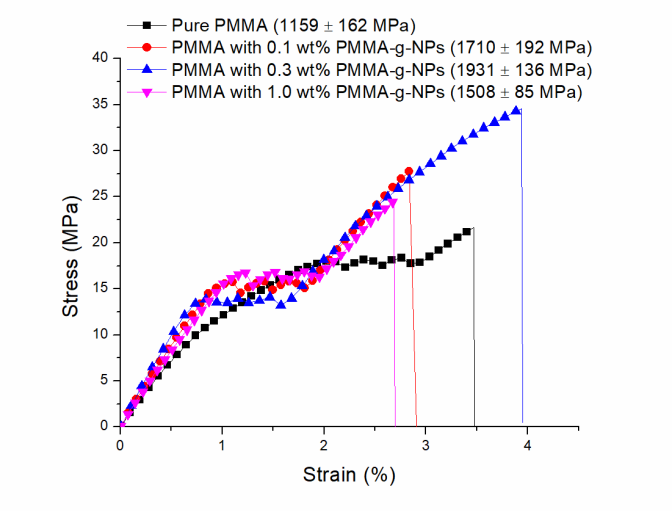

Figure 3.5. Representative tensile tests show an increase in the tensile modulus and UTS as the loading level of PMMA-g-NPs increases. While the sets of data shown are from single measurements, values of the tensile modulus given in the legend are based on measurements of five replicate samples.

herein, this is a reasonable conclusion. Nevertheless, while the nanocomposites have identical deformation patterns, the addition of PMMA-g-NPs into PMMA has a considerable impact on the mechanical properties of parts printed by FFF. For instance, as compared to unfilled PMMA, increasing the loading level of PMMA-g-NPs up to 0.3 wt% (based on Si wt%) increases the tensile modulus by 52% and the UTS by 116%. Increases in the tensile modulus and UTS of polymer nanocomposites are generally attributed to favorable interactions between the inorganic additive and polymer matrix. For instance, increases in the UTS of polymer-grafted nanocomposites are attributed to increases in the number density of interfacial interactions between graft chains and matrix chains, which improve the polymer-grafted nanocomposites ability to dissipate stress.[79,101,105,134]

Although both the UTS and tensile modulus increase with increasing PMMA-g-NP content, the elongation at break remains essentially unaffected. Some researchers report that the addition of nanoparticles decreases the elongation at break, while others observe increases in the elongation at break when nanoparticles were added.[9,69–72,121] As a result of these diverging reports and to avoid speculation, an explanation for the elongation at break values is not provided.

Overall, the results obtained from DMA measurements and from tensile tests clearly indicate that incorporating PMMA-g-NPs in PMMA resin to create nanocomposite filaments increases the mechanical properties of FFF-printed specimens. The average values from DMA and tensile measurements are reported in Table 3.2. As seen in Table 3.2, the mechanical properties increase as the loading level of PMMA-g-NPs increases, and there is a signature of an optimal loading level. Additionally, results from DMA strain-sweep and tensile measurements agree with constant-strain temperature ramp measurements. For instance, all measurements exhibit an increase in the modulus as the loading level of PMMA-g-NPs incorporated into FFF-printed PMMA nanocomposites increases. Additionally, the pattern of increasing modulus as the loading level of PMMA-g-NPs increases up to 0.3 wt% is observed across multiple measurement techniques.

These macroscopic assessments demonstrate how molecular engineering, conveyed by tailoring polymer-particle interactions at the nanoscale via polymer-decorated nanoparticles, dictates the macroscopic performance of FFF-printed parts. Coupling these assessments with SAXS and rheology results allow inferences to be made regarding the mechanism of reinforcement. Specifically, SAXS results indicate that the nanostructure does not change as the loading level of PMMA-g-NPs increases, but increasing the loading

Table 3.2. Mechanical properties of PMMA nanocomposite samples containing PMMA-g-NPs manufactured by FFF.[a]

Loading Level[b]	Ultimate Tensile Strength (MPa)	Tensile Modulus (MPa)	Elongation at break (%)	Young's Modulus (MPa)
Pure PMMA	18 ± 3	1159 ± 162	2.3 ± 0.9	1223 ± 157
PMMA w/ 0.1 wt% PMMA-g-NPs	30 ± 4	1710 ± 192	2.7 ± 0.1	1852 ± 116
PMMA w/ 0.3 wt% PMMA-g-NPs	39 ± 5	1931 ± 136	3.1 ± 0.7	1988 ± 126
PMMA w/ 1.0 wt% PMMA-g-NPs	25 ± 1	1508 ± 85	2.6 ± 0.1	1799 ± 54

[a]All values (average ± the standard deviation) result from measurement of 5 replicate samples.

[b] Loading level based on wt% of Si.

level of PMMA-g-NPs has an observable impact on the rheological response. These sets of results suggest that the nanostructure of all nanocomposites are organized in connected sheets (surface fractals) and increasing the loading level by an order of a magnitude (0.1 wt% to 1.0 wt%) increases the number density of interfacial interactions between graft chains with neighboring polymer-decorated particles and matrix chains. Increases in the number density of interactions within the particle network are demonstrated to enhance stress-transmission from the polymer matrix to the nanoparticle additives, which provide mechanical reinforcement as seen in DMA and tensile tests. These inferences align with a previous report by Kumar *et al*., who demonstrated that polystyrene-g-NPs arranged in surface fractals participate in interfacial interactions with matrix chains and the graft chains on surrounding particles.[101] While a percolated network is not observed here, we similarly

infer that interfacial interactions, conveyed as entanglements and interdiffusion across the polymer matrix/additive interface, allow stress to be dissipated to particle clusters within the nanocomposites which increase the performance of FFF-printed parts.[101]

Although the incorporation of polymer grafted nanoparticles improves the material properties of 3D printed parts, the decrease in the mechanical properties observed when loading level of PMMA-g-NPs increases to 1.0 wt% suggests there is an optimal loading level. This pattern of behavior – the presence of an optimal loading level that maximizes mechanical properties –has been reported in various nanocomposite studies.[9,135–137] As described by Schadler *et al.*, a drop off in performance observed at higher loading levels is attributed to the formation of an agglomerated state.[9] The presence of a large agglomerated state could be present at 1.0 wt% but the size of these structures cannot be detected from the q-range covered by SAXS. Therefore, additional research utilizing USAXS and higher loadings levels than 1.0 wt% are needed to clarify the reason for the relative decrease in performance.

It is useful to frame the impact of the technological innovation manifest in the approach and results by comparing the results reported here to those of observed in our previous effort when bare (unfunctionalized) Si NPs were incorporated into FFF-printed parts. Specifically, SAXS results demonstrate that PMMA-g-NPs arrange in larger, connected sheets compared to bare (unfunctionalized) Si NPs that are arrange in well-dispersed mass fractals.[121] Additionally and as seen in melt rheology master curves displayed in Figure B.7 and B8 in Appendix B, compared to bare Si NPs, incorporating PMMA-g-NPs results in significant increases to both the elastic response, G'(ω), and complex viscosity at comparable loading levels. Increases in the melt properties for

nanocomposites containing PMMA-g-NPs are accompanied by a marked improvement in the mechanical properties. For example, at the highest loading level of bare Si NPs previously studied (1 wt%) only a 41% increase in the Young's modulus was observed, whereas incorporating PMMA-g-NPs at 0.3 wt% lead to a 61% increase in the Young's modulus.[121] Furthermore, not only are the improvements in the Young's modulus observed for nanocomposites containing PMMA-g-NPs well above those obtained when bare Si NPs were incorporated, but even the Young's modulus value obtained at the lowest loading level (0.1 wt%) of PMMA-g-NPs surpass those obtained at the highest loading level (1.0 wt%) of bare Si NPs.[121] Additionally, at low loading levels (0.1 wt% and 0.3 wt%), incorporating PMMA-g-NPs led to a noticeable improvement in the UTS, Young's modulus, storage modulus, and loss modulus compared to equivalent loading levels when bare Si NPs were utilized.[121] These results highlight how tailoring interactions on the nanoscale, expressed here by polymer-grafted nanoparticle, can be effectively managed to control the mechanical properties of polymer nanocomposites.

3.5 Conclusions

This research effort demonstrates that the thermomechanical properties of parts manufactured by FFF can be enhanced by tailoring the interfacial interactions between the polymer matrix and additive. Specifically, attaching PMMA chains to silica nanoparticles provides a novel route to increase the number density of interfacial interactions between the polymer matrix and nanoparticle additive, which increases the stress-transfer within the nanocomposite and improves the mechanical properties. This inference is supported by SAXS and rheology measurements, which suggest that PMMA-g-NPs arrange in

connected sheets which dissipate stress through graft chain interactions with the polymer matrix and the graft chains of nearby PMMA-g-NPs. The results reported herein provide proof-of-concept that the thermomechanical properties of parts fabricated by FFF can be enhanced by tailoring the interfacial interactions between the additive and polymer matrix.

CHAPTER 4: SELF-COMPLEMENTARY MULTIPLE HYDROGEN BONDING ADDITIVES ENHANCE THERMOMECHANICAL PROPERTIES OF PMMA STRUCTURES CREATED BY FUSED FILAMENT FABRICATION

This chapter describes work submitted to ACS Macromolecules in 2019. I synthesized all of the copolymer additives and generated all of the printed parts in this work and performed all of the thermomechanical characterizations. Coauthors include William K. Ledford and Abigail A. Allison who helped with filament preparation and additive characterization, Steven Patterson and Jamie M. Messman who completed tensile measurements, Brad Lokitz who helped with instrument training, Deanna L. Pickel who provided insight regarding specimen fabrication, and Prof. S. Michael Kilbey II, who advised this work.

4.1 Abstract

Nonbonded interactions provide a way to guide the assembly and alter the physical properties of soft polymeric materials. Here, self-complementary hydrogen bonding interactions conveyed through polymeric additives dramatically enhance thermomechanical properties of poly(methyl methacrylate) specimens printed by Fused Filament Fabrication (FFF). Random copolymer additives comprised of methyl methacrylate (MMA) and a methacrylate monomer containing 2-ureido-4-pyrimidone (UPy) pendant groups (UPyMA), which self-dimerize through quadruple hydrogen bonding interactions, were incorporated at 1 wt% in a high molecular weight PMMA matrix. Results from dynamic mechanical analysis show that as the UPyMA comonomer content in the p(MMA-r-UPyMA) copolymer additive increases up to 5 mol%, there is a 50% increase in the Young's modulus and a 62% increase in the storage modulus. Concomitantly, there is an 85% increase in ultimate tensile strength and a 100% increase in tensile modulus. Additionally, melt rheology measurements indicate that the storage modulus and complex viscosity of the multicomponent blends are unaffected by the

incorporation of p(MMA-r-UPyMA) additives, regardless of the UPyMA content. In aggregate, these results suggest that using reversible, non-bonded intermolecular interactions, such as multidentate hydrogen-bonding, provides a novel route to overcome the mechanical property limitations of FFF-printed materials without affecting melt processability.

4.2 Introduction

Advances in supramolecular chemistry have fostered the development of tailored polymers that are triggered to organize and assemble by non-bonded interactions. Of the three principle mechanisms used by nature to drive self-assembly – hydrogen bonding, metal ion coordination, and π-stacking – hydrogen bonding interactions are used most often to create responsive or functional polymeric materials.[138] The fact that hydrogen bonding interactions can be broken at elevated temperatures has stimulated the development of a variety of novel thermoresponsive polymers that exhibit excellent mechanical properties at use temperatures and low viscosities during melt processing.[23–27,139,140] One of the first examples along these lines was work by Meijer *et al.*, who described how functionalizing hydroxyl end groups of a telechelic poly(ethylene oxide-co-propylene) copolymer with 2-ureido-4[1*H*]-pyrimidone (UPy) groups impacted thermomechanical properties of the copolymer in the melt state.[28] Specifically, unfunctionalized PEO-co-PPO copolymers were covalently crosslinked through terminal hydroxyl groups and the melt state characteristics were compared to telechelic PEO-co-PPO copolymers functionalized with UPy groups, which crosslink through thermoreversible physical interactions. They showed that in comparison to the covalently crosslinked polymers, PEO-co-PPO copolymers

functionalized with UPy end groups displayed an increase in the plateau modulus, enhanced shear-thinning, and exhibited a rubbery plateau region in the storage modulus. These enhancements were attributed to hydrogen bonding interactions between UPy groups, which are known to self-dimerize in a donor-donor-acceptor-acceptor fashion. They concluded that the reversibility of the self-complementary, tetradentate hydrogen bonding interactions between UPy groups allows the copolymers to assemble efficiently, creating a more interconnected, thermodynamically stable network. On the other hand, covalent crosslinking of the unfunctionalized copolymer is irreversible, leading to a kinetically hindered network.[28]

In addition to attaching UPy groups to polymer chain ends, Meijer *et al.* also examined how varying the interaction strength of hydrogen bonding groups impacted the properties of telechelic oligomers.[141–143] For example, they investigated how the melt state properties of telechelic PEO-co-PPO systems were affected when terminal hydroxyl groups were either covalently crosslinked, modified with urea groups, or modified with UPy (which has a high self-dimerization constant). In comparison to the covalently crosslinked copolymer, they found that telechelic copolymers modified with hydrogen bonding groups exhibit a higher plateau modulus due to the formation of a highly interconnected, thermodynamically stable network. However, even though UPy or urea-functionalized copolymers created a thermally-reversible, hydrogen bonding network, the bulk viscosity of copolymers modified with urea was noticeably higher than those containing UPy groups. Meijer *et al.* attributed this behavior to differences in the hydrogen bonding interactions that lead to the formation of two distinct polymer networks. Specifically, they determined that copolymer systems with urea groups organize in

microphase separated, hydrogen bonding arrays, while those with UPy groups dimerize in a unidirectional, end to end arrangement.[141]

These seminal reports stimulated numerous studies that examine how incorporating self-complementary multiple hydrogen bonding (SCMHB) groups along the backbone of macromolecules impact the resultant thermomechanical properties.[144–147] For example, Long *et al.* investigated how the thermomechanical properties of random copolymers containing 2-ethylhexyl methacrylate and 2-ureido-4[1*H*]-pyrimidone methacrylate (UPyMA) were affected as the UPyMA comonomer content increased. The role of noncovalent associations on properties were probed by tensile tests, creep compliance measurements, and melt rheology. They showed that the tensile strength increased by 400% as the UPyMA comonomer content increased to 3 mol%. Moreover, storage modulus master curves obtained from rheology measurements show that the plateau modulus was elevated and lengthened significantly as UPyMA comonomer content increased. Improvements in the thermomechanical properties of these copolymers were attributed the formation of a physically crosslinked material due to self-complementary, multiple hydrogen bonding of UPy groups, which have a high self-dimerization constant.[23] Additionally, Coates *et al.* examined how the mechanical properties of polyolefin films were affected as the comonomer content of a UPy-containing 1-hexene derivative increased from 0 mol% to 2 mol%.[147] Specifically, they synthesized polyolefins by copolymerizing 1-hexene and a 1-hexene derivative containing a terminal UPy-group. As compared to homopolymer films of poly(1-hexene), copolymer films containing UPy motifs displayed a 1600% increase in the ultimate tensile strength at a UPy comonomer content of 2 mol%. This increase was attributed to physical crosslinks between UPy groups,

which inhibits polymer chains from moving past one another during deformation. As a result, the amount of stress required to deform the films increased significantly.

Inspired by these research efforts, with this work I detail for the first time how the addition of copolymers containing UPy groups provide reinforcement to 3D-printed parts made by FFF. It is well known that polymeric structures created by FFF exhibit inferior properties compared to monolithic structures fabricated by conventional processing methods such as injection molding or blow molding. Moreover, although the FFF process relies on melt extrusion, rapid cooling of the printed bead gives rise to exceptionally weak interfaces because chains from adjacent beads do not have time to entangle across bead interfaces before cooling below their glass transition temperature. Motivated by these issues and the potential for reinforcement through supramolecular assembly across bead interfaces, I systematically examine how increasing the composition of p(MMA-r-UPyMA) additives affects the mechanical and thermal properties of PMMA-printed parts. While melt rheology suggests that the thermoreversible nature SCMHB negates any impact on processing of the blends, assessments of macroscale performance indicate that the self-dimerization of the UPy groups in the random comonomer additive is responsible for significant increases in thermomechanical properties of FFF-printed parts. These fundamental studies suggest that multiplexed nonbonded interactions can be used to enhance the thermomechanical properties of parts created by the non-isothermal, non-equilibrium FFF process.

4.3 Experimental Methods

4.3.1 Materials and Copolymer Synthesis

Materials. To remove the inhibitor, methyl methacrylate (MMA) (Aldrich, 99%) was passed through a basic alumina column. 2,2'-Azobis(2-methylpropionitrile) (AIBN, Aldrich, 98%) was recrystallized from methanol. Atactic poly(methyl methacrylate) beads (Polysciences Inc., MW = 100,000 g mol^{-1}) were heated *in vacuo* at 100 °C before use. All other materials were used as received unless specifically stated otherwise.

Monomer and Copolymer Syntheses. The self-dimerizing hydrogen bonding monomer, 2-ureido-4[1*H*]-pyrimidone methacrylate (UPyMA), was synthesized according to protocols described by Long *et al*.[23,27] In a typical procedure, 54.80 g (35.4 mmol) of 2-isocyanatoethyl methacrylate and 40.18 g (32.1 mmol) of 2-amino-4-hydroxy-6-methylpyrimidone were added into a flame-dried 250 mL round bottom flask containing 200 mL of DMSO under an argon atmosphere. (Note: as suggested by Long *et al*., 2-amino-4-hydroxy-6-methylpyrimidine was heated overnight *in vacuo* at 100 °C before use.[23,27]) The round bottom flask was immersed in an oil bath pre-heated to 150 °C for 30 minutes and then it was removed and allowed to cool to room temperature, which causes the product, UPyMA, to precipitate from solution. The solid product was isolated by vacuum filtration, rinsed with methanol to remove residual DMSO and starting materials, and then dried at room temperature *in vacuo* overnight. The UPyMA monomer was characterized by ^{1}H NMR. (See Figure C.1 in Appendix C.)

Random copolymers consisting of MMA and UPyMA comonomers were synthesized via free radical polymerization. The preparation of a copolymer targeted to be 3 mol % UPyMA is offered as an example: First, 1.75 g (17.5 mmol) of MMA and 156 mg

(0.562 mmol) of UPyMA were added to a 100 mL round bottom flask containing 4 mg (0.0225 mol) of AIBN dissolved in 50 mL of THF and a magnetic stir bar. The flask was sealed with a rubber septum, the contents were sparged with argon, and then the flask was lowered into an oil bath pre-heated to 60 °C. After 24 h, the reaction was quenched by immersing the flask in liquid nitrogen. Once the reaction mixture thawed, it was filtered to remove any undissolved UPyMA monomer. The filtrate was precipitated into chilled hexanes and the solid copolymer was collected and dried overnight *in vacuo* at 30 °C. The molar composition and molecular weight of the p(MMA-r-UPyMA) additives were determined via ^{1}H NMR and GPC and results are presented in Figure C.2 and Figure C.3, respectively, as seen in Appendix C. Copolymers having different compositions were made by adjusting the ratio of MMA:UPyMA while keeping the total monomer concentration constant at 18.1 mmol. Throughout the manuscript, the p(MMA-r-UPyMA) copolymers are referred to by the UPyMA comonomer feed composition.

4.3.2 Extrusion of Filament and FFF

Filament Preparation. To create multicomponent PMMA filaments containing the SCMHB copolymer additive, PMMA beads were combined with the UPyMA-containing copolymer at 1 wt% loading with respect to the copolymer additive. A 1 wt% additive loading level was chosen based on the view that additives should be effective at low levels as well as my previous research involving nanocomposite filaments.[121] Due to the capacity of the extruder, 400 mg of the p(MMA-r-UPyMA) additive was added to 39.6 g of PMMA beads and the mixture was blended at high speed using a Magic Bullet® 250 W. This mixture was added to the hopper and extruded through a 2.85 mm circular die using a

Filabot EX2 extruder. The Filabot EX2 extruder is a single screw with one heating zone and an L/D ratio of 10:1. Multicomponent filaments were extruded with the heating zone set to 180 °C and a screw speed of 25 RPM. After extrusion, the diameter of the multicomponent filaments was measured with calipers at numerous locations to verify that the filament diameter varied by < 0.2 mm.

3D Printing of Test Specimens by FFF. A Lulzbot Mini 3D printer was used to fabricate PMMA specimens containing p(MMA-r-UPyMA) additives. DMA and tensile specimens conforming to ASTM D7028 and ASTM D638 (standard V) specifications, respectively, were generated using Autodesk® AutoCad® 2017s (student version). Once a template was created in AutoCad, the file was exported as an STL file and then imported into the Cura software used by the Lulzbot for 3D printing. At least five samples of each type (DMA and tensile bars) were printed for each testing method. Specimens were printed in the x-y plane using an extrusion temperature of 240 °C and a bed temperature of 110 °C. Samples were fabricated using a +45/−45 raster angle and the printer settings were as follows: 0.5 mm nozzle size, 0.425 mm initial layer thickness, 0.25 mm layer height with a 100% fill density. (The remaining settings were left at standard values for ABS established by the Cura software.) The print bed was allowed to cool to room temperature prior to sample removal to minimize deformation prior to mechanical testing.

4.3.3 Instrumentation and Characterization

^{1}H NMR spectra of random copolymers in deuterated chloroform at 25 °C were obtained using a Varian VNMRS 500MHz spectrometer. Number-average molecular weight, M_n, and dispersity, Đ, of each copolymer were determined at 25 °C using an

Agilent 1260 Infinity II GPC using THF at a flow rate of 1.0 mL/min as the mobile phase. The Agilent GPC was equipped with a Wyatt Dawn® Helios® 8 Multi-Angle Light Scattering Detector, ViscoStar® III, and an Optilab® T-rEX™. Molecular weights reported herein are obtained via conventional calibration analysis using polystyrene standards. The glass transition temperature, T_g, of each copolymer additive was measured using a TA Instruments Q-2000 Differential Scanning Calorimeter. In a typical procedure, 5-10 mg of the copolymer was sealed in an aluminum pan, which was subjected to a heat/cool/heat cycle from 50-160 °C at a rate of 10 °C/min. T_g values are reported as the midpoint of the transition recorded on the second heating ramp. A MTS Criterion Model 43 Test System equipped with a 10 kN load cell was used for tensile measurements. Tensile testing adhered to the ASTM D638 standard, which utilizes a 1 mm/s elongation rate and a grip separation distance of 25.4 mm.

A TA Instruments DMA Q800 equipped with a dual cantilever clamp was utilized to investigate the thermomechanical properties of FFF-printed multicomponent blends. To determine the Young's Modulus, the samples were first equilibrated at 30 °C and then subjected to a constant-frequency strain sweep using a frequency of 1 Hz while completing an amplitude sweep from 20 to 2000 μm. Storage and loss moduli and T_g were determined from constant-strain temperature ramp experiments using a 0.1% strain and a temperature ramp from 30 to 140 °C at 10 °C/ min. T_g values are reported as the peak maximum of tan δ. The frequency-dependent complex viscosity and storage modulus of FFF-printed multicomponent blends were determined using a TA Instruments Discovery Hybrid Rheometer-3. For these measurements, a constant-strain frequency sweep was completed

at various temperatures to construct master curves via time-temperature superposition. Specifically, an FFF-printed sample was equilibrated at 180 °C and then the molten polymer was compressed between parallel plates (25 mm diameter) to set an interplate gap of 1000 μm. Next, a series of frequency sweeps from 0.1 to 100 Hz using a strain of 0.1% were completed at various temperatures, beginning at 180 °C and decreasing to 130 °C using decrements of 10 °C. Frequency-dependent master curves were created using time-temperature superposition analysis (using the TRIOS software provided by TA Instruments). The master curves displayed later in this *Article* were generated by setting the reference temperature of the frequency sweeps to 180 °C and the shift factors, a_t (WLF type), used to construct the frequency-dependent complex viscosity and storage modulus master curves are displayed in Figure C.4 in Appendix C.

4.4 Results and Discussion

Four methacrylate-based copolymers containing the UPyMA comonomer in different molar proportions (1 mol%, 3 mol%, 5 mol%, and 10 mol% relative to MMA; indexed to feed composition) were synthesized and characterized. These copolymers were used to investigate how hydrogen-bonding interactions, conveyed through pendant UPy groups along the backbone, impact the thermomechanical properties of FFF-printed parts. For convenience, these copolymer additives will be referred to as p(MMA-r-UPyMA). Table 4.1 reports the molecular characteristics of the copolymers. Molecular compositions determined by ^{1}H NMR show that the incorporation of the UPyMA comonomer can be tailored, and the compositions closely follow the comonomer ratios used during free radical polymerization. The set of functional H-bonding copolymers have comparable molecular

Table 4.1. Molecular characteristics of p(MMA-r-UPyMA) additives synthesized via free radical polymerization.

Sample Name	Monomer Feed Ratio MMA:UPyMA (mol %)	UPyMA Content in Copolymer [a] (mol %)	M_w [b] (g mol^{-1})	Đ [b]	T_g [c] (° C)
p(MMA-r-UPyMA) 1%	99:1	0.6	31,820	1.39	117
p(MMA-r-UPyMA) 3%	93:7	3.5	29,120	2.20	125
p(MMA-r-UPyMA) 5%	95:5	4.8	32,950	1.45	132
p(MMA-r-UPyMA) 10%	90:10	9.6	24,630	1.35	141

[a] Determined by ^{1}H NMR spectroscopy.

[b] Determined by GPC.

[c] Determined via DSC.

weights and a monotonic increase in the glass transition temperature, T_g, is observed as the relative amount (mol %) of UPyMA comonomer increases. The increase in T_g observed for these UPy-containing copolymers is consistent with previous reports by Long *et al.*, who ascribe the increase in T_g as the UPyMA content increases to strong interactions between the UPy pendant groups.[23,27]

Using this set of copolymers, multicomponent filaments were successfully produced by compounding the p(MMA-r-UPyMA) additives with PMMA pellets and extruding the resulting blend. For convenience and because all multicomponent blends contain the same loading level of the copolymer additive (1 wt%), parts printed from multicomponent filaments will be referred to as PMMA with X mol% UPyMA, where "PMMA" designates the matrix polymer and "X mol% UPyMA" captures the UPyMA content of the random copolymer additive as set by comonomer feed ratio. The conditions

reported in the Experimental section and used to extrude the multicomponent filament, including the process temperature, screw speed, etc., represent an optimized condition for the system. (Results of trial extrusion and printing are not presented.) As noted earlier, the p(MMA-r-UPyMA) additives were incorporated at a loading level of 1 wt%, a choice that is guided by the general notion that additives should be effective at low loading levels and also based on my previous report showing that silica nanoparticles at 1 wt% loading gave the greatest enhancement in thermomechanical properties of FFF-printed nanocomposites.[121] Also, fixing the loading level of the copolymer additive and molecular weight allows the impact of UPyMA content to be systematically examined.

DMA measurements and tensile tests were used to examine how increasing UPyMA content impacts the mechanical properties of the additive modified FFF-printed parts. Representative DMA curves displayed in Figure 4.1 show that increasing the UPyMA content in the copolymer additive up to 5 mol% increases the Young's modulus of FFF-printed specimens made from the multicomponent filaments. Specifically, incorporating the UPyMA comonomer up to 5 mol% led to a 50% increase in the Young's modulus as compared to PMMA parts fabricated from virgin (unmodified) filaments. It is important to note that the values of Young's modulus reported in the legend of Figure 4.1 are averages resulting from measurements of five samples (± the standard deviation), while the data plotted in the figure is a set of individual samples.

While DMA measurements probe the linear response regime, tensile tests also were completed to examine how the presence of additives that offer SCMHB impact mechanical properties of FFF-printed parts that are strained through failure. Representative stress-strain curves from tensile testing shown in Figure 4.2 indicate that increasing the UPyMA

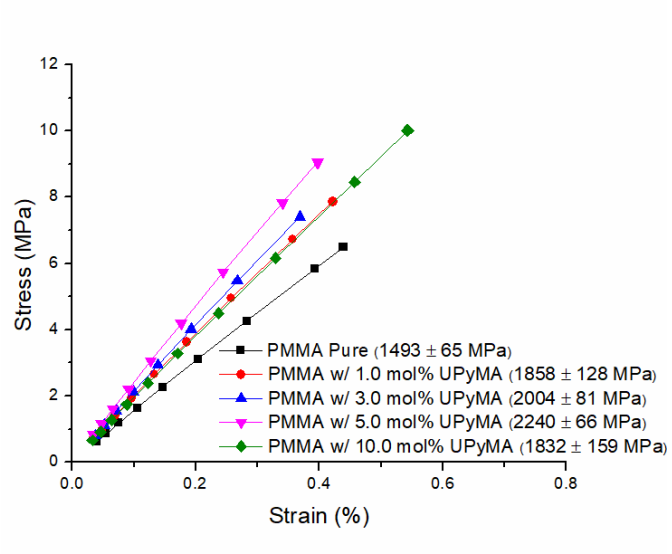

Figure 4.1 DMA results show an increase in the Young's modulus of all FFF-printed parts containing copolymer additives compared to the unmodified PMMA. Moreover, the Young's modulus increases as the UPyMA composition increase from 1 mol% to 5 mol%. Values of the Young's modulus given in the legend are averages based on measurements of five replicate samples.

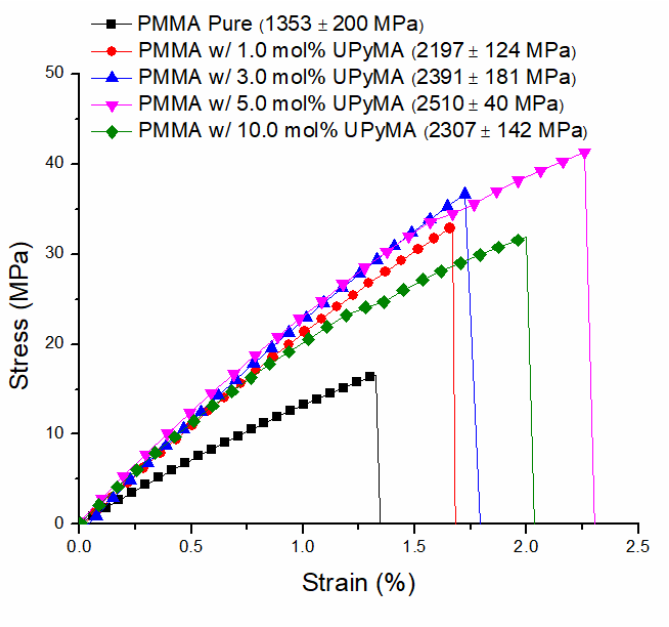

Figure 4.2. Multicomponent blends containing random copolymer additives having SCMHB UPy groups show increases in tensile modulus and ultimate tensile strength as the UPyMA content present in the copolymer additive increases up to 5 mol%. A representative trace from a series of replicate tests is shown for each copolymer additive, and the values of tensile modulus provided in the legend are based on measurements of five replicate samples.

comonomer content up to 5 mol% increases the mechanical properties, which is similar to the trend observed from DMA. Here again, values in the legend report the average tensile modulus obtained from five samples (and the corresponding standard deviation). While the deformation behavior of all FFF-printed samples is similar, the mechanical properties of FFF-printed parts are significantly affected by the addition of copolymer additives containing UPy pendant groups. For example and as shown in Table 4.2, the tensile modulus increases as the UPyMA comonomer content increases: there is an 85% increase in the tensile modulus relative to pure (unmodified) PMMA samples when the UPyMA content in the random copolymer is increased up to 5%. In addition to the enhancements observed in the tensile modulus, the ultimate tensile strength (UTS) also increases as the UPyMA content increases. For instance, an average UTS of 42 MPa is observed for FFF-printed parts enriched with the copolymer additive having 5 mol% UPyMA comonomer, while parts created using pure PMMA had an average UTS of 21 MPa. The trends observed herein agree with previous investigations of single component systems in which incorporation of UPy comonomers was used to improve the mechanical properties of the resulting polymeric materials.[23,147] For example, in their study of poly(ethylhexyl methacrylate-co-UPyMA) copolymers, Long *et al.* showed that in comparison to poly(ethylhexyl methacrylate) homopolymers, a random copolymer having 3 mol% UPyMA increased the UTS by 400% and the tensile modulus by 10-fold. Both the enhanced stiffness and tensile strength were ascribed to physical crosslinking due to hydrogen bonding interactions conveyed through the UPy pendant groups.[23] Although the magnitude of the changes seen for the UPy-containing copolymers incorporated as additives are not as large because PMMA is the majority component, they are significant

Table 4.2. Mechanical properties of FFF-printed parts containing p(MMA-r-UPyMA) copolymer additives.

Sample Name [a]	Young's Modulus (MPa)	Tensile Modulus (MPa)	Ultimate Tensile Strength (MPa)	Elongation at break (%)
Pure PMMA	1493 ± 65	1353 ± 200	21± 6	2.4 ± 1
PMMA w/ 1 mol% UPyMA	1858 ± 128	2197 ± 124	35 ± 2	1.7 ± 0.1
PMMA w/ 3 mol% UPyMA	2004 ± 81	2391 ± 181	38 ± 5	1.8 ± 0.2
PMMA w/ 5 mol% UPyMA	2240 ± 66	2510 ± 40	42 ± 5	2.3 ± 0.7
PMMA w/ 10 mol% UPyMA	1832 ± 159	2307 ± 142	37 ± 1	2.4 ± 0.5

[a] All p(MMA-r-UPyMA) additives were incorporated into a PMMA matrix [Mw = 100,000 g mol^{-1}] at 1 wt% loading.

and it is inferred that the increases in stiffness and tensile strength are due to hydrogen bonding interactions between UPy motifs.

The results presented in Figure 4.2 also show that while the UTS and tensile modulus increase when additives are present, the addition of UPyMA copolymers does not affect the average elongation at break (failure strain) or the characteristic deformation pattern. As reflected in the representative stress-strain curves presented in Figure 4.2, all samples show elastic deformation followed by brittle fracture. Because the deformation behavior of the additive modified composite material is similar to that of the unfilled material (here, pure PMMA), it suggests that the macroscopic deformation process is mainly governed by the matrix polymer and is not influenced by the addition of the additive.[133]

While these results are a powerful demonstration of how molecular assembly, which operates at the nanoscale, leads to a significant improvement in the macroscopic performance of printed materials, it is worth noting that a decrease in the mechanical properties is observed when the UPyMA content is increased to 10 mol%. Although additional studies are being completed to determine the origin of this effect, it is believed that this is a direct result of competition between intermolecular and intramolecular hydrogen bonding. It is reasonable to hypothesize that as the UPy content in the random copolymers increases, there is a concomitant increase in intramolecular hydrogen bonding, which reduces the density of "active" physical crosslinks present in the FFF-printed parts. This supposition is consistent with a report by Long *et al*. that focused on the behavior of UPy-containing random copolymers.[23] Specifically, they noted that in comparison to copolymers containing lower UPy content (i.e. 1-7 mol% in the random copolymer), copolymers containing 10 mol% UPy had a significantly higher complex viscosity and exhibited a different viscosity-temperature profile. Also, they reported that tensile testing of the random copolymer containing more than 7 mol% UPy could not be completed because those samples experienced brittle fracture when clamped in the instrument. Based on these observations, they suggested that the random copolymer system has a critical concentration of UPy groups, above which the polymeric materials exhibit different properties and patterns of behavior.[23] Thus, the decrease in performance observed in the multicomponent blends used to make FFF-printed parts when UPyMA content in the additive reaches 10 mol% suggests that a critical concentration of UPy-pendant groups has been reached. Additional experiments to access higher UPy content in order to test this supposition of there being an upper limiting concentration were unsuccessful due to

solubility issues that arose during polymerizations. Similar issues were reported by Long *et al.*[23] Therefore copolymers containing more than 10 mol% UPyMA were not used to make filaments and FFF-printed parts.

Average properties for all specimens examined via DMA strain-sweep measurements and tensile testing are reported in Table 4.2. The results clearly show that the mechanical properties of FFF-printed specimens containing random copolymer additives containing UPyMA comonomers increases as the random copolymer composition increase up to 5 mol% UPyMA. Furthermore, not only do the mechanical properties increase as the UPyMA comonomer content increases, but this trend is also consistent across numerous measurement techniques.

Because self-assembly by hydrogen bonding interactions is temperature dependent, additional measurements were completed to investigate the temperature dependence of thermomechanical properties of printed parts containing the SCMHB additives. Specifically, constant-strain temperature ramp measurements were used to investigate how increasing the UPy content in p(MMA-r-UPyMA) additives impact the storage modulus, loss modulus and glass transition temperature of FFF-printed parts. As seen in Figure 4.3A, the addition of UPy-containing copolymers increases the glass transition temperature of samples made from the multicomponent blends (113 °C) relative to pure PMMA (109 °C). While all of the multicomponent FFF-printed samples show a higher T_g relative to that of the unmodified PMMA, progressively increasing the UPyMA content in the copolymer additive does not produce an observable, corresponding change in the T_g of the printed samples. This is likely a product of the low loading level of the random copolymers as well as the broad transition from an amorphous glass to a viscoelastic fluid. Nevertheless, the

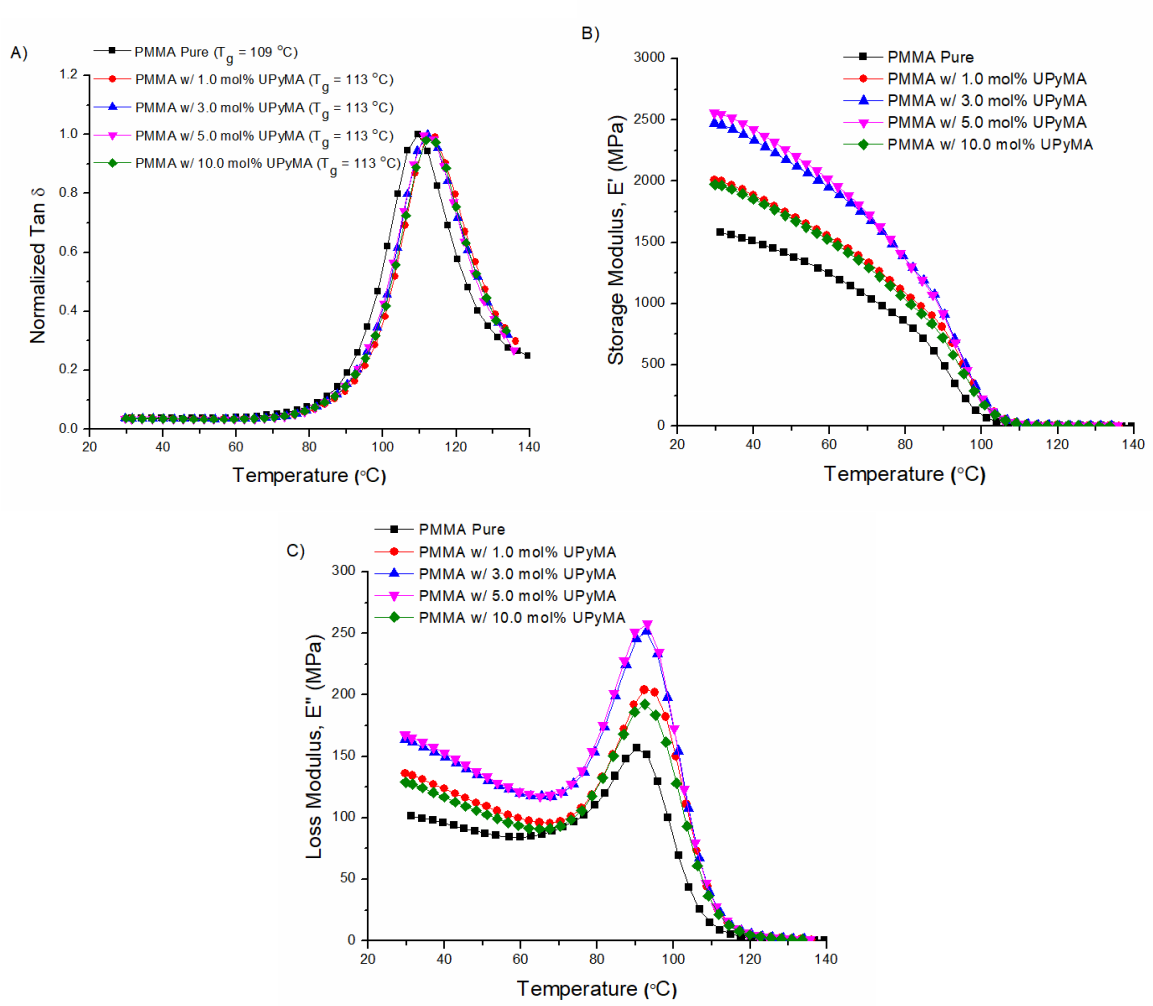

Figure 4.3. Constant-strain temperature ramp measurements of PMMA-based samples containing SCMHB random copolymer additives produced by FFF as a function of the UPyMA content show that the (A) glass transition temperature, (B) storage modulus, and (C) loss modulus increase with increasing UPyMA content. These enhancements are attributed to hydrogen bonding interactions between UPy groups, which serve as physical crosslinks.

signal of an increase in the T_g due to the presence of hydrogen bonding additives agrees with previous reports describing how hydrogen bonding additives affect thermal transitions of polymer blends.[148–151] For example, Inoue *et al.* showed that increasing the loading level of a small molecule hydrogen bonding additive, 4,4'-thiodiphenol, in poly(ε-caprolactone) (PCL) from 0 to 40 wt% increased the T_g of the polymer blend by 20 °C.[149] They ascribe the increase in T_g to the formation of a hydrogen-bonded network that produces a physically-crosslinking polymer network and suggests this lowers the "flexibility" of the matrix polymer and manifests as an increase in the T_g of the blend.[148,149] Although I maintained the loading level of the UPy-containing copolymer additives constant at 1 wt%, the increase in T_g similarly suggests that the hydrogen bonding interactions provided by the random copolymer additives leads to the formation of a hydrogen-bonded network.

In addition and as seen in Figure 4.3B and 4.3C, although all samples show similar patterns of behavior, the thermomechanical properties in the glassy regime are significantly impacted by the addition of p(MMA-r-UPyMA) additives. For instance, at the initial temperature used in these measurements (30 °C), both the storage modulus, E', and loss modulus, E", are markedly higher compared to the unmodified PMMA samples. At a random copolymer composition of 5 mol% UPyMA, there is >60% increase in both E' and E", which are dramatic improvements given that the p(MMA-r-UPyMA) copolymers are added at only 1 wt%. Also, the results indicate that the storage and loss moduli increase as the UPyMA comonomer content increases up to 5 mol% but decreases thereafter. The enhancements in E' and E" as a function of UPy-content appear to be sustained until T ~90 °C, at which point, the curves begin to overlay one another. This pattern of behavior is compelling and suggests that at temperatures below the dissociation temperature (reported

to be 80 °C)[24,27], hydrogen bonding interactions between UPy groups are active, leading to enhancements in thermomechanical properties of FFF-printed parts. Additionally, it is expected that as the temperature approaches and exceeds the dissociation temperature, self-complementary quadruple H-bonding of UPy groups is disrupted, thereby diminishing and eventually eliminating the enhancements in thermomechanical properties. While the data in Figures 4.3B and 4.3C are consistent with this view, it is noted that PMMA begins to transition from a glass to a viscoelastic rubber in the same temperature window. (See Figure 4.3A.) Thus, additional studies utilizing a matrix polymer with a T_g that is distinctly above the dissociation temperature of UPy groups would be needed to separately assess the impact of dissociation of UPy groups on the thermomechanical properties of FFF-printed parts. The increase in the storage and loss moduli as a function of UPy-content is consistent with previous reports showing that the thermomechanical properties of polymer blends can be improved by hydrogen-bonding interactions.[148,151–153] For example, Abetz *et al.* showed that the storage and loss moduli of styrene-b-styrene-r-butadiene-b-styrene (S-S/B-S) triblock copolymers increased when the butadiene units present in the middle block were modified such that they presented hydrogen bonding groups.[152] Specifically, they showed that modifying butadiene repeat units with benzoic acid enhanced the storage and loss moduli relative to unfunctionalized S-S/B-S copolymers, and increasing the number of benzoic acid groups increased the moduli. This behavior was attributed to physical crosslinking through self-complementary, hydrogen bonding between carboxylic acid groups.[152]

In addition to DMA and tensile tests, which highlight how the macroscopic properties of FFF-printed parts are impacted by the incorporation of copolymer additives

containing hydrogen bonding motifs, low-amplitude oscillatory-shear measurements were completed to examine melt flow characteristics. The angular frequency-dependent storage modulus and complex viscosity of FFF-printed PMMA parts containing no copolymer additive (designated as Pure PMMA) and multicomponent samples containing p(MMA-r-UPyMA) additives with increasing UPyMA comonomer content (1-10 mol%) are shown in Figure 4.4. These results suggest that neither the storage modulus nor the complex viscosity are affected by the incorporation of p(MMA-r-UPyMA) additives. Specifically, the frequency dependent storage modulus, G'(ω), which is shown in Figure 4.4A, suggests that the melt flow behavior of multicomponent blends containing p(MMA-r-UPyMA) additives is similar to that of the homopolymer PMMA, regardless of the UPyMA content: All of the G'(ω) curves overlay one another and exhibit similar rheological behavior. Specifically, all samples exhibit a viscous response at low frequencies and an elastic response at high frequencies. Moreover, all samples exhibit the same power law exponent at high (½) and low (1) frequencies, regardless of UPy content. A power law exponent of ½ is expected at high frequencies for an entangled polymer melt, but it is noted that the behavior of all samples deviate from the power law exponent of 2 expected for a monodisperse entangled melt at low frequencies.[25,154] This is attributed to the fact that the matrix PMMA has a large dispersity (Đ= 1.5), which leads to a deviation from the rheological response expected for a monodisperse melt.[154] Additionally, all blends exhibit liquid-like behavior in the terminal regime regardless of the UPyMA content. Specifically, there is no evidence of a secondary plateau and G"(ω) > G'(ω).[25] Both of these characteristics (G"(ω) > G'(ω) and the absence of a secondary plateau in the terminal regime) are indicative of a liquid-like response and suggest that physical crosslinks

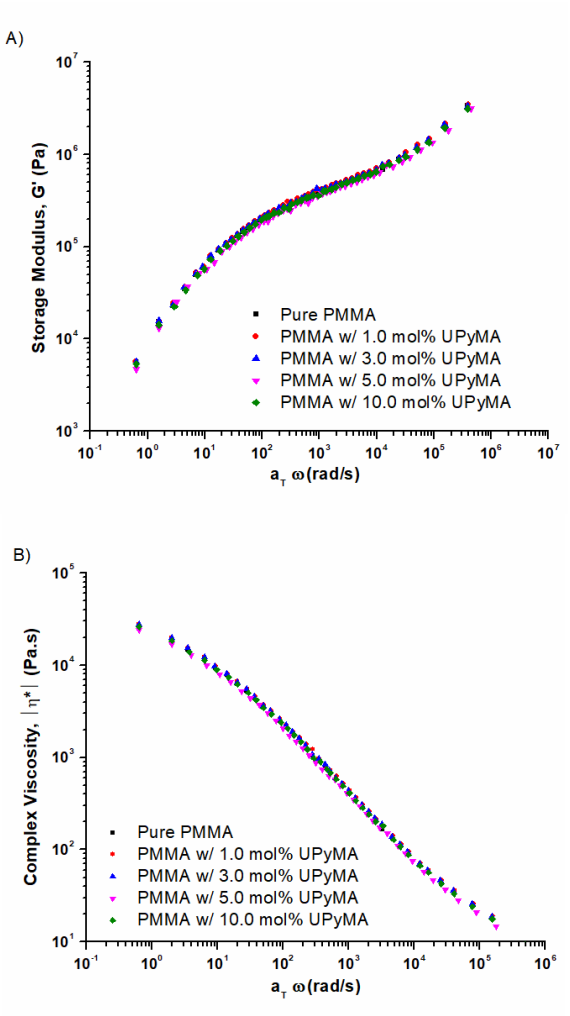

Figure 4.4. Melt rheology measurements show that the storage modulus (A) and complex viscosity (B) of FFF-printed PMMA multicomponent blends are unaffected by the presence of p(MMA-r-UPyMA) additives. A reference temperature of 180 °C was used for time-temperature superposition.

between UPy groups are avoided in the melt state.[25] (A master curve for each blend highlighting the relationship between G'(ω) and G"(ω) is displayed in Figure C.5, as displayed in Appendix C.) Furthermore and as seen from the frequency-dependent complex viscosity, |η*|, which is shown in Figure 4.4B, the frequency dependent complex viscosity of the multicomponent polymer blends is consistent with the behavior of the pure PMMA homopolymer: All curves overlay one another, exhibiting a plateau at low frequencies and shear-thinning behavior at high frequencies. These results are consistent with non-Newtonian behavior despite the presence of the hydrogen bonding motifs along chain backbones. These results agree with a report by Long *et al.* who determined that the melt characteristics of copolymers comprised of butyl acrylate and UPyMA comonomers were nearly identical to that of butyl acrylate homopolymers at T > 80 °C, which was assigned as the dissociation temperature of the UPy groups.[27]

4.5 Conclusions

Random copolymer additives containing UPy groups, which offer self-complementary, multidentate hydrogen bonding interactions, have a dramatic impact on the performance and properties of PMMA specimens printed by FFF. Mechanical property characterizations demonstrate substantial increases in the Young's modulus and ultimate tensile strength (increases of 50-100%) when p(MMA-r-UPyMA) additives containing up to 5 mol% UPy are incorporated in FFF-printed parts, while rheometric studies indicate that the addition the copolymer additives does not impact the melt flow characteristics, regardless of the UPy-content. This behavior – a dramatic increase in mechanical properties but no change in melt properties – is significant but not unexpected for the p(MMA-r-

UPyMA) thermoresponsive additives investigated. This behavior is a direct result of the reversible, non-bonded hydrogen-bonding interactions provided by UPy groups, which operate at the nanoscale but manifest in the macroscopic behaviors. Although FFF is a non-equilibrium, non-isothermal process, the significant enhancements in mechanical properties at low additive loading levels suggest that self-assembly through weak and reversible intermolecular interactions have outstanding potential in the context of polymer additive manufacturing, especially in consideration of the enormous composition, chemical, and topological design space accessible with polymers.

CHAPTER 5: SUMMARY, CONCLUSIONS, AND FUTURE WORKS

5.1 Summary

Understanding how interfacial interactions can be manipulated to drive assembly at the nanoscale and provide reinforcement at the macroscale is crucial for expanding the known boundaries of material-property space for 3D printed materials. Specifically, my dissertation research examines how controlling interfacial interactions across the matrix /nanoparticle interface in polymer nanocomposites and how using hydrogen bonding interactions in multicomponent blends impacts the resultant properties of parts printed by Fused Filament Fabrication (FFF). The structure-property relationships established from these research endeavors provide a foundation for future efforts that use nanoscopic additives to control the performance of parts printed by the non-isothermal, nonequilibrium FFF process. The first research effort describes how the thermomechanical properties of FFF-printed PMMA parts are impacted by the addition of unfunctionalized (bare) Si NPs. This research work demonstrates that increases in the macroscopic performance of PMMA nanocomposites containing Si NPs are due to favorable, hydrogen bonding interactions between hydroxyl groups on Si NP surface and carbonyl groups within the backbone of PMMA chains. The number density of polymer-particle interactions increase as the loading level of Si NPs increases, which enhances stress transmission and results in an increase in the performance of PMMA printed nanocomposites. This effort is noteworthy because it highlights the importance of interfacial interactions as a way to enhance the performance of polymer nanocomposites in the context of 3D printing.

The second major theme of my dissertation research describes the first example of incorporating polymer-grafted nanoparticles in FFF-printed nanocomposites. In that research effort, I examined how attaching end-tethered chains to the surface of Si NPs

controls organization on the nanoscale and alters the macroscopic properties polymer-grafted nanocomposites. Specifically, PMMA-grafted nanoparticles (PMMA-g-NPs) having low molecular weight graft chains and an intermediate grafting density are demonstrated to arrange in surface fractals, or connected sheets, throughout PMMA nanocomposites generated by FFF. Macroscopic assessments coupled with rheology measurements suggest that these interconnected sheet-like nanostructures effectively dissipate stress throughout the nanocomposite through graft chain interactions with matrix chains and graft chains on neighboring particles. Additionally, the mechanical performance of FFF-printed parts described in this work surpass those obtained when bare Si NPs were used, which further highlights how manipulating interfacial interactions in polymer nanocomposites, conveyed here by grafted polymer chains, controls organization on the nanoscale and affects the performance of polymer nanocomposites. This work is significant because it emphasizes how the performance of polymer nanocomposites depend on both the spatial distribution of nanoparticles and interfacial interactions. From this research effort, additional studies examining how variation in the grafting density of chains or graft chain length impact nanoscale organization can be completed. These research efforts may provide a useful way to effectively control the stress-transmission from the matrix chains to Si NPs and also may provide a way to promote particle diffusion across bead-bead interfaces.

Lastly, I examined how the melt characteristics and thermomechanical properties of FFF-printed PMMA parts were affected by the addition of polymeric additives containing self-complementary, hydrogen bonding groups. These research studies provide the first example showing how thermoreversible, hydrogen bonding interactions offer

mechanical reinforcement at use temperatures, but exhibit no delirious impact on the processability at temperatures above the dissociation temperature of the hydrogen bonding interaction. Specifically, I synthesized random copolymer additives consisting of methyl methacrylate and 2-ureido-4[1*H*]-pyrimidone methacrylate (UPyMA). By varying the UPyMA content, the number density of self-complementary, hydrogen bonding interactions between UPy groups could be manipulated. Results from macroscopic assessments demonstrate that increasing the number of physical crosslinks, conveyed by the self-dimerization of UPy groups, increased the mechanical properties of PMMA parts printed by FFF, but no changes in the melt characteristics were observed. Results from this research show that the properties of parts printed from these multicomponent blends depend on the self-dimerization strength of the hydrogen bonding groups and the number density of non-bonded interactions. This work is impactful because it demonstrates how the strength and number density of non-bonded, physical interactions can tuned to effectively manage the properties of FFF-printed materials at use and production temperatures.

While these research efforts provide strong proof for the concept that the performance of FFF-printed parts are dictated by the interactions on the nanoscale, improvements in the properties of FFF-printed parts are limited by the amount of additive that can be successfully incorporated in PMMA filaments. For instance, all multicomponent or nanocomposite filaments generated herein (by using either Si NPs, PMMA-g-NPs, or SCMHB copolymer additives) exhibit degradation in the structural integrity of filaments and the appearance of macroscopic agglomerates as the loading level of the additive increases above 1.0 wt%. These problems are attributed to inefficient mixing

during either mechanical mixing or melt extrusion. Two methods are suggested for resolving this problem: First, it may be useful to use a different preparation procedure to incorporate additives in PMMA filament. For instance, instead of using a mechanical mixing procedure, one may use a solution mixing method which has been used previously to create nanocomposites. By allowing the matrix chains and additive to mix in solution, a more homogenous nanocomposite (or blend) may be obtained, and this strategy may help to eliminate macroscopic agglomerates. In addition to altering how the different components are mixed prior to filament extrusion, it may be useful to consider using an extruder with a longer length-to-diameter (L/D) ratio of the extrusion screw and multiple heating zones, as these may enhance mixing during melt processing. This method also may decrease the presence of macroscopic agglomerates and allow structurally stable filaments that can be used for printing to be generated.

5.2 Future Work

My dissertation work provides clear proof that the addition of additives, either inorganic particles or self-complementary, multiple hydrogen bonding macromolecules, enhance the performance of FFF-printed parts and provides motivation for future studies aimed at investigating how manipulating nanoscale interactions can be used to control the macroscopic properties of printed materials. As demonstrated in Chapters 2 and 3, the ability to control interfacial interactions across the particle/matrix interface provides a novel way to control both the nanoscale organization and properties of polymer nanocomposites. Due to the ability to synthetically control the characteristics of polymer-grafted nanoparticles, such as the grafting dentistry, graft chain molecular weight and

chemical composition of the graft chain, there is a need to develop structure-property relationships regarding the incorporation of polymer-grafted nanoparticles into materials created by the non-isothermal, nonequilibrium (*vide infra*) FFF process. In addition to tailoring interactions in polymer nanocomposites, incorporating surface-active additives into filaments provides a novel route to address the principal issue of weak interbead interfaces in printed parts. By promoting diffusion across bead-bead interfaces, surface-active additives offer a compelling approach for increasing the performance of printed materials. I believe that both of these areas, tailoring the properties of polymer-grafted nanoparticles and using surface-active additives, are worthy of further exploration, and each will be discussed briefly.

5.2.1 Random Copolymer Grafted Nanocomposites

As mentioned previously, it is well established that incorporating nanoparticles in polymeric materials can improve the mechanical, optical, and electrical properties of the nanocomposite due to the superposition of specific material properties. However, nanocomposite properties are sensitive to both the arrangement of nanoparticles throughout the polymer matrix and the interactions between the additive and matrix. As highlighted in Chapters 2 and 3, the nanoscale organization and stress-transmission from matrix chains to nanoparticles can be effectively managed by tailoring interactions across the matrix/particle interface. The polymer-grafted nanocomposites examined in my dissertation work were athermal systems in which the matrix chains and graft chains have the same chemical composition. Athermal systems are entropically controlled, and as a result, there are two possible states when the grafting density is high enough to “cover”

polymer-surface interactions: polymer-grafted nanoparticles will disperse in the matrix when the molecular weight of the matrix chains is less than the molecular weight of the graft chains, but they will form anisotropic clusters when the molecular weight of the matrix chains is greater than the molecular weight of the graft chains. Because it is synthetically challenging to graft high molecular weight chains on nanoparticle surfaces, it is difficult to achieve a dispersed nanoparticle state in so-called "symmetric" systems because matrix chain molecular weights are typically high (nominally 100 kDa). Thus, polymer-grafted nanoparticles often arrange in clusters, as evident from the studies presented in Chapter 3. As a result, a novel method to control the interfacial interactions between the graft and matrix polymers to promote dispersion and improve thermomechanical properties in high molecular weight matrices is desirable.

To address this challenge, a profitable theme for future efforts may be to investigate how the composition of random copolymer grafted nanoparticles (RCGNPs) affects particle organization at the nanoscale and the thermomechanical properties, such as the glass transition temperature, T_g, and storage and loss moduli of FFF-printed parts. The methacrylate monomers presented in Figure 5.1 provide a way to explore how changing the T_g, by comonomer type and level of incorporation, affects interfacial interactions across the matrix/particle interface and controls the resultant nanocomposite properties.

Specifically, this line of research is focused around addressing two main questions: How does the choice of comonomer and copolymer composition affect (1) the spatial distribution of random copolymer-grafted nanoparticles (RCGNPs), and (2) the thermomechanical and melt characteristics of the resulting nanocomposite? To complete these studies, random copolymers of varying compositions can be polymerized from

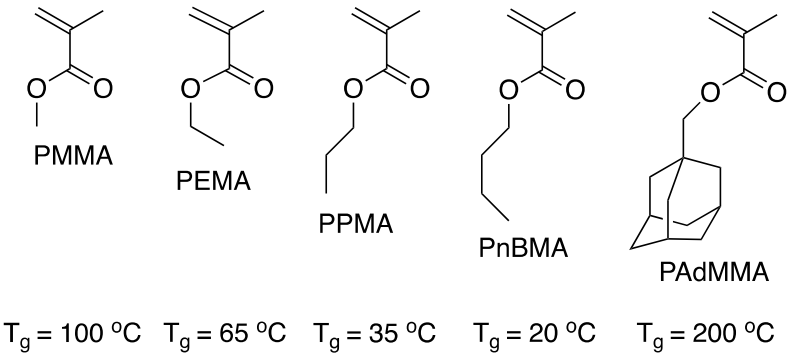

Figure 5.1. A series of methacrylate-based monomers that provide access to various copolymer Tg values. Using random copolymer-grafts based on various methacrylate comonomers offers an innovative way to change the nature of the interfacial layer and potentially control interactions across the grafted-nanoparticle/PMMA matrix interface.

nanoparticle surfaces and blended with PMMA pellets to create random copolymer-grafted nanocomposite filaments. To answer the first question, SAXS and WAXS measurements can be used to analyze the nanostructure of the random copolymer grafted-nanocomposites. The second question will be answered by using various techniques, such as DMA and rheology, to evaluate how the properties of PMMA parts printed by FFF are impacted by the addition of the RCGNPs. These studies will provide fundamental insight into how the spatial arrangement and thermomechanical properties of polymer nanocomposites can be managed by tailoring interactions across the particle/matrix interface by random copolymer grafts.

This research is essential to understanding design-structure-property relationships of polymer grafted nanocomposites that are potentially useful in FFF, and there is fundamental value to these studies because a detailed study of random copolymer grafted

nanoparticles in polymer matrices has not been completed. The design-structure-property relationships established by this research will be useful for future implementation of tailored nanocomposites in a variety of applications, including 3D printed materials.

5.2.2 Surface-Active Additives Promote Diffusion Across Bead-Bead Interfaces

As noted in the introductory chapter, FFF-printed parts have poor mechanical properties due to the formation of voids and weak interfacial adhesion between adjacent filaments that results from limited diffusion of polymer chains across bead-bead interfaces during the printing process. Thus, in addition to manipulating interfacial interactions in polymer nanocomposites to control the organization of nanoparticles on the nanoscale and the stress-transmission from the polymer matrix to the inorganic additives, promoting diffusion across interbead interfaces offers an attractive route to improve the properties of FFF-printed materials. Recent research efforts suggest that incorporating linear additives of the same chemical type but lower molecular weight than the polymer matrix is useful because the lower molecular weight chains will diffuse across interbead interfaces, thereby increasing the mechanical properties of printed parts.[155] However, these claims are speculative, as there is no quantitative information linking the diffusion of additives to the increase in performance that was observed. Thus, it is imperative to examine this issue in detail, and a set of studies that quantitatively link additive design to surface-activity and composition across bead-bead interfaces is sorely needed. One way to do this is to use non-linear chains that offer a high number of end groups that can be detected.

At the end of my dissertation work, I began some initial studies to assess the practically of such studies. In that work, surface-active polystyrene bottlebrushes (PS BBs)

were incorporated into filaments and subsequently used to produce printed parts. PS BBs were chosen based on previous research efforts showing that they migrate to polymer thin film interfaces. Specifically, thin film blends containing linear PS chains and PS BBs additives show spontaneously segregation of the PS BBs to both the film/air interface and the film/substrate. The segregation of PS BBs to the surface and substrate is attributed to a strong, entropy-controlled surface attraction. Inspired by these results and the need to promote diffusion across bead-bead interfaces in 3D printed materials, a full phase study devoted to studying FFF filaments made by blending linear PS and PS BBs and extruding, printing, and characterizing those samples should be pursued. Figure 5.2 shows schematically the analogous entropy-driven segregation of PS BBs additives to bead surfaces.

This research will address two main questions: (1) do PS BBs accumulate at filament interfaces, and (2) does the accumulation and diffusion of PS BBs across filament interfaces improve the mechanical properties of FFF-printed parts? To address the first question, first PS BBs will be synthesized via ring-opening polymerization using macromonomers. The macromonomers can be made using RAFT polymerization, which

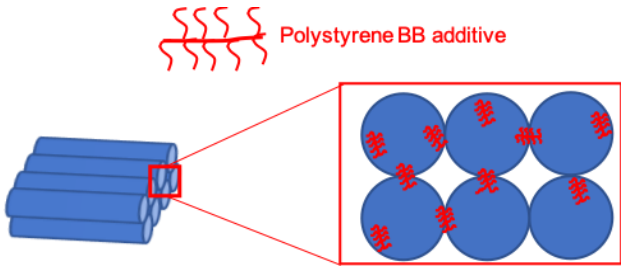

Figure 5.2. Surface active polymer bottlebrushes can promote diffusion across interbead interfaces and increase the mechanical properties of FFF-printed parts.

creates side chains. Because the side chains are functionalized with a dithioester or trithiocarbonate (from the chain transfer agent), scanning electron microscopy – energy dispersive X-ray spectroscopy (SEM-EDS) can be used to determine the elemental composition of sulfur across the beads. The elemental sulfur composition at filament interfaces can be compared to composition in bulk or at the center of the filament, providing a quantitative description of the concentration of PS BBs at bead-bead interfaces. Parametric studies of various processing parameters, such as the extrusion temperature and screw speed, printing temperature and print speed, and build plate temperature will provide a basis for effectively tailoring the amount of PS BBs that accumulates at interfaces. Finally, mechanical tests, such as T-peel tests and tensile tests, should be completed to determine how increasing BB content at filament interfaces impacts the performance of parts printed by FFF.

Overall, this research effort will offer insight regarding how the melt processability of polymer filaments is affected by the addition of BB additives. Additionally, this effort will provide the first quantitative report examining how varying the temperature and time during extrusion and printing impact the surface migration of PS BBs and how this impacts the resultant properties of the printed parts.

5.3 Conclusions

Overall, my dissertation research establishes structure-property relationships for polymer nanocomposites and multicomponent filaments that are used to print FFF parts. Research efforts described herein examine how interactions on the nanoscale can be effectively used to address the inferior mechanical properties associated with parts

manufactured by FFF. Specifically, I have demonstrated that incorporating either inorganic nanoparticles or thermoresponsive copolymer additives into FFF-printed parts significantly impact the thermomechanical properties of printed structures and, to varying degrees depending on the nature of the additive, alter melt flow characteristics. My research provides a foundation for future research efforts aimed at investigating how altering the design of polymer-grafted nanoparticles (such as grafting density, graft chain composition, graft chain molecular weight, etc.) or the number density and interaction strength of self-complementary hydrogen bonding groups impacts the resultant properties of advanced polymeric materials fabricated by FFF.

LIST OF REFERENCES

(1) Richard, J.; Randal, R. *Polymers at Surfaces and Interfaces*; Cambridge University Press, 1999.

(2) Barner-Kowollik, C.; Goldmann, A. S.; Schacher, F. H. Polymer Interfaces: Synthetic Strategies Enabling Functionality, Adaptivity, and Spatial Control. *Macromolecules* **2016**, *49* (14), 5001–5016.

(3) J. T., K. Tailoring Polymer Interfacial Properties by End Group Modification. In *Polymer Surfaces, Interfaces and Thin Films*; World Scientific Publishing, 2000.

(4) Allara, D. L.; Atre, S. V.; Parikh, A. N. Self-Assembled Molecular Films as Polymer Surface Models. In *Polymer Surfaces and Interfaces II*; John Wiley & Sons, Ltd, 1993.

(5) Vetaphone. Corona Treatment. *Technology*. 2016.

(6) Aden, B.; Street, D. P.; Hopkins, B. W.; Lokitz, B. S.; Kilbey, S. M. Tailoring Surface Properties through in Situ Functionality Gradients in Reactively Modified Poly(2-Vinyl-4,4-Dimethyl Azlactone) Thin Films. *Langmuir* **2018**, *34* (18), 5204–5213.

(7) Pesek, S. L.; Lin, Y.-H.; Mah, H. Z.; Kasper, W.; Chen, B.; Rohde, B. J.; Robertson, M. L.; Stein, G. E.; Verduzco, R. Synthesis of Bottlebrush Copolymers Based on Poly(Dimethylsiloxane) for Surface Active Additives. *Polymer* **2016**, *98*, 495–504.

(8) Ramanathan, T.; Liu, H.; Brinson, L. C. Functionalized SWNT/Polymer Nanocomposites for Dramatic Property Improvement. *Journal of Polymer Science Part B: Polymer Physics* **2005**, *43* (17), 2269–2279.

(9) Ash, B. J.; Siegel, R. W.; Schadler, L. S. Mechanical Behavior of Alumina/Poly(Methyl Methacrylate) Nanocomposites. *Macromolecules* **2004**, *37* (4), 1358–1369.

(10) Meng, S.; He, H.; Jia, Y.; Yu, P.; Huang, B.; Chen, J. Effect of Nanoparticles on the Mechanical Properties of Acrylonitrile–Butadiene–Styrene Specimens Fabricated by Fused Deposition Modeling. *J. Appl. Polym. Sci.* **2017**, *134* (7), 1–9.

(11) Torrado, A. R.; Shemelya, C. M.; English, J. D.; Lin, Y.; Wicker, R. B.; Roberson, D. A. Characterizing the Effect of Additives to ABS on the Mechanical Property Anisotropy of Specimens Fabricated by Material Extrusion 3D Printing. *Additive Manufacturing* **2015**, *6*, 16–29.

(12) Jayaraman, A. Polymer Grafted Nanoparticles: Effect of Chemical and Physical Heterogeneity in Polymer Grafts on Particle Assembly and Dispersion. *Journal of Polymer Science Part B: Polymer Physics* **2013**, *51* (7), 524–534.

(13) Jiao, Y.; Akcora, P. Assembly of Polymer-Grafted Magnetic Nanoparticles in Polymer Melts. *Macromolecules* **2012**, *45* (8), 3463–3470.

(14) Kumar, S. K.; Jouault, N.; Benicewicz, B.; Neely, T. Nanocomposites with Polymer Grafted Nanoparticles. *Macromolecules* **2013**, *46* (9), 3199–3214.

(15) Chevigny, C.; Dalmas, F.; Di Cola, E.; Gigmes, D.; Bertin, D.; Boué, F.; Jestin, J. Polymer-Grafted-Nanoparticles Nanocomposites: Dispersion, Grafted Chain Conformation, and Rheological Behavior. *Macromolecules* **2011**, *44* (1), 122–133.

(16) Harton, S. E.; Kumar, S. K. Mean-Field Theoretical Analysis of Brush-Coated Nanoparticle Dispersion in Polymer Matrices. *J. Polym. Sci. B Polym. Phys.* **2008**, *46* (4), 351–358.

(17) Green, P. F. The Structure of Chain End-Grafted Nanoparticle/Homopolymer Nanocomposites. *Soft Matter* **2011**, *7* (18), 7914.

(18) Estridge, C. E.; Jayaraman, A. Assembly of Diblock Copolymer Functionalized Spherical Nanoparticles as a Function of Copolymer Composition. *The Journal of Chemical Physics* **2014**, *140* (14), 144905.

(19) Akcora, P.; Liu, H.; Kumar, S. K.; Moll, J.; Li, Y.; Benicewicz, B. C.; Schadler, L. S.; Acehan, D.; Panagiotopoulos, A. Z.; Pryamtisyn, V.; et al. Anisotropic Self-Assembly of Spherical Polymer-Grafted Nanoparticles. *Nature Materials* **2009**, *8*, 354–359.

(20) Moll, J. F.; Akcora, P.; Rungta, A.; Gong, S.; Colby, R. H.; Benicewicz, B. C.; Kumar, S. K. Mechanical Reinforcement in Polymer Melts Filled with Polymer Grafted Nanoparticles. *Macromolecules* **2011**, *44* (18), 7473–7477.

(21) De Greef, T. F. A.; Smulders, M. M. J.; Wolffs, M.; Schenning, A. P. H. J.; Sijbesma, R. P.; Meijer, E. W. Supramolecular Polymerization. *Chemical Reviews* **2009**, *109* (11), 5687–5754.

(22) Amabilino, D. B.; Smith, D. K.; Steed, J. W. Supramolecular Materials. *Chemical Society Reviews* **2017**, *46* (9), 2404–2420.

(23) Elkins, C. L.; Park, T.; McKee, M. G.; Long, T. E. Synthesis and Characterization of Poly(2-Ethylhexyl Methacrylate) Copolymers Containing Pendant, Self-

Complementary Multiple-Hydrogen-Bonding Sites. *Journal of Polymer Science Part A: Polymer Chemistry* **2005**, *43* (19), 4618–4631.

(24) McKee, M. G.; Elkins, C. L.; Park, T.; Long, T. E. Influence of Random Branching on Multiple Hydrogen Bonding in Poly(Alkyl Methacrylate)S. *Macromolecules* **2005**, *38* (14), 6015–6023.

(25) Lewis, C. L.; Stewart, K.; Anthamatten, M. The Influence of Hydrogen Bonding Side-Groups on Viscoelastic Behavior of Linear and Network Polymers. *Macromolecules* **2014**, *47* (2), 729–740.

(26) Lei, Y.; Lodge, T. P. Effects of Component Molecular Weight on the Viscoelastic Properties of Thermoreversible Supramolecular Ion Gels Viahydrogen Bonding. *Soft Matter* **2012**, *8* (7), 2110–2120.

(27) Yamauchi, K.; Lizotte, J. R.; Long, T. E. Thermoreversible Poly(Alkyl Acrylates) Consisting of Self-Complementary Multiple Hydrogen Bonding. *Macromolecules* **2003**, *36* (4), 1083–1088.

(28) Sijbesma, R. P.; Beijer, F. H.; Brunsveld, L.; Folmer, B. J. B.; Hirschberg, J. H. K. K.; Lange, R. F. M.; Lowe, J. K. L.; Meijer, E. W. Reversible Polymers Formed from Self-Complementary Monomers Using Quadruple Hydrogen Bonding. *Science* **1997**, *278* (5343), 1601–1604.

(29) MATYJASZEWSKI, K.; GAYNOR, S. G. FREE RADICAL POLYMERIZATION. In *Applied Polymer Science: 21st Century*; Craver, C. D., Carraher, C. E., Eds.; Pergamon: Oxford, 2000; pp 929–977.

(30) Shenoy, A. *Rheology of Filled Polymer Systems*; Springer-Science+Business Media, B.V., 1999.

(31) Morrison, F. *Understanding Rheology*; Oxford University Press, 2001.

(32) Leblanc, J. L. Rubber±®ller Interactions and Rheological Properties in ®lled Compounds. *Prog. Polym. Sci.* **2002**, 61.

(33) Hsich, H. S. Y. Composite Rheology — I. Elastomer-Filler Interaction and Its Effect on Viscosity. *Journal of Materials Science* **1982**, *17* (2), 438–446.

(34) Berman, B. 3-D Printing: The New Industrial Revolution. *Business Horizons* **2012**, *55* (2), 155–162.

(35) Levy, G. N.; Schindel, R.; Kruth, J.-P. Rapid Manufacturing and Rapid Tooling with Layer Manufacturing (LM) Technologies, State of the Art and Future Perspectives. *CIRP Annals-Manufacturing Technology* **2003**, *52* (2), 589–609.

(36) Tong, J.; Bowen, C. R.; Persson, J.; Plummer, A. Mechanical Properties of Titanium-Based Ti–6Al–4V Alloys Manufactured by Powder Bed Additive Manufacture. *Materials Science and Technology* **2017**, *33* (2), 138–148.

(37) Campbell, I.; Bourell, D.; Gibson, I. Additive Manufacturing: Rapid Prototyping Comes of Age. *Rapid Prototyping Journal* **2012**, *18* (4), 255–258.

(38) Vaezi, M.; Seitz, H.; Yang, S. A Review on 3D Micro-Additive Manufacturing Technologies. *International Journal of Advanced Manufacturing Technology* **2013**, *67* (5–8), 1721–1754.

(39) Murphy, S. V.; Atala, A. 3D Bioprinting of Tissues and Organs. *Nature Biotechnology* **2014**, *32* (8), 773–785.

(40) Melchels, F. P. W.; Domingos, M. A. N.; Klein, T. J.; Malda, J.; Bartolo, P. J.; Hutmacher, D. W. Additive Manufacturing of Tissues and Organs. *Progress in Polymer Science* **2012**, *37* (8), 1079–1104.

(41) Gross, B. C.; Erkal, J. L.; Lockwood, S. Y.; Chen, C.; Spence, D. M. Evaluation of 3D Printing and Its Potential Impact on Biotechnology and the Chemical Sciences. *Analytical Chemistry* **2014**, *86* (7), 3240–3253.

(42) Christian Polzin; Sebastian Spath; Hermann Seitz. Characterization and Evaluation of a PMMA-based 3D Printing Process. *Rapid Prototyping Journal* **2013**, *19* (1), 37–43.

(43) Leary, M.; Piola, R.; Shimeta, J.; Toppi, S.; Mayson, S.; McMillan, M.; Brandt, M. Additive Manufacture of Anti-Biofouling Inserts for Marine Applications. *Rapid Prototyping Journal* **2016**, *22* (2), 416–434.

(44) Bagsik, A.; Schöppner, V. Mechanical Properties of Fused Deposition Modeling Parts Manufactured with Ultem* 9085. In *ANTEC*; 2011; pp 1–5.

(45) Ivanova, O.; Williams, C.; Campbell, T. Additive Manufacturing (AM) and Nanotechnology: Promises and Challenges. *Rapid Prototyping Journal* **2013**, *19* (5), 353–364.

(46) Carneiro, O. S.; Silva, A. F.; Gomes, R. Fused Deposition Modeling with Polypropylene. *Materials & Design* **2015**, *83*, 768–776.

(47) Casavola, C.; Cazzato, A.; Moramarco, V.; Pappalettere, C. Orthotropic Mechanical Properties of Fused Deposition Modelling Parts Described by Classical Laminate Theory. *Materials & Design* **2016**, *90*, 453–458.

(48) Boschetto, A.; Bottini, L. Design for Manufacturing of Surfaces to Improve Accuracy in Fused Deposition Modeling. *Robotics and Computer-Integrated Manufacturing* **2016**, *37*, 103–114.

(49) Sun, Q.; Rizvi, G. M.; Bellehumeur, C. T.; Gu, P. Effect of Processing Conditions on the Bonding Quality of FDM Polymer Filaments. *Rapid Prototyping Journal* **2008**, *14* (2), 72–80.

(50) Upadhyay, K.; Dwivedi, R.; Singh, A. K. Determination and Comparison of the Anisotropic Strengths of Fused Deposition Modeling P400 ABS. In *Advances in 3D Printing & Additive Manufacturing Technologies*; Wimpenny, D. I., Pandey, P. M., Kumar, L. J., Eds.; Springer Singapore: Singapore, 2017; pp 9–28.

(51) Rodriguez, J. F.; Thomas, J. P.; Renaud, J. E. Characterization of the Mesostructure of Fused-deposition Acrylonitrile-butadiene-styrene Materials. *Rapid Prototyping Journal* **2000**, *6* (3), 175–186.

(52) Turner, B. N.; Gold, S. A. A Review of Melt Extrusion Additive Manufacturing Processes: II. Materials, Dimensional Accuracy, and Surface Roughness. *Rapid Prototyping Journal* **2015**, *21* (3), 250–261.

(53) Peng, F.; Zhao, Z.; Xia, X.; Cakmak, M.; Vogt, B. D. Enhanced Impact Resistance of Three-Dimensional-Printed Parts with Structured Filaments. *ACS Applied Materials & Interfaces* **2018**, *10* (18), 16087–16094.

(54) Tjong, S. C. Structural and Mechanical Properties of Polymer Nanocomposites. *Materials Science and Engineering: R: Reports* **2006**, *53* (3–4), 73–197.

(55) Sumita, M.; Tsukihi, H.; Miyasaka, K.; Ishikawa, K. Dynamic Mechanical Properties of Polypropylene Composites Filled with Ultrafine Particles. *J. Appl. Polym. Sci.* **1984**, *29* (5), 1523–1530.

(56) Petrovic, Z.; Zhang, W. Glassy and Elastomeric Polyurethanes Filled with Nano-Silica Particles. *Materials Science Forum 352*.

(57) Kumar, S. K.; Benicewicz, B. C.; Vaia, R. A.; Winey, K. I. *50th Anniversary Perspective* : Are Polymer Nanocomposites Practical for Applications? *Macromolecules* **2017**, *50* (3), 714–731.

(58) Harton, S. E.; Kumar, S. K.; Yang, H.; Koga, T.; Hicks, K.; Lee, H.; Mijovic, J.; Liu, M.; Vallery, R. S.; Gidley, D. W. Immobilized Polymer Layers on Spherical Nanoparticles. *Macromolecules* **2010**, *43* (7), 3415–3421.

(59) Jancar, J.; Douglas, J. F.; Starr, F. W.; Kumar, S. K.; Cassagnau, P.; Lesser, A. J.; Sternstein, S. S.; Buehler, M. J. Current Issues in Research on Structure–Property Relationships in Polymer Nanocomposites. *Polymer* **2010**, *51* (15), 3321–3343.

(60) Gawande, M. B.; Goswami, A.; Felpin, F.-X.; Asefa, T.; Huang, X.; Silva, R.; Zou, X.; Zboril, R.; Varma, R. S. Cu and Cu-Based Nanoparticles: Synthesis and Applications in Catalysis. *Chemical Reviews* **2016**, *116* (6), 3722–3811.

(61) Wiria, F. E.; Leong, K. F.; Chua, C. K.; Liu, Y. Poly-Epsilon-Caprolactone/Hydroxyapatite for Tissue Engineering Scaffold Fabrication via Selective Laser Sintering. *Acta Biomaterials* **2007**, *3*, 1–12.

(62) Chung, H.; Das, S. Functionally Graded Nylon-11/Silica Nanocomposites Produced by Selective Laser Sintering. *Materials Science and Engineering A* **2008**, No. 487, 251–257.

(63) Menard, K. *Dynamic Mechanical Analysis: A Practical Introduction*, 1st ed.; CRC Press, 1999.

(64) Beaucage, G. Approximations Leading to a Unified Exponential/Power-Law Approach to Small-Angle Scattering. *Journal of Applied Crystallography* **1995**, *28* (6), 717–728.

(65) Ilavsky, J.; Jemian, P. R.; Allen, A. J.; Zhang, F.; Levine, L. E.; Long, G. G. Ultra-Small-Angle X-Ray Scattering at the Advanced Photon Source. *Journal of Applied Crystallography* **2009**, *42* (3), 469–479.

(66) Beaucage, G. Small-Angle Scattering from Polymeric Mass Fractals of Arbitrary Mass-Fractal Dimension. *Journal of Applied Crystallography* **1996**, *29* (2), 134–146.

(67) Hasan, O. A.; Boyce, M. C.; Li, X. S.; Berko, S. An Investigation of the Yield and Postyield Behavior and Corresponding Structure of Poly(Methyl Methacrylate). *Journal of Polymer Science Part B: Polymer Physics* **1993**, *31* (2), 185–197.

(68) Gorga, R. E.; Cohen, R. E. Toughness Enhancements in Poly(Methyl Methacrylate) by Addition of Oriented Multiwall Carbon Nanotubes. *Journal of Polymer Science Part B: Polymer Physics* **2004**, *42* (14), 2690–2702.

(69) Nielsen, L. E. Simple Theory of Stress-Strain Properties of Filled Polymers. *Journal of Applied Polymer Science* **1966**, *10* (1), 97–103.

(70) Zhang, H.; Zhang, Z.; Friedrich, K.; Eger, C. Property Improvements of in Situ Epoxy Nanocomposites with Reduced Interparticle Distance at High Nanosilica Content. *Acta Materialia* **2006**, *54* (7), 1833–1842.

(71) Zayed, S. M.; Alshimy, A. M.; Fahmy, A. E. Effect of Surface Treated Silicon Dioxide Nanoparticles on Some Mechanical Properties of Maxillofacial Silicone Elastomer. *Int J Biomater* **2014**, *2014*.

(72) Wu, C. L.; Zhang, M. Q.; Rong, M. Z.; Friedrich, K. Tensile Performance Improvement of Low Nanoparticles Filled-Polypropylene Composites. *Composites Science and Technology* **2002**, *62* (10–11), 1327–1340.

(73) Bray, D. J.; Dittanet, P.; Guild, F. J.; Kinloch, A. J.; Masania, K.; Pearson, R. A.; Taylor, A. C. The Modelling of the Toughening of Epoxy Polymers via Silica Nanoparticles: The Effects of Volume Fraction and Particle Size. *Polymer* **2013**, *54* (26), 7022–7032.

(74) Natarajan, B.; Li, Y.; Deng, H.; Brinson, L. C.; Schadler, L. S. Effect of Interfacial Energetics on Dispersion and Glass Transition Temperature in Polymer Nanocomposites. *Macromolecules* **2013**, *46* (7), 2833–2841.

(75) Bansal, A.; Yang, H.; Li, C.; Cho, K.; Benicewicz, B. C.; Kumar, S. K.; Schadler, L. S. Quantitative Equivalence between Polymer Nanocomposites and Thin Polymer Films. *Nature Materials* **2005**, *4* (9), 693–698.

(76) Salavagione, H. J.; Martínez, G.; Gómez, M. A. Synthesis of Poly(Vinyl Alcohol)/Reduced Graphite Oxide Nanocomposites with Improved Thermal and Electrical Properties. *Journal of Materials Chemistry* **2009**, *19* (28), 5027.

(77) Rittigstein, P.; Priestley, R. D.; Broadbelt, L. J.; Torkelson, J. M. Model Polymer Nanocomposites Provide an Understanding of Confinement Effects in Real Nanocomposites. *Nature Materials* **2007**, *6* (4), 278–282.

(78) Ramanathan, T.; Stankovich, S.; Dikin, D. A.; Liu, H.; Shen, H.; Nguyen, S. T.; Brinson, L. C. Graphitic Nanofillers in PMMA Nanocomposites—An Investigation of Particle Size and Dispersion and Their Influence on Nanocomposite Properties. *J. Polym. Sci. B Polym. Phys.* **2007**, *45* (15), 2097–2112.

(79) Akcora, P.; Kumar, S. K.; García Sakai, V.; Li, Y.; Benicewicz, B. C.; Schadler, L. S. Segmental Dynamics in PMMA-Grafted Nanoparticle Composites. *Macromolecules* **2010**, *43* (19), 8275–8281.

(80) Senses, E.; Akcora, P. An Interface-Driven Stiffening Mechanism in Polymer Nanocomposites. *Macromolecules* **2013**, *46* (5), 1868–1874.

(81) Zheng, W.; Wong, S.-C. Electrical Conductivity and Dielectric Properties of PMMA/Expanded Graphite Composites. *Composites Science and Technology* **2003**, *63* (2), 225–235.

(82) Kumar, M.; Shanmuga Priya, N.; Kanagaraj, S.; Pugazhenthi, G. Melt Rheological Behavior of PMMA Nanocomposites Reinforced with Modified Nanoclay. *Nanocomposites* **2016**, *2* (3), 109–116.

(83) Pötschke, P.; Fornes, T. D.; Paul, D. R. Rheological Behavior of Multiwalled Carbon Nanotube/Polycarbonate Composites. *Polymer* **2002**, *43* (11), 3247–3255.

(84) Zhang, H.-B.; Zheng, W.-G.; Yan, Q.; Jiang, Z.-G.; Yu, Z.-Z. The Effect of Surface Chemistry of Graphene on Rheological and Electrical Properties of Polymethylmethacrylate Composites. *Carbon* **2012**, *50* (14), 5117–5125.

(85) Zhang, Q.; Archer, L. A. Poly(Ethylene Oxide)/Silica Nanocomposites: Structure and Rheology. *Langmuir* **2002**, *18* (26), 10435–10442.

(86) Bartholome, C.; Beyou, E.; Bourgeat-Lami, E.; Cassagnau, P.; Chaumont, P.; David, L.; Zydowicz, N. Viscoelastic Properties and Morphological Characterization of Silica/Polystyrene Nanocomposites Synthesized by Nitroxide-Mediated Polymerization. *Polymer* **2005**, *46* (23), 9965–9973.

(87) Cassagnau, P. Melt Rheology of Organoclay and Fumed Silica Nanocomposites. *Polymer* **2008**, *49* (9), 2183–2196.

(88) Cassagnau, P. Payne Effect and Shear Elasticity of Silica-Filled Polymers in Concentrated Solutions and in Molten State. *Polymer* **2003**, *44* (8), 2455–2462.

(89) Elias, L.; Fenouillot, F.; Majeste, J. C.; Cassagnau, P. Morphology and Rheology of Immiscible Polymer Blends Filled with Silica Nanoparticles. *Polymer* **2007**, *48* (20), 6029–6040.

(90) Inoubli, R.; Dagréou, S.; Lapp, A.; Billon, L.; Peyrelasse, J. Nanostructure and Mechanical Properties of Polybutylacrylate Filled with Grafted Silica Particles. *Langmuir* **2006**, *22* (15), 6683–6689.

(91) Krishnamoorti, R.; Vaia, R. A.; Giannelis, E. P. Structure and Dynamics of Polymer-Layered Silicate Nanocomposites. *Chemistry of Materials* **1996**, *8* (8), 1728–1734.

(92) Sinha Ray, S.; Maiti, P.; Okamoto, M.; Yamada, K.; Ueda, K. New Polylactide/Layered Silicate Nanocomposites. 1. Preparation, Characterization, and Properties. *Macromolecules* **2002**, *35* (8), 3104–3110.

(93) Hadipoespito, G.; Yang, Y.; Choi, H.; Ning, G.; Li, X. Digital Micromirror Device Based Microstereolithography for Micro Structures of Transparent Photopolymer and Nanocomposites. In *Solid Freeform Fabrication Symposium, Austin, TX*; 2003; pp 13–24.

(94) Chryssolouris, G.; Stavropoulos, P.; Tsoukantas, G.; Salonitis, K.; Stournaras, A. Nanomanufacturing Processes: A Critical Review. *International Journal of Materials and Product Technology* **2003**, *21*, 535–543.

(95) Kumar, S.; Kruth, J.-P. Composites by Rapid Prototyping Technology. *Materials & Design* **2010**, *31* (2), 850–856.

(96) Jayaraman, A.; Nair, N. Integrating PRISM Theory and Monte Carlo Simulation to Study Polymer-Functionalised Particles and Polymer Nanocomposites. *Molecular Simulation* **2012**, *38* (8–9), 751–761.

(97) Jayaraman, A.; Schweizer, K. S. Effective Interactions, Structure, and Phase Behavior of Lightly Tethered Nanoparticles in Polymer Melts. *Macromolecules* **2008**, *41* (23), 9430–9438.

(98) Kalb, J.; Dukes, D.; Kumar, S. K.; Hoy, R. S.; Grest, G. S. End Grafted Polymernanoparticles in a Polymeric Matrix: Effect of Coverage and Curvature. *Soft Matter* **2011**, *7* (4), 1418–1425.

(99) Beaucage, G.; Kammler, H. K.; Pratsinis, S. E. Particle Size Distributions from Small-Angle Scattering Using Global Scattering Functions. *Journal of Applied Crystallography* **2004**, *37* (4), 523–535.

(100) Maillard, D.; Kumar, S. K.; Fragneaud, B.; Kysar, J. W.; Rungta, A.; Benicewicz, B. C.; Deng, H.; Brinson, L. C.; Douglas, J. F. Mechanical Properties of Thin Glassy Polymer Films Filled with Spherical Polymer-Grafted Nanoparticles. *Nano Letters* **2012**, *12* (8), 3909–3914.

(101) Akcora, P.; Kumar, S. K.; Moll, J.; Lewis, S.; Schadler, L. S.; Li, Y.; Benicewicz, B. C.; Sandy, A.; Narayanan, S.; Ilavsky, J.; et al. "Gel-like" Mechanical Reinforcement in Polymer Nanocomposite Melts. *Macromolecules* **2010**, *43* (2), 1003–1010.

(102) Liu, S.; Senses, E.; Jiao, Y.; Narayanan, S.; Akcora, P. Structure and Entanglement Factors on Dynamics of Polymer-Grafted Nanoparticles. *ACS Macro Letters* **2016**, *5* (5), 569–573.

(103) Bansal, A.; Yang, H.; Li, C.; Benicewicz, B. C.; Kumar, S. K.; Schadler, L. S. Controlling the Thermomechanical Properties of Polymer Nanocomposites by Tailoring the Polymer–Particle Interface. *J. Polym. Sci. B Polym. Phys.* **2006**, *44* (20), 2944–2950.

(104) Vaziri, H. S.; Omaraei, I. A.; Abadyan, M.; Mortezaei, M.; Yousefi, N. Thermophysical and Rheological Behavior of Polystyrene/Silica Nanocomposites: Investigation of Nanoparticle Content. *Materials & Design* **2011**, *32* (8), 4537–4542.

(105) Rong, M. Z.; Zhang, M. Q.; Zheng, Y. X.; Zeng, H. M.; Walter, R.; Friedrich, K. Structure–Property Relationships of Irradiation Grafted Nano-Inorganic Particle Filled Polypropylene Composites. *Polymer* **2001**, *42* (1), 167–183.

(106) Mitchell, C. A.; Bahr, J. L.; Arepalli, S.; Tour, J. M.; Krishnamoorti, R. Dispersion of Functionalized Carbon Nanotubes in Polystyrene. *Macromolecules* **2002**, *35* (23), 8825–8830.

(107) Kumar, S. K.; Ganesan, V.; Riggleman, R. A. Perspective: Outstanding Theoretical Questions in Polymer-Nanoparticle Hybrids. *The Journal of Chemical Physics* **2017**, *147* (2), 020901.

(108) Trombly, D. M.; Ganesan, V. Curvature Effects upon Interactions of Polymer-Grafted Nanoparticles in Chemically Identical Polymer Matrices. *J. Chem. Phys.* **2010**, *133* (15), 154904.

(109) Kumar, S. K.; Krishnamoorti, R. Nanocomposites: Structure, Phase Behavior, and Properties. *Annual Review of Chemical and Biomolecular Engineering* **2010**, *1* (1), 37–58.

(110) Xu, C.; Ohno, K.; Ladmiral, V.; Milkie, D. E.; Kikkawa, J. M.; Composto, R. J. Simultaneous Block Copolymer and Magnetic Nanoparticle Assembly in Nanocomposite Films. *Macromolecules* **2009**, *42* (4), 1219–1228.

(111) Bellini, A.; Güçeri, S. Mechanical Characterization of Parts Fabricated Using Fused Deposition Modeling. *Rapid Prototyping Journal* **2003**, *9* (4), 252–264.

(112) Thrimurthulu, K.; Pandey, P. M.; Venkata Reddy, N. Optimum Part Deposition Orientation in Fused Deposition Modeling. *International Journal of Machine Tools and Manufacture* **2004**, *44* (6), 585–594.

(113) N. Turner, B.; Strong, R.; A. Gold, S. A Review of Melt Extrusion Additive Manufacturing Processes: I. Process Design and Modeling. *Rapid Prototyping Journal* **2014**, *20* (3), 192–204.

(114) Ahn, S.; Montero, M.; Odell, D.; Roundy, S.; Wright, P. K. Anisotropic Material Properties of Fused Deposition Modeling ABS. *Rapid Prototyping Journal* **2002**, *8* (4), 248–257.

(115) Kaveh, M.; Badrossamay, M.; Foroozmehr, E.; Hemasian Etefagh, A. Optimization of the Printing Parameters Affecting Dimensional Accuracy and Internal Cavity for HIPS Material Used in Fused Deposition Modeling Processes. *Journal of Materials Processing Technology* **2015**, *226*, 280–286.

(116) Kim, E.; Shin, Y.-J.; Ahn, S.-H. The Effects of Moisture and Temperature on the Mechanical Properties of Additive Manufacturing Components: Fused Deposition Modeling. *Rapid Prototyping Journal* **2016**, *22* (6), 887–894.

(117) Peng, F.; Zhao, Z.; Xia, X.; Cakmak, M.; Vogt, B. D. Enhanced Impact Resistance of Three-Dimensional-Printed Parts with Structured Filaments. *ACS Applied Materials & Interfaces* **2018**, *10* (18), 16087–16094.

(118) Dul, S.; Fambri, L.; Pegoretti, A. Fused Deposition Modelling with ABS–Graphene Nanocomposites. *Composites Part A: Applied Science and Manufacturing* **2016**, *85*, 181–191.

(119) Gnanasekaran, K.; Heijmans, T.; Bennekom, S. van; Woldhuis, H.; Wijnia, S.; With, G. de; Friedrich, H. 3D Printing of CNT- and Graphene-Based Conductive Polymer Nanocomposites by Fused Deposition Modeling. *Applied Materials Today* **2017**, *9*, 21–28.

(120) Parandoush, P.; Lin, D. A Review on Additive Manufacturing of Polymer-Fiber Composites. *Composite Structures* **2017**, *182*, 36–53.

(121) Street, D. P.; Mah, A. H.; Patterson, S.; Pickel, D. L.; Bergman, J. A.; Stein, G. E.; Messman, J. M.; Kilbey, S. M. Interfacial Interactions in PMMA/Silica Nanocomposites Enhance the Performance of Parts Created by Fused Filament Fabrication. *Polymer* **2018**, *157*, 87–94.

(122) Li, C.; Han, J.; Ryu, C. Y.; Benicewicz, B. C. A Versatile Method To Prepare RAFT Agent Anchored Substrates and the Preparation of PMMA Grafted Nanoparticles. *Macromolecules* **2006**, *39* (9), 3175–3183.

(123) Street, D. P.; Kilbey, S. M. Enhancing Thermomechanical Properites of PMMA through Fused Deposition Modeling Using Nanocomposite Filaments.

(124) Kinning, D. J.; Thomas, E. L. Hard-Sphere Interactions between Spherical Domains in Diblock Copolymers. *Macromolecules* **1984**, *17* (9), 1712–1718.

(125) Martin, T. B.; Mongcopa, K. I. S.; Ashkar, R.; Butler, P.; Krishnamoorti, R.; Jayaraman, A. Wetting–Dewetting and Dispersion–Aggregation Transitions Are Distinct for Polymer Grafted Nanoparticles in Chemically Dissimilar Polymer Matrix. *Journal of the American Chemical Society* **2015**, 150813151435003.

(126) Vaia, R. A. Polymer Nanocomposites with Prescribed Morphology: Going beyond Nanoparticle-Filled Polymers. 16.

(127) Jouault, N.; Vallat, P.; Dalmas, F.; Said, S.; Jestin, J.; Boué, F. Well-Dispersed Fractal Aggregates as Filler in Polymer−Silica Nanocomposites: Long-Range Effects in Rheology. *Macromolecules* **2009**, *42* (6), 2031–2040.

(128) Cassagnau, P. Payne Effect and Shear Elasticity of Silica-Filled Polymers in Concentrated Solutions and in Molten State. *Polymer* **2003**, *44* (8), 2455–2462.

(129) Goffin, A.-L.; Raquez, J.-M.; Duquesne, E.; Siqueira, G.; Habibi, Y.; Dufresne, A.; Dubois, P. Poly(ε-Caprolactone) Based Nanocomposites Reinforced by Surface-Grafted Cellulose Nanowhiskers via Extrusion Processing: Morphology, Rheology, and Thermo-Mechanical Properties. *Polymer* **2011**, *52* (7), 1532–1538.

(130) Zhu, A.; Cai, A.; Zhou, W.; Shi, Z. Effect of Flexibility of Grafted Polymer on the Morphology and Property of Nanosilica/PVC Composites. *Applied Surface Science* **2008**, *254* (13), 3745–3752.

(131) Wang, M.; Shi, J.-H.; Pramoda, K. P.; Goh, S. H. Microstructure, Crystallization and Dynamic Mechanical Behaviour of Poly(Vinylidene Fluoride) Composites Containing Poly(Methyl Methacrylate)-Grafted Multiwalled Carbon Nanotubes. *Nanotechnology* **2007**, *18* (23), 235701.

(132) Eitan, A.; Fisher, F. T.; Andrews, R.; Brinson, L. C.; Schadler, L. S. Reinforcement Mechanisms in MWCNT-Filled Polycarbonate. *Composites Science and Technology* **2006**, *66* (9), 1162–1173.

(133) Koerner, H.; Liu, W.; Alexander, M.; Mirau, P.; Dowty, H.; Vaia, R. A. Deformation–Morphology Correlations in Electrically Conductive Carbon Nanotube—Thermoplastic Polyurethane Nanocomposites. *Polymer* **2005**, *46* (12), 4405–4420.

(134) Taniike, T.; Toyonaga, M.; Terano, M. Polypropylene-Grafted Nanoparticles as a Promising Strategy for Boosting Physical Properties of Polypropylene-Based Nanocomposites. *Polymer* **2014**, *55* (4), 1012–1019.

(135) Ash, B. J.; Rogers, D. F.; Wiegand, C. J.; Schadler, L. S.; Siegel, R. W.; Benicewicz, B. C.; Apple, T. Mechanical Properties of Al2O3/Polymethylmethacrylate Nanocomposites. *Polym Compos* **2002**, *23* (6), 1014–1025.

(136) Ng, C. B.; Ash, B. J.; Schadler, L. S.; Siegel, R. W. A Study of the Mechanical and Permeability Propertied OS Nano- and Micron TiO2 Filled Epoxy Composites. *Advanced Composites Letters 10* (3), 101.

(137) Zhang, J.; Wang, X.; Lu, L.; Li, D.; Yang, X. Preparation and Performance of High-Impact Polystyrene (HIPS)/Nano-TiO2 Nanocomposites. *Journal of Applied Polymer Science* **2003**, *87* (3), 381–385.

(138) Tirrell, M. Modular Materials by Self-Assembly. *AIChE Journal* **2005**, *51* (9), 2386–2390.

(139) Pekkanen, A. M.; Mondschein, R. J.; Williams, C. B.; Long, T. E. 3D Printing Polymers with Supramolecular Functionality for Biological Applications. *Biomacromolecules* **2017**, *18* (9), 2669–2687.

(140) de Greef, T. F. A.; Meijer, E. W. Materials Science: Supramolecular Polymers. *Nature* **2008**, *453* (7192), 171–173.

(141) Lange, R. F. M.; Van Gurp, M.; Meijer, E. W. Hydrogen-Bonded Supramolecular Polymer Networks. *Journal of Polymer Science Part A: Polymer Chemistry* **1999**, *37* (19), 3657–3670.

(142) Folmer, B. J. B.; Sijbesma, R. P.; Kooijman, H.; Spek, A. L.; Meijer, E. W. Cooperative Dynamics in Duplexes of Stacked Hydrogen-Bonded Moieties. *Journal of the American Chemical Society* **1999**, *121* (39), 9001–9007.

(143) Hirschberg, J. H. K. K.; Beijer, F. H.; van Aert, H. A.; Magusin, P. C. M. M.; Sijbesma, R. P.; Meijer, E. W. Supramolecular Polymers from Linear Telechelic Siloxanes with Quadruple-Hydrogen-Bonded Units. *Macromolecules* **1999**, *32* (8), 2696–2705.

(144) Hilger, C.; Stadler, R. New Multiphase Architecture from Statistical Copolymers by Cooperative Hydrogen Bond Formation. *Macromolecules* **1990**, *23* (7), 2095–2097.

(145) Hilger, C.; Stadler, R. Cooperative Structure Formation by Combination of Covalent and Association Chain Polymers: 4. Designing Functional Groups for Supramolecular Structure Formation. *Polymer* **1991**, *32* (17), 3244–3249.

(146) Hilger, C.; Draeger, M.; Stadler, R. Molecular Origin of Supramolecular Self-Assembling in Statistical Copolymers. *Macromolecules* **1992**, *25* (9), 2498–2501.

(147) Rieth, L. R.; Eaton, R. F.; Coates, G. W. Polymerization of Ureidopyrimidinone-Functionalized Olefins by Using Late-Transition Metal Ziegler–Natta Catalysts: Synthesis of Thermoplastic Elastomeric Polyolefins. *Angewandte Chemie International Edition* **2001**, *40* (11), 2153–2156.

(148) Watanabe, T.; He, Y.; Asakawa, N.; Yoshie, N.; Inoue, Y. Hydrogen-Bonding Interaction between Poly(ε-Caprolactone) and Low-Molecular-Weight Amino Compounds. *Polymer International* **2001**, *50* (4), 463–468.

(149) He, Y.; Asakawa, N.; Inoue, Y. Studies on Poly(ε-Caprolactone)/Thiodiphenol Blends: The Specific Interaction and the Thermal and Dynamic Mechanical Properties. *Journal of Polymer Science Part B: Polymer Physics* **2000**, *38* (14), 1848–1859.

(150) Kuo, S.-W. Hydrogen-Bonding in Polymer Blends. *Journal of Polymer Research* **2008**, *15* (6), 459–486.

(151) He, Y.; Zhu, B.; Inoue, Y. Hydrogen Bonds in Polymer Blends. *Progress in Polymer Science* **2004**, *29* (10), 1021–1051.

(152) Wittenberg, E.; Meyer, A.; Eggers, S.; Abetz, V. Hydrogen Bonding and Thermoplastic Elastomers – a Nice Couple with Temperature-Adjustable Mechanical Properties. *Soft Matter* **2018**, *14* (14), 2701–2711.

(153) Qiu, S.; Gan, X.; Gao, C.; Zheng, X.; Yu, H.; Fan, H. Hydrogen Bond Effect of Azido Polyurethane Elastomer by Dynamic Mechanical Analysis. *Journal of Polymer Science Part B: Polymer Physics* **2006**, *44* (19), 2841–2851.

(154) Shabbir, A.; Goldansaz, H.; Hassager, O.; van Ruymbeke, E.; Alvarez, N. J. Effect of Hydrogen Bonding on Linear and Nonlinear Rheology of Entangled Polymer Melts. *Macromolecules* **2015**, *48* (16), 5988–5996.

(155) Levenhagen, N. P.; Dadmun, M. D. Bimodal Molecular Weight Samples Improve the Isotropy of 3D Printed Polymeric Samples. *Polymer* **2017**, *122*, 232–241.

APPENDICES

Appendix A – Supporting Information for Chapter 2: Interfacial Interactions in PMMA/Silica Nanocomposites Enhance the Performance of Parts Created by Fused Filament Fabrication

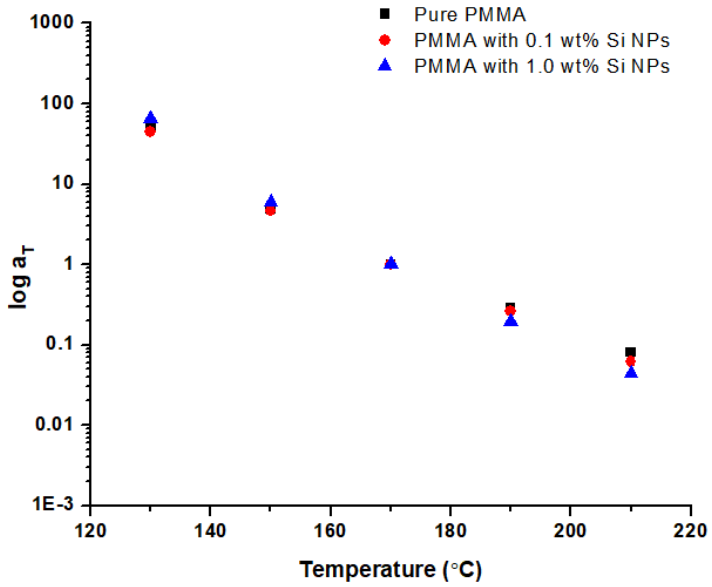

Figure A.1. Frequency shift factors (a_T) for FFF-printed PMMA nanocomposites.

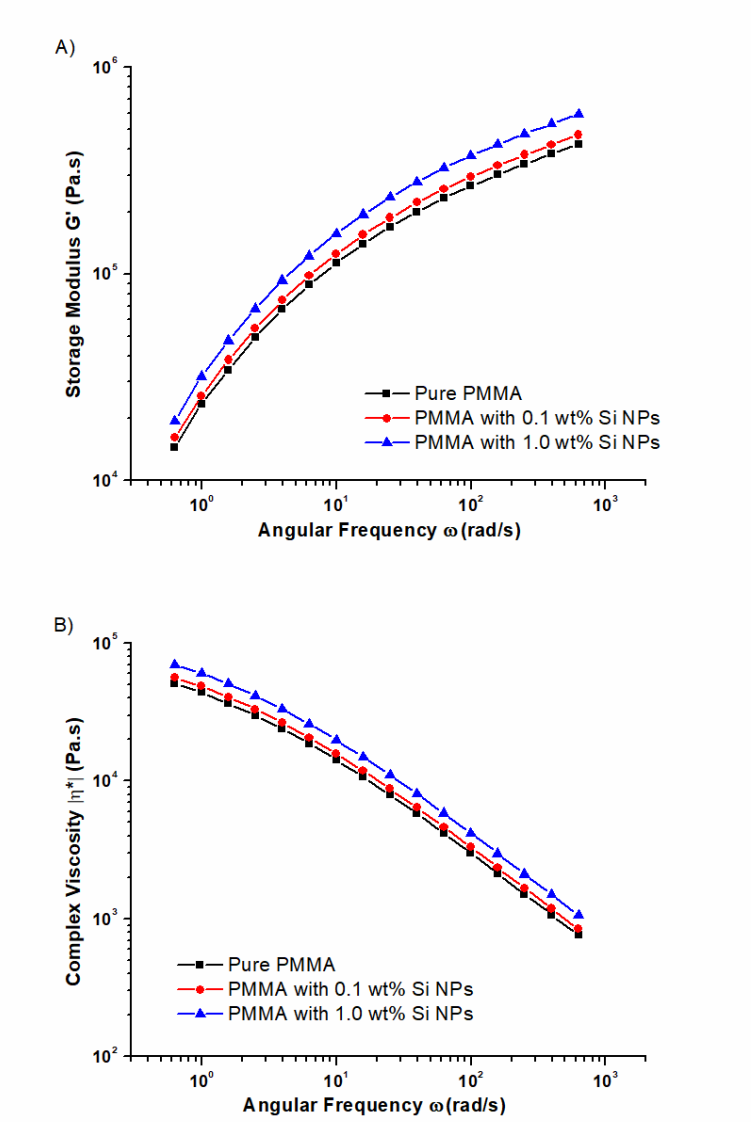

Figure A.2. Small amplitude oscillatory shear measurements completed at 170 °C display a monotonic increase in the storage (A) and complex viscosity (B) as the loading level of Si NPs increases.

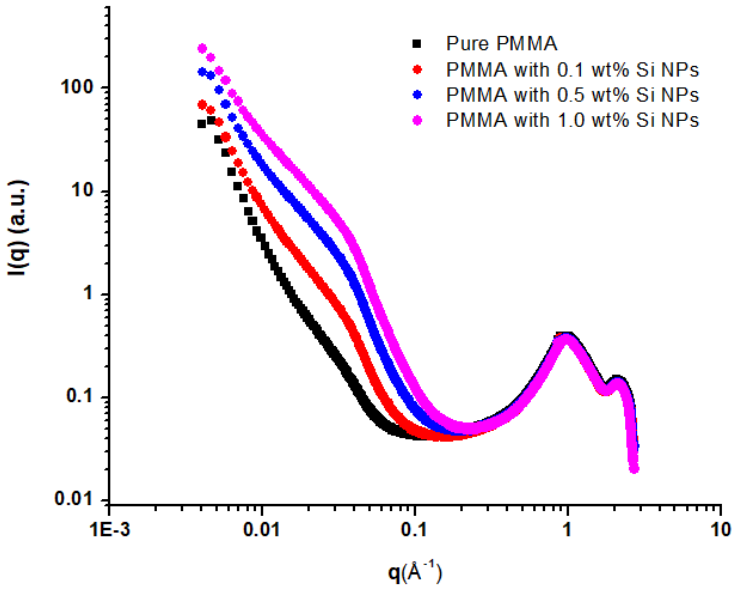

Figure A.3. Uncorrected SAXS and WAXS results of FFF-printed PMMA nanocomposites with increasing loading levels of Si NPs. As noted in the *Article*, the WAXS signal (0.85 < q ($Å^{-1}$) < 2.69) is the same for all samples.

Appendix B – Supporting Information for Chapter 3: Tailoring Interfacial Interactions Using Polymer Grafted Nanoparticles Improves Performance of Parts Manufactured by 3D Printing

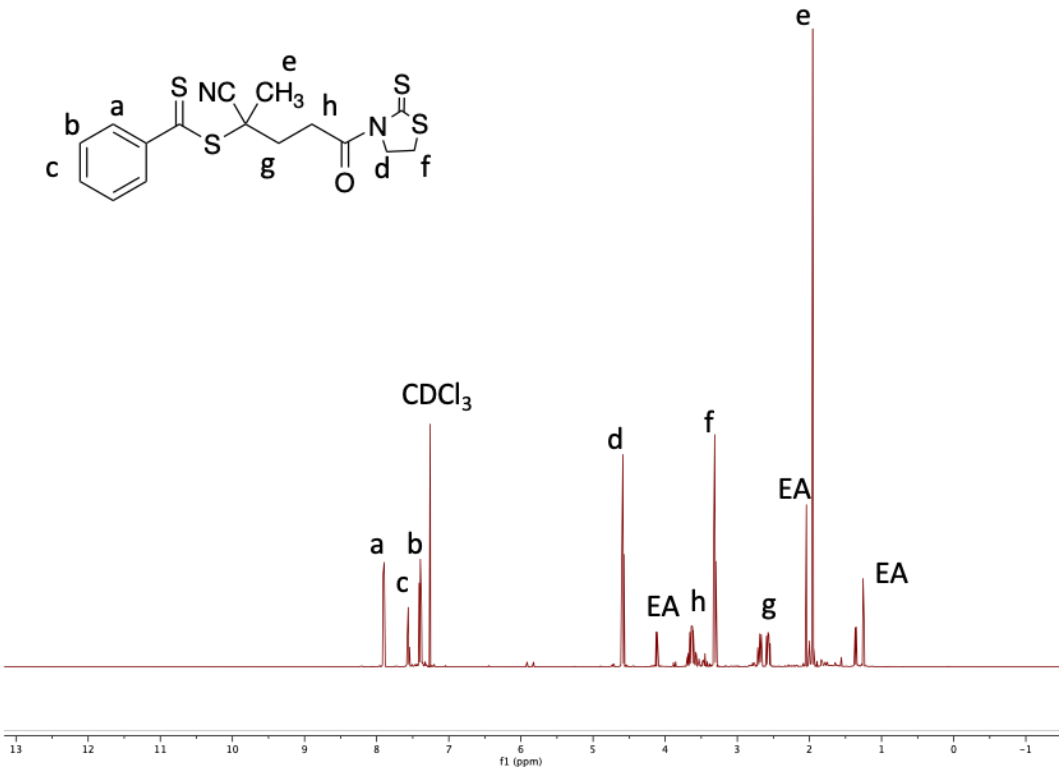

Figure B.1. ^{1}H NMR spectrum (500 MHz, 25 °C, $CDCl_3$) of the modified CTA; δ (ppm): 7.90 (d,2H,CH), 7.56 (t, 1H, CH), 4.59(t, 2H, CH_2), 3.62 (m, 2H, CH_2), 3.30 (t, 2H, CH_2), 2.50-2.70 (m, 2H, CH_2), 1.95 (s, 3H, CH_3). Solvent residual peaks for chloroform and ethyl acetate (EA) are identified.

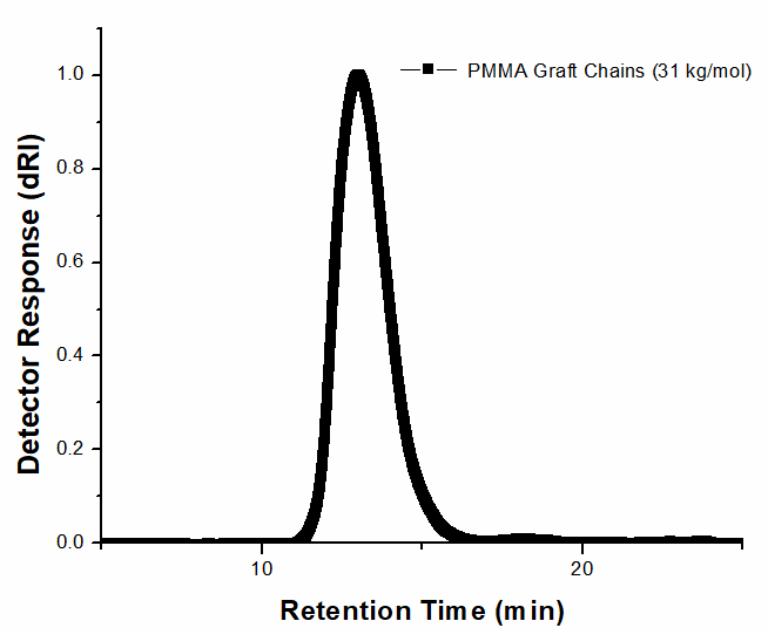

Figure B.2. GPC trace of PMMA graft chains cleaved (using HF) from 14 nm Si NPs measured using dRI detection.

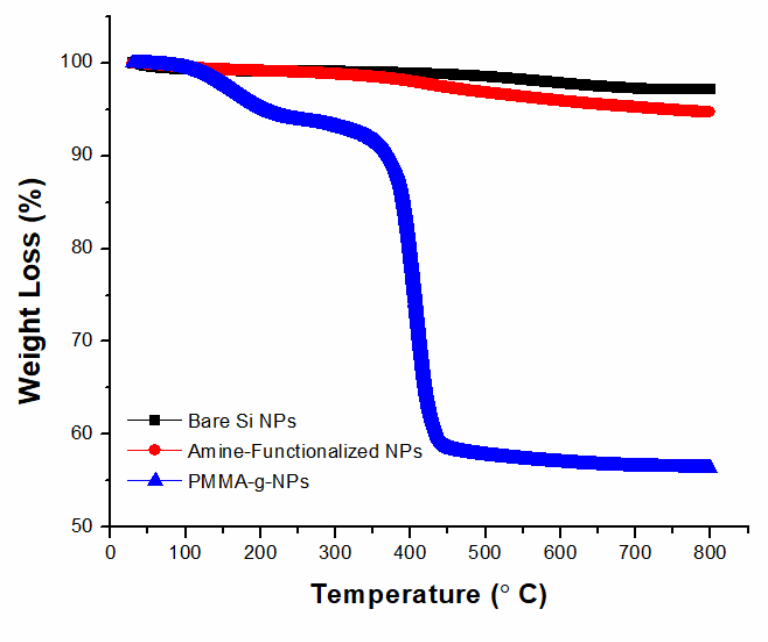

Figure B.3. TGA traces reflect an increase in mass loss after bare Si NPs (black trace) are functionalized with the aminosilane (red trace) and after PMMA chains are grown from the NP surface (blue trace).

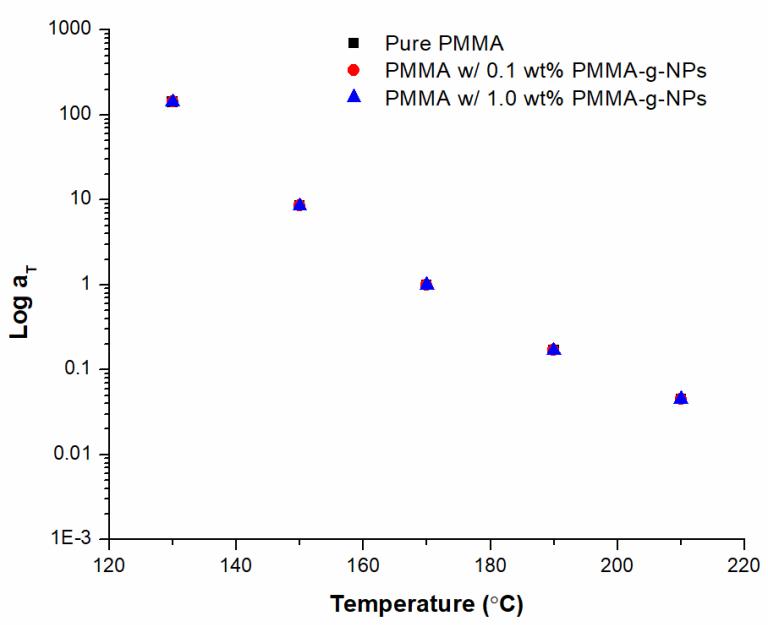

Figure B.4. WLF-type frequency shift factors, a_T, generated using time-temperature superposition for PMMA nanocomposites containing PMMA-g-NPs.

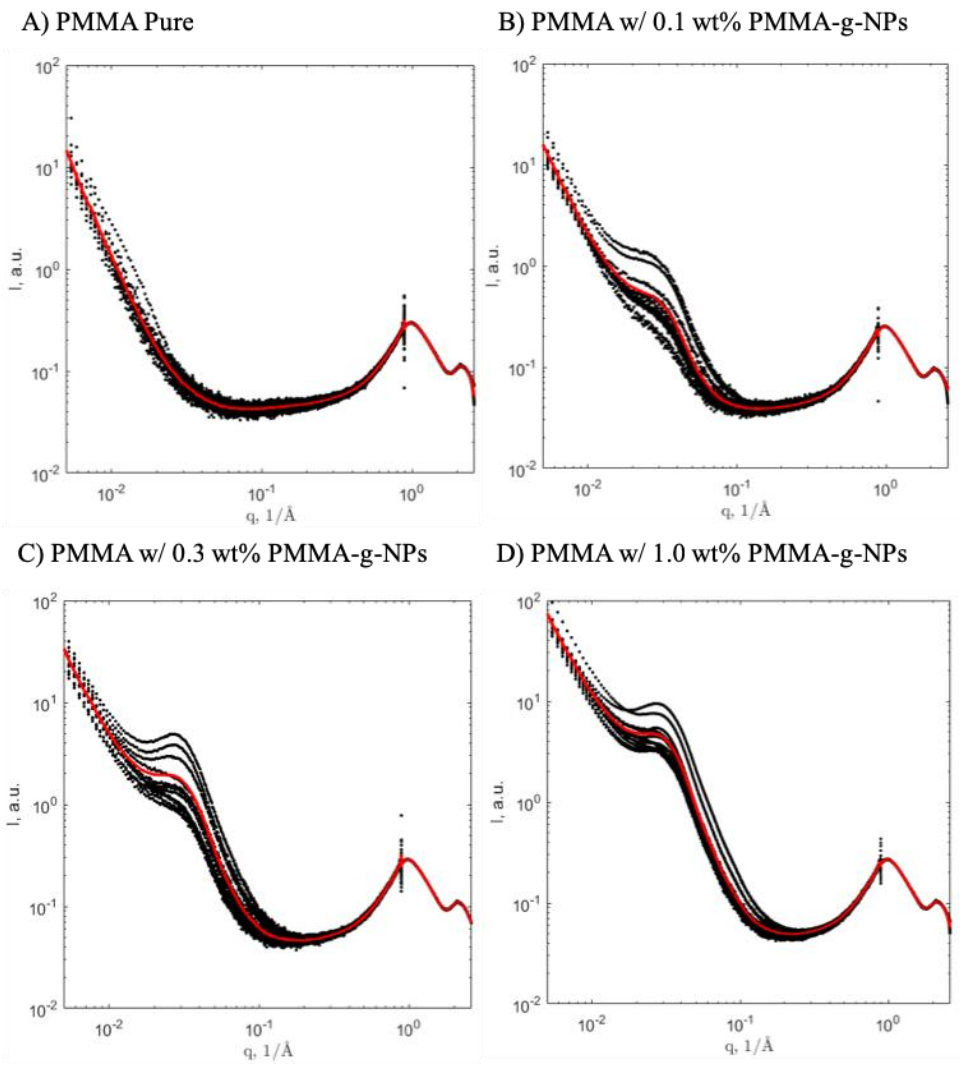

Figure B.5. Uncorrected SAXS and WAXS data for FFF-printed PMMA nanocomposites containing PMMA-g-NPs at various loading levels. The red line represents the average trace.

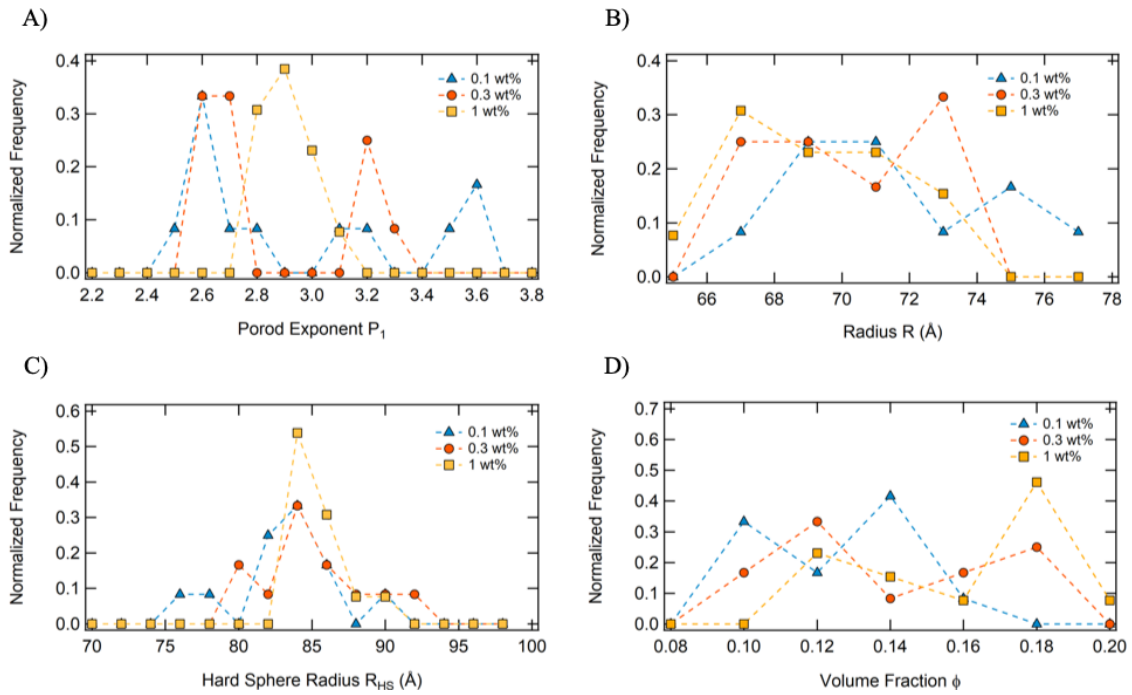

Figure B.6. SAXS parameter plots for the (A) Porod Exponent, (B) Radius, (C) Hard Sphere Radius, and (D) volume fraction.

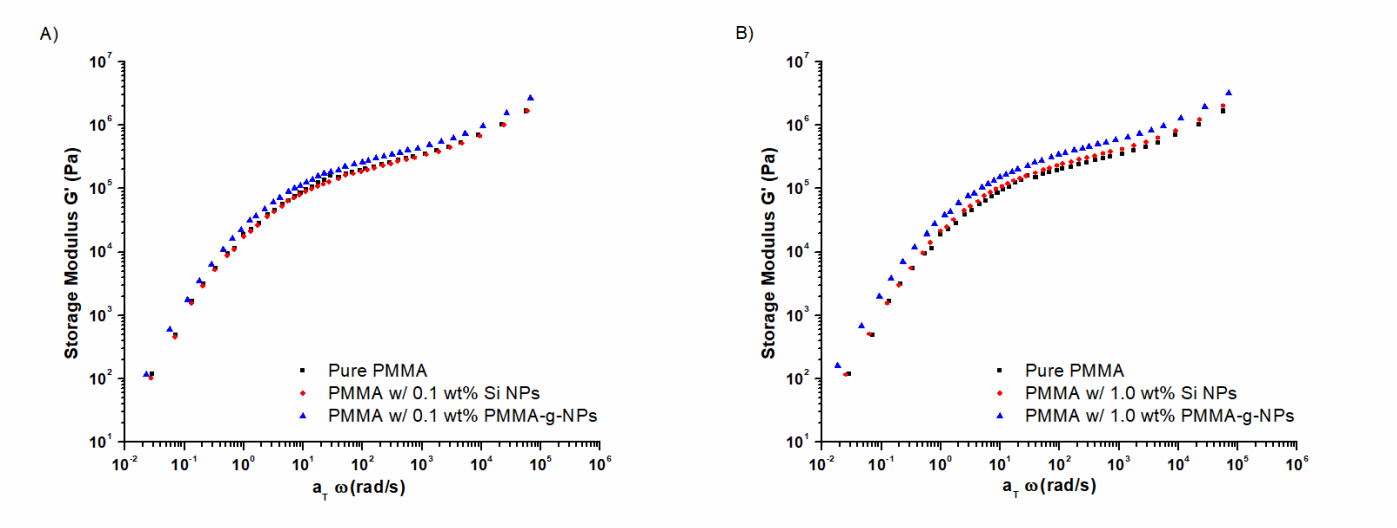

Figure B.7. Angular frequency-dependent storage modulus master curves show how the melt flow characteristics of FFF-printed PMMA parts are significantly affected by the addition of PMMA-g-NPs compared to bare (unfunctionalized) Si NPs at (A) 0.1 wt% and (B) 1.0 wt%.

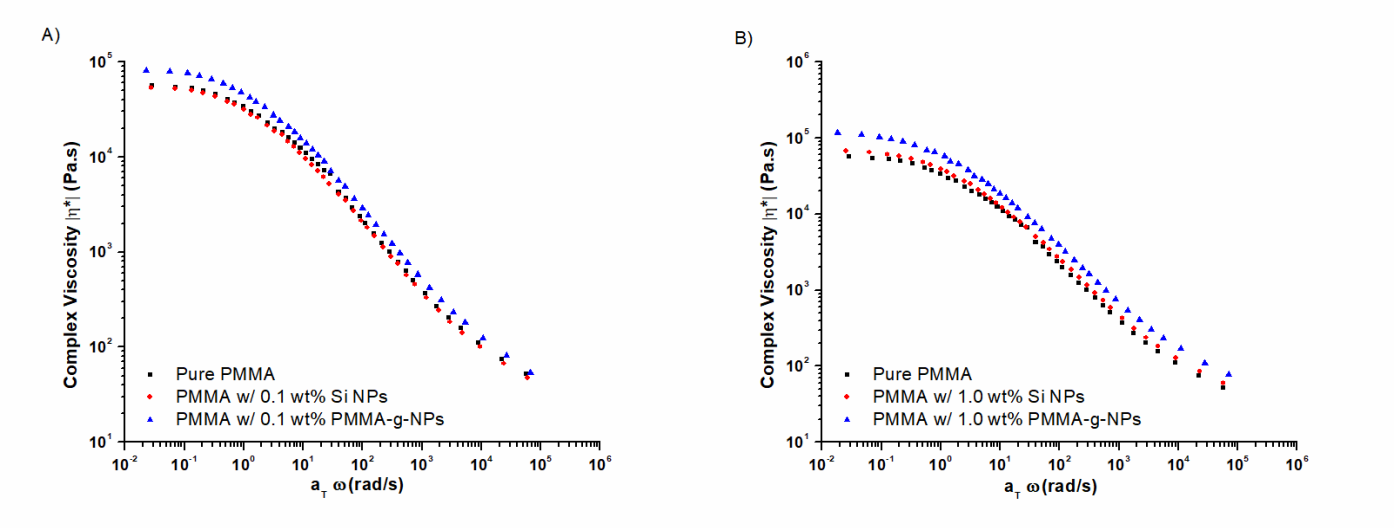

Figure B.8. Angular frequency-dependent complex viscosity master curves reflect an increase in the melt flow properties of PMMA parts containing PMMA-g-NPs compared to bare Si NPs at equivalent loading levels, such as (A) 0.1 wt% and (B) 1.0 wt%.

Appendix C – Supporting Information for Chapter 4: Self-Complementary Multiple Hydrogen Bonding Additives Enhance Thermomechanical Properties of PMMA Structures Created by Fused Filament Fabrication

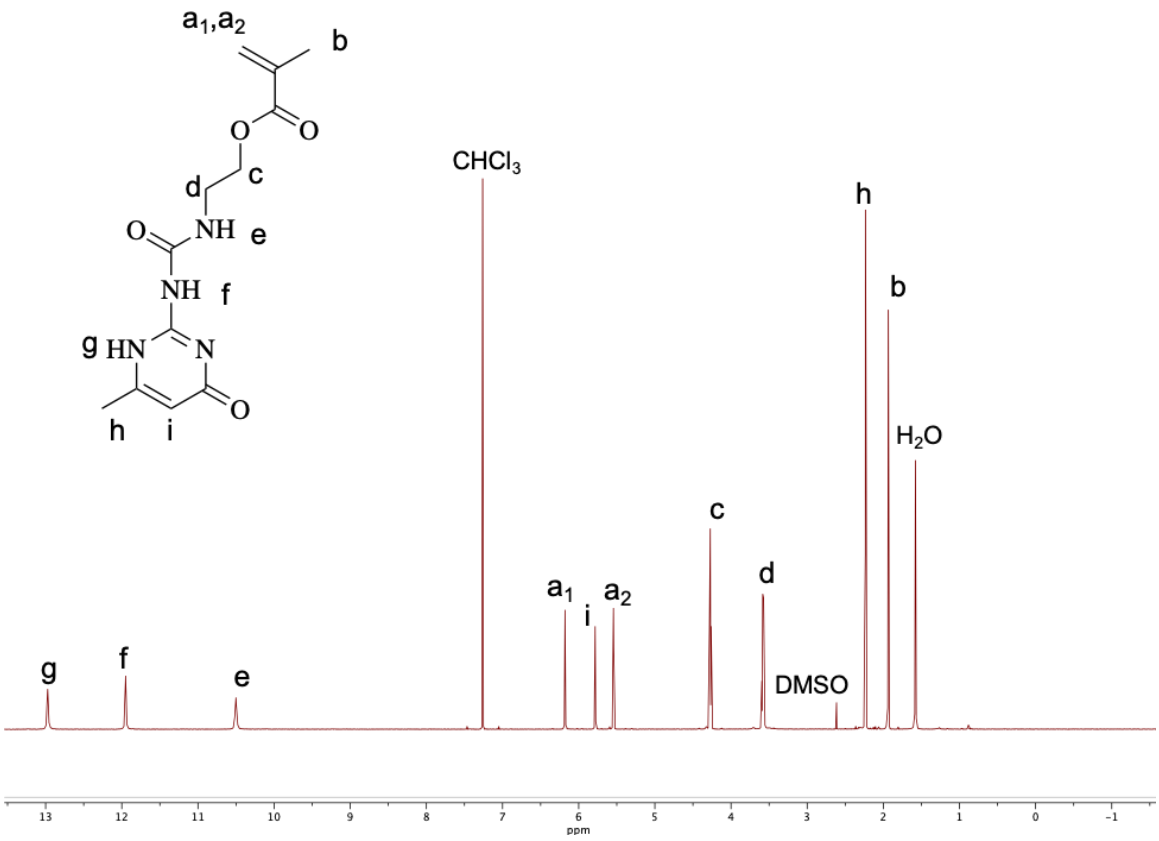

Figure C.1. ^{1}H NMR spectrum (500 MHz, 25 °C, $CDCl_3$) of UPyMA monomer; δ (ppm): 12.97 (s,1H,NH), 11.95 (s, 1H, NH), 10.50 (s, 1H, NH), 6.18 (s, 1H, CH), 5.78 (s, 1H, CH), 5.54 (s, 1H, CH), 4.27 (s, 2H, CH_2), 3.58 (s, 2H, CH_2), 2.23 (s, 3H, CH_3), 1.93 (s, 3H, CH_3).

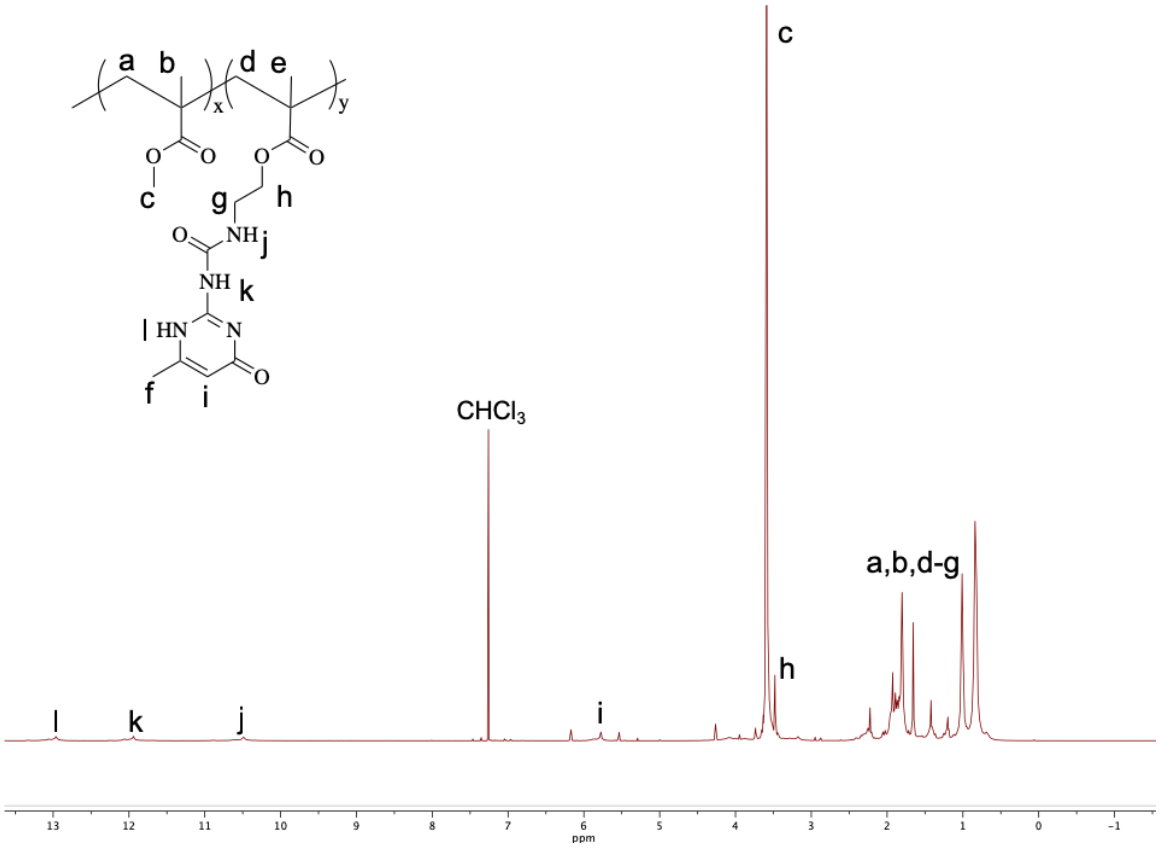

Figure C.2. Representative ^{1}H NMR spectrum (500 MHz, 25 °C, $CDCl_3$) of MMA-r-UPyMA copolymer (3 mol% UPyMA); δ (ppm): 12.96 (s, 1H, NH in UPyMA units), 11.94 (s, 1H, NH in UPyMA units), 10.49 (s, 1H, NH in UPyMA units), 5.78 (s, 1H, CH in UPyMA units), 3.59 (s, 3H, CH_3 in MMA units), 3.48 (s, 2H, CH_2 in UPyMA units), 0.8-2.3 (b, CH_2, CH_3 in MMA and UPyMA units).

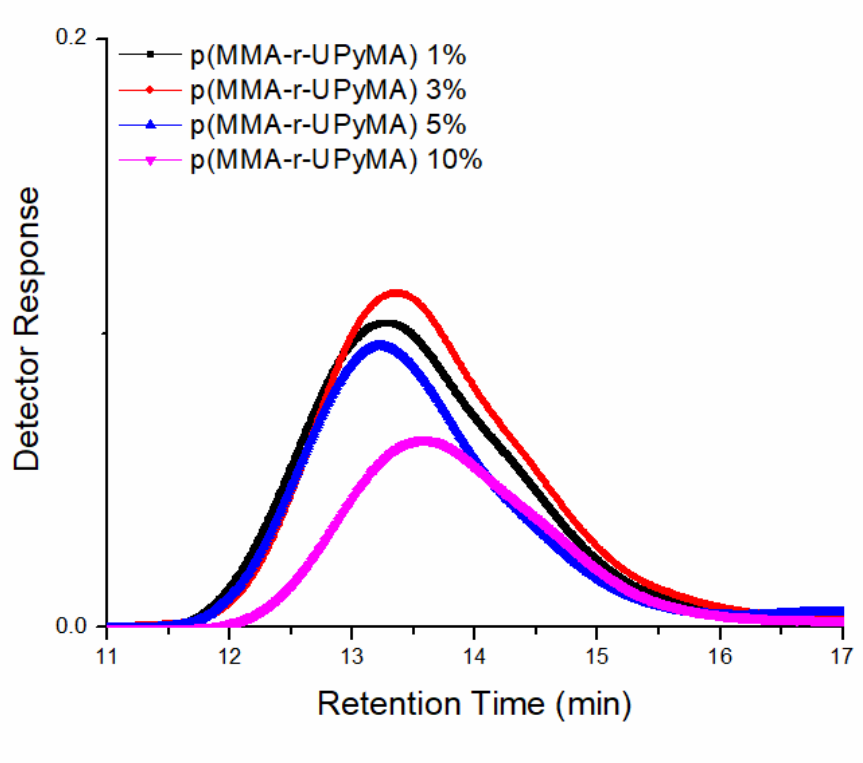

Figure C.3. GPC traces of p(MMA-r-UPyMA) copolymer additives synthesized via free radical polymerization measured using dRI detection.

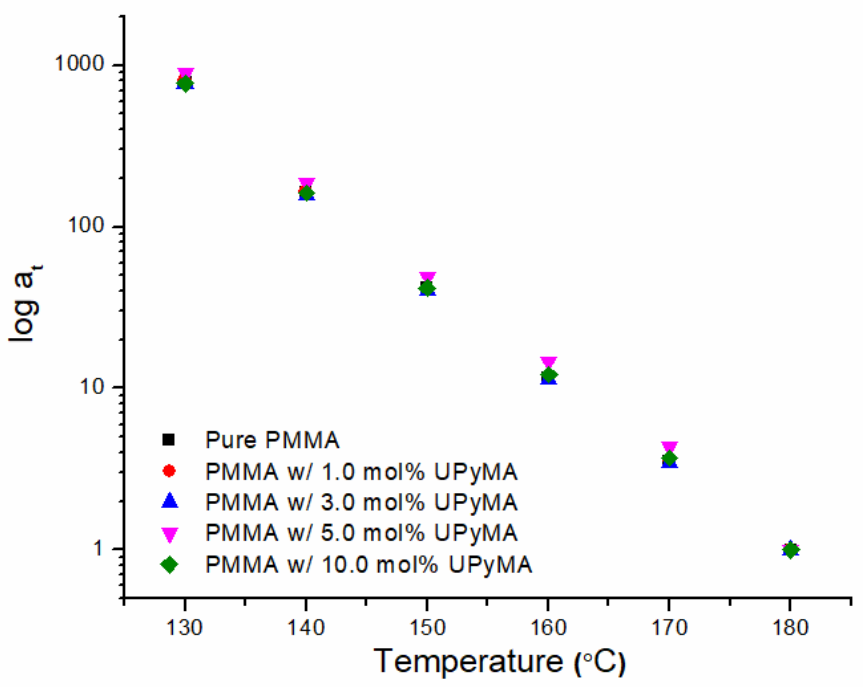

Figure C.4. Frequency shift factors (a_t) generated by time-temperature superposition for PMMA multicomponent blends printed via FFF.

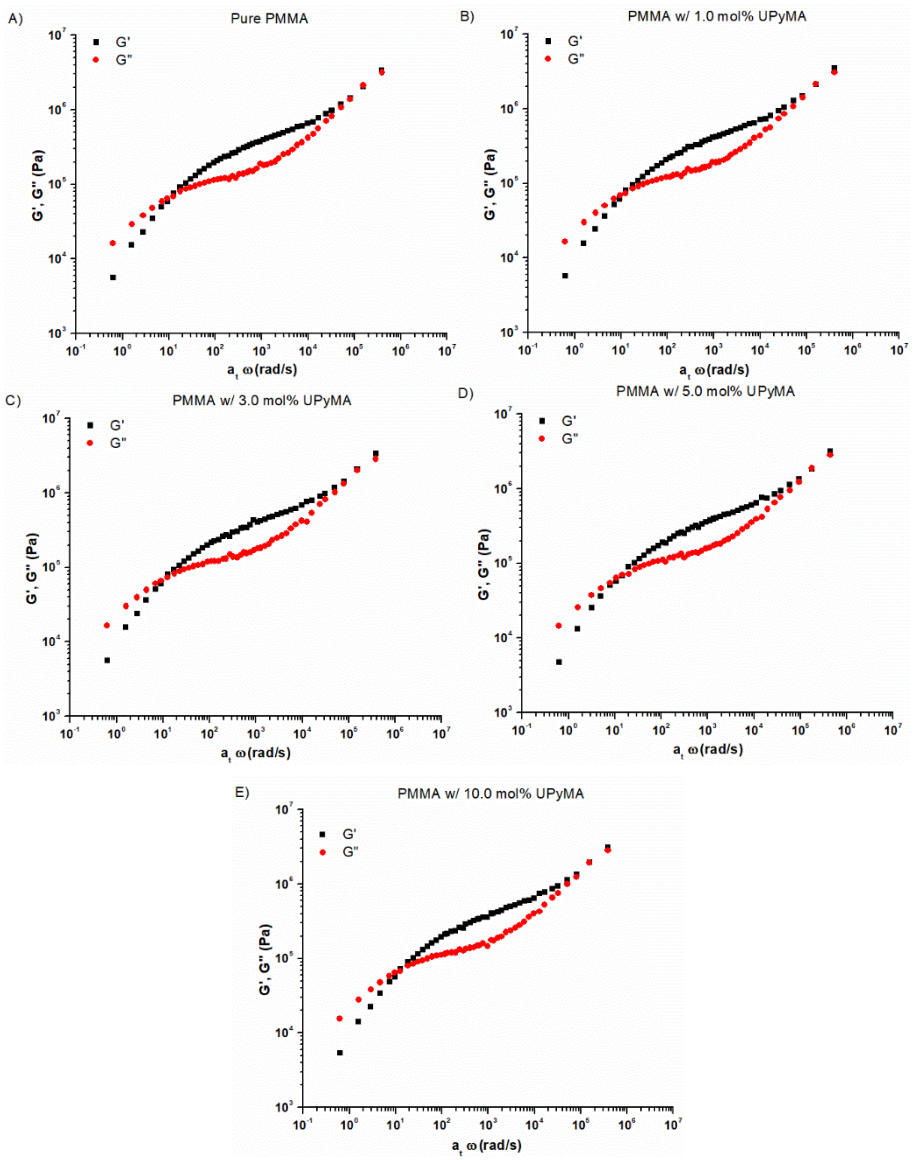

Figure C.5. Storage and loss moduli master curves measured for the PMMA matrix polymer (A) and multicomponent blends with 1 wt.% random copolymer additive of different composition (B-E) display liquid-like behavior in the terminal regime, G”(ω) > G’(ω), regardless of the UPyMA content. This suggest that at temperatures exceeding the dissociation temperature (taken to be T = 80 °C) the physical crosslinks are, in essence, broken.

VITA

Dayton Phillip Street was born and raised in Kingsport, Tennessee. In 2010, he graduated from Sullivan South High School. After high school, Dayton attended East Tennessee State University (ETSU) and earned a Bachelor of Science degree in Chemistry. Throughout his time at ETSU, Dayton completed undergraduate research with Dr. Hua Mei and worked at Eastman Chemical Company. As an undergraduate researcher, he was the recipient of an honors undergraduate research award for his work pertaining to fluorinated monomers for proton exchange membranes. After graduating from ETSU in 2014, Dayton enrolled at the University of Tennessee-Knoxville to continue his academic studies. Dayton joined the research group of Professor S. Michael Kilbey II and earned his Ph.D. in Polymer Chemistry in 2019. His dissertation research focused on manipulating interfacial interactions between polymer matrices and nanoscopic additives in order to manipulate the nanoscale structure and enhance the macroscopic properties of polymeric parts printed by Fused Filament Fabrication. In addition to his academic studies, Dayton was heavily involved in the Association of Chemistry Graduate Students, serving as the Vice President, Secretary and Philanthropist, and he was elected to represent the graduate student body on the Graduate Research Recruiting Committee. Furthermore, Dayton volunteered annually for the Forensic Chemistry Camp for middle school students. In 2018 Dayton was selected to receive an National Research Council fellowship that will enable him to join the Air Force Research Laboratory as a postdoctoral research fellow.